



**UNIL** | Université de Lausanne

Unicentre

CH-1015 Lausanne

<http://serval.unil.ch>

---

*Year : 2015*

## Stability of Nanoparticle Agglomerates under Mechanical Stress and its Effects on their Release into the Air

DING Yaobo

DING Yaobo, 2015, Stability of Nanoparticle Agglomerates under Mechanical Stress and its Effects on their Release into the Air

Originally published at : Thesis, University of Lausanne

Posted at the University of Lausanne Open Archive <http://serval.unil.ch>

Document URN : urn:nbn:ch:serval-BIB\_7F04C24BA8BF9

### **Droits d'auteur**

L'Université de Lausanne attire expressément l'attention des utilisateurs sur le fait que tous les documents publiés dans l'Archive SERVAL sont protégés par le droit d'auteur, conformément à la loi fédérale sur le droit d'auteur et les droits voisins (LDA). A ce titre, il est indispensable d'obtenir le consentement préalable de l'auteur et/ou de l'éditeur avant toute utilisation d'une oeuvre ou d'une partie d'une oeuvre ne relevant pas d'une utilisation à des fins personnelles au sens de la LDA (art. 19, al. 1 lettre a). A défaut, tout contrevenant s'expose aux sanctions prévues par cette loi. Nous déclinons toute responsabilité en la matière.

### **Copyright**

The University of Lausanne expressly draws the attention of users to the fact that all documents published in the SERVAL Archive are protected by copyright in accordance with federal law on copyright and similar rights (LDA). Accordingly it is indispensable to obtain prior consent from the author and/or publisher before any use of a work or part of a work for purposes other than personal use within the meaning of LDA (art. 19, para. 1 letter a). Failure to do so will expose offenders to the sanctions laid down by this law. We accept no liability in this respect.



**UNIL** | Université de Lausanne

Faculté de biologie  
et de médecine

**Institut Universitaire Romand de Santé au Travail (IST)**

**Stability of Nanoparticle Agglomerates under  
Mechanical Stress and its Effects on their Release  
into the Air**

**Thèse de doctorat ès sciences de la vie (PhD)**

présentée à la

Faculté de Biologie et de Médecine  
de l'Université de Lausanne

par

**Yaobo DING**

Master en Science et Génie des Matériaux  
Diplômé de l'Ecole Polytechnique Fédérale de Lausanne (EPFL), Suisse

**Jury**

Prof. Bernard Burnand, Président  
Dr. Michael Riediker, Directeur de thèse  
Prof. Gerhard Kasper, Expert  
Dr. Keld Alstrup Jensen, Expert  
Dr. Olivier Le Bihan, Expert

Lausanne 2015

# Imprimatur

Vu le rapport présenté par le jury d'examen, composé de

<i>Président · e</i>	Monsieur Prof. Bernard <b>Burnand</b>
<i>Directeur · rice de thèse</i>	Monsieur Dr Michael <b>Riediker</b>
<i>Experts · es</i>	Monsieur Prof. Gerhard <b>Kasper</b>
	Monsieur Dr Olivier <b>Le Bihan</b>
	Monsieur Dr Keld Alstrup <b>Jensen</b>

le Conseil de Faculté autorise l'impression de la thèse de

**Monsieur Yaobo Ding**

Master in Materials Science and Engineering de l' Ecole Polytechnique Fédérale  
de Lausanne

intitulée

**Stability of Nanoparticle Agglomerates under Mechanical Stress  
and its Effects on their release into the air**

Lausanne, le 15 décembre 2015

pour le Doyen  
de la Faculté de biologie et de médecine



Prof. Bernard Burnand

## **Abstract**

Occupational exposure to airborne engineered nanomaterials (ENMs) poses potential health risks to workers at nanotechnology workplaces. It is important to understand the release scenarios of nanoparticle aerosols in processes and activities associated with human exposure. The release mechanisms, including release rate and physicochemical properties of nanoparticles, determine their subsequent transport behaviors as well as biological hazard effects. The number size distribution of ENMs aerosols is one of the most important parameters influencing these processes. The mechanical stability of nanoparticle agglomerates, in turn, affects their size distributions. The deagglomeration potential of these agglomerates determines the possibilities of them to deform under external energy inputs, resulting in modified size distribution and number concentration which eventually alter their exposure risks. Environmental conditions, such as relative humidity, may play a role in the deagglomeration process due to effects such as adhesion by capillary condensation of moisture.

The general goal of this thesis was to assess the release scenarios of ENMs from workplace processes and activities. The sub-objectives include: 1. Investigate deagglomeration potential of nanoparticles under varied environmental conditions. 2. Investigate nano-objects release from ENM polymer composites; 3. Assess real-life ENM releases at workplaces.

Different laboratory aerosolization systems which featured distinct energy inputs in powder aerosolizations were compared. TiO<sub>2</sub> nanopowders with distinct surface hydrophilicity were tested. Scanning mobility particle sizers (SMPS), aerodynamic particle sizers (APS) and optical particle counters (OPC) were used to measure particle number concentration and size distribution. Transmission electron microscopes (TEM) were employed for morphological analysis of airborne particle samples. Aerosol characteristics (size distribution and number concentration) differed by different testing methods. The velocities of aerosolization air flow were used to estimate energy level in these systems, and the particle modal size were shown to be inversely proportional to this parameter. In general, the hydrophilic aerosol particles had larger diameters and lower numbers than their hydrophobic counterparts. However, this also depended on the testing methods. The air velocity was found to be an effective parameter to rank process energies in similar aerosolization systems.

A fluidized-bed system for testing deagglomeration potentials of airborne nanoparticle using critical orifices (exerting shear forces onto particles by pressure drop) and a humidifier, was developed. Its performance was compared to a similar setup from a partner institution. A variety of nanopowders with distinct surface coatings were tested. A broad range of energies and humidity conditions were used. A SMPS and an OPC were used to measure particle number concentration and size distribution. TEMs were employed for morphological analysis of airborne particle samples. Mean particle size decreased and number concentration increased when pressure drops were applied. Particle number fraction below 100 nm was increased, and those above 350 nm were reduced. Opposite observations were made under humid conditions, especially for small particles. Moreover, the humidity applied reduced the effects of pressure drop. The results suggest that deagglomeration of airborne nanoparticle agglomerates is possible under the energy ranges applied in the study. However, humid atmosphere may promote their agglomeration and enhance their stabilities, reducing release of nanoparticles into the environment. The system can be used for routine test of deagglomeration potentials of ENMs and to rank them. Such a ranking would facilitate prioritizing exposure and risk assessments based on the concern level of relevant ENMs.

An automatic drilling setup and a manual sawing setup were established to study nanoparticle release from different types of nanocomposites. Drilling speed and bit size were varied in the experiments. Particle size and number concentration were measured by a SMPS and diffusion size classifier miniatures (DISCmini). Nanofiller distributions in the raw composites and released particles were analyzed by scanning electron microscopes (SEM) and TEMs. The drilling tests released higher numbers of particles than the sawing did. Faster drilling speeds and larger drilling bit increased particle generation. The nanofillers did not alter release behaviors of the nanocomposites in the drilling experiments. However, sawing differed in the release levels between the composites and the blank samples. Moreover, polymer fumes were generated by the sawing heat. Most of the released particles were polymer matrix materials with nanofiller protrusions from the surface. The results emphasized the importance of process type and parameters in determining composite releases. Secondary emissions such as the polymer fumes call for the need of exposure and risk assessments for such scenarios.

A systematic literature review of ENM release in different industrial sectors and research laboratories was performed. Well defined information search strategies and templates were used to collect and store relevant data in this field. Release scenarios, such as aerosol particle size and number concentration, were compared for different activities. Availability of the contextual information that is relevant for human exposure estimation was assessed. It was found that exposure related data are not always available in current literature. Properties of released ENM aerosols seem to depend on the type of the activities. High energy processes tend to generate higher level of particle concentrations in smaller size ranges. This information derived from the review can be useful for determining the concern level of specific industrial processes for risk assessments in a tiered approach. For exposure assessment, the availability of exposure-relevant data can be improved by following a better data reporting practice.

## Résumé

L'exposition professionnelle aux nanomatériaux manufacturés dans l'air présente des risques potentiels pour la santé des travailleurs dans les secteurs de la nanotechnologie. Il est important de comprendre les scénarios de libération des aérosols de nanoparticules dans les processus et les activités associées à l'exposition humaine. Les mécanismes de libération, y compris les taux de libération et les propriétés physico-chimiques des nanoparticules, déterminent leurs comportements de transport ainsi que les effets biologiques néfastes. La distribution de taille des particules d'aérosols est l'un des paramètres les plus importants dans ces processus. La stabilité mécanique d'agglomérats de nanoparticules affecte leurs distributions de tailles. Les potentiels de désagglomération de ces agglomérats déterminent les possibilités de leur déformation sous énergies externes. Cela rend les changements possibles dans leur distribution de taille et de la concentration en nombre qui vont finalement modifier leurs risques d'exposition. Les conditions environnementales, telles que l'humidité relative, peuvent influencer les processus de désagglomération par l'adhérence de condensation capillaire de l'humidité.

L'objectif général de cette thèse était d'évaluer les scénarios de libération des nanomatériaux manufacturés des processus et activités sur le lieu de travail. Les sous-objectifs étaient les suivants: 1. Etudier les potentiels de désagglomération des nanoparticules dans des conditions environnementales variées. 2. Etudier la libération des nano-objets à partir de nanocomposites polymères; 3. Evaluer la libération de nanoparticules sur le lieu de travail dans des situations concrètes.

Nous avons comparé différents systèmes de laboratoire qui présentaient différents niveaux d'énergie dans l'aérosolisation des poudres. Des nanopoudres de  $\text{TiO}_2$  avec des hydrophilicités de surface distinctes ont été testées. Un spectromètre à mobilité électrique (SMPS), un spectromètre à mobilité aérodynamique (APS) et un spectromètre optique (OPC) ont été utilisés pour mesurer la concentration de particules et la distribution de taille des particules. La microscopie électronique à transmission (TEM) a été utilisée pour l'analyse morphologique d'échantillons de particules dans l'air. Les propriétés des aérosols (distribution de taille et concentration en nombre) étaient différentes suivant la méthode employée. Les vitesses des flux d'air d'aérosolisation ont été utilisées pour estimer le niveau d'énergie dans ces systèmes, et il a été montré que les tailles modales des particules étaient inversement proportionnelles à la vitesse

appliquée. En général, les particules hydrophiles ont des diamètres plus grands et des nombres inférieurs à ceux des particules hydrophobes. Toutefois, cela dépend aussi des méthodes utilisées. La vitesse de l'air peut donc être un paramètre efficace pour le classement de l'énergie des procédés pour des systèmes d'aérosolisation similaires.

Nous avons développé un système laboratoire pour tester les potentiels de désagglomération des nanoparticules dans l'air en utilisant des orifices critiques et un humidificateur. Sa performance a été comparée à un système similaire dans un institut partenaire. Une variété de nanopoudres différentes a été testée. Le niveau d'énergie appliquée et l'humidité ont été modifiés. Le SMPS et l'OPC ont été utilisés pour mesurer la concentration de particules et la distribution de la taille. Un TEM a été utilisé pour l'analyse morphologique d'échantillons de particules dans l'air. Le diamètre moyen des particules a diminué et la concentration en nombre s'est accrue lorsque des énergies externes ont été appliquées. Le nombre de particules inférieures à 100 nm a été augmenté, et celui au-dessus de 350 nm réduits. Les conditions humides ont faits exactement le contraire, en particulier pour les petites particules. En outre, ils ont réduits les effets de la différence de pression due à l'orifice. Les résultats suggèrent que la désagglomération d'agglomérats de nanoparticules dans l'air est possible dans la gamme d'énergie appliquée. Cependant, l'atmosphère humide peut favoriser leur agglomération et améliorer leurs stabilités en réduisant la libération de nanoparticules dans l'environnement. Nous proposons d'utiliser notre système pour le test de routine des potentiels de désagglomération des nanomatériaux manufacturés et de les classer. Un tel classement faciliterait la priorisation de l'exposition et du risque encouru en fonction du niveau d'ENM.

Un système de perçage automatique et un système de sciage manuel ont été développés pour étudier la libération de nanoparticules à partir de différents types de nanocomposites. La vitesse de perçage et taille de la mèche ont été modifiées dans les expériences. La distribution de taille des particules et leur concentration en nombre ont été mesurées par un SMPS et un *miniature diffusion size classifier* (DISCmini). Les distributions de nanoparticules dans les composites et les particules libérées ont été analysés par un TEM et un microscope électronique à balayage (SEM). Les tests de perçage ont libérés un plus grand nombre de particules que le sciage. Des vitesses de perçage plus rapide et les mèches plus grandes ont augmentés la génération de particules. Les charges de nanoparticules manufacturées dans les composites ne modifient pas leurs comportements de libération dans les expériences de perçage. Toutefois, le sciage

différencie les niveaux de libération entre les composites et les échantillons blancs. De plus, les vapeurs de polymères ont été générées par la chaleur de sciage. La plupart des particules libérées sont des polymères contenant des nanoparticules ou sur leurs surface. Les résultats ont souligné l'importance du type de processus et paramètres pour déterminer la libération de nanoparticules de composites. Les émissions secondaires telles que les fumées polymères appellent à la nécessité d'évaluations de l'exposition et de risque pour de tels scénarios.

Une revue systématique de la littérature sur le sujet de libérations de nanoparticules dans l'air dans les secteurs industriels et laboratoires de recherche a été effectuée. Des stratégies de recherche des informations pertinentes et de stockage ont été développées. Les mécanismes de libération, tels que la taille de particules d'aérosol et de leur concentration en nombre, ont été comparés pour différentes activités. La disponibilité de l'information contextuelle qui est pertinente pour l'estimation de l'exposition humaine a été évaluée. Il a été constaté que les données relatives à l'exposition ne sont pas toujours disponibles dans la littérature actuelle. Les propriétés des aérosols libérés semblent dépendre de la nature des activités. Des procédés à haute énergie ont tendance à générer des plus hauts niveaux de concentrations de particules dans les gammes de plus petite taille. Les résultats peuvent être utiles pour déterminer la priorité des procédés industriels pour l'évaluation les risques associés dans une approche à plusieurs niveaux. Pour l'évaluation de l'exposition, la disponibilité de l'information peut être améliorée par le développement d'une meilleure méthode de communication des données.

## 摘 要

职业性的接触工程纳米材料气溶胶对于在相关工作岗位的工人具有潜在的健康风险。对于在人为工业操作及过程中纳米颗粒气溶胶污染物的排放机制理解有待加强。包括排放率和纳米颗粒的物理化学性质在内的排放机制，决定了它们接下来的传输过程以及生物毒性。工程纳米材料气溶胶的粒径分布是影响这些过程的最重要的参数之一。其粒径分布又受到纳米颗粒聚集体力学稳定性的影响。这些聚集体的稳定性决定了它们在外部能量的作用下是否会解体并且导致粒径分布和浓度的改变，最终影响工人的暴露风险。环境条件，比如相对湿度，可能影响纳米颗粒聚集体的稳定性。

本论文的主要目标在于评估工业操作过程中纳米气溶胶的排放机制。次级目标包括：

1. 研究纳米气溶胶团聚颗粒在不同环境条件下解团聚的可能性。
2. 研究在纳米高分子复合机械操作中排放的气溶胶污染物。
3. 评估工作场所中纳米气溶胶的排放。

实验使用了不同能量水平的纳米粉体雾化系统对具有不同表面性质的二氧化钛纳米粉体进行测试，并利用扫描电迁移率粒径谱仪（SMPS），空气动力学粒径谱仪（APS），光学颗粒物粒径谱仪（OPC）和透射电镜（TEM）测量并分析粒子浓度，粒径分布和空气悬浮物样本的形态。实验发现系统产生的纳米气溶胶性质（粒径分布和浓度）随测试方法的不同而变化。雾化的能量水平可用气流速度来估测，并且气溶胶粒子平均尺寸和其成反比。疏水性气溶胶颗粒通常较亲水性颗粒大且浓度更低。实验结果表明在类似的粉体雾化系统中，雾化过程的能量水平可用气流速度进行有效分级。

实验开发出可用于碎化纳米气溶胶颗粒团聚体的流化床系统。系统使用一个临界流孔对粒子实施剪切作用。此外，系统环境的相对湿度可用一台整合的加湿器控制。此系统的

性能和合作研究所的一个类似系统作了比较。实验在较大能量和湿度范围下对具有不同表面性质的纳米粉体气溶胶进行了测试，并利用 SMPS，光学颗粒物粒径谱仪 ( OPC ) 和透射电镜测量并分析气溶胶浓度及粒径分布的改变和空气悬浮粒子的形态。剪切作用导致气溶胶颗粒的平均尺寸减小，浓度增加。小于 100 纳米的粒子浓度增加，大于 350 纳米的粒子浓度降低。但是，相对湿度的增加对其产生了相反的影响，其作用对直径较小的颗粒尤其显著。此外，相对潮湿的环境还减小了剪切力造成的粒子尺寸改变的程度。实验结果表明纳米气溶胶颗粒聚集体在一定的外部能量下可被打碎。湿度在这一过程中可促进他们的团聚和加其强稳定性，并降低浓度。此系统可被用于纳米气溶胶颗粒团聚体稳定性的常规测试和分级。其结果有助于区分对于不同材料风险评估的优先次序。

实验搭建了自动钻孔和手动切割平台用于研究从不同种类高分子纳米复合物中排放出的空气污染物，并使用钻头速度和尺寸作为实验变量。实验利用 SMPS，便携式扩散粒径分级谱仪，扫描电镜和透射电镜监测并分析排放颗粒的尺寸，浓度以及形态。在实验中，钻孔操作相较于切割操作排放出更高浓度的气溶胶污染物。更快的钻头速度和更大的钻头尺寸提高了排放水平。在钻孔测试中，含有纳米填充物的样本和空白样本的排放水平并无明显区别。但是，切割实验造成纳米复合物不同的排放机制，并且发现操作产生的热量可导致高分子挥发物的释放。实验中产生的大部分气溶胶颗粒为高分子基底材料，并且在表面可观察到纳米填充物突起。实验结果表明操作种类和条件对于纳米复合物的气溶胶污染物排放机制具有重要影响。此外，有必要对类似机械操作产生的次级产物 ( 例如高分子挥发物 ) 进行人体健康风险的评估。

本论文还对工业和科研环境中纳米气溶胶污染物的排放进行了系统的文献综述。综述评估了文献中有关工人暴露风险背景信息的可用性，并比较了在不同工业操作过程中污染物的排放机制（气溶胶粒径和浓度）。结果表明文献通常不包括此类背景信息。释放的纳米颗粒气溶胶的性质取决于操作种类。高能过程更易产生高浓度且平均粒径小的气溶胶颗粒。此结果有助于对工业过程的污染物排放水平和风险程度进行分级评估。此外，可通过完善与工人暴露风险相关的背景信息的搜集过程来改进评估质量。

# Table of Contents

1. Introduction .....	12
1.1 Engineered nanomaterials (ENMs) and their applications.....	12
1.2 Hazard.....	12
1.3 Exposure.....	13
1.4 Concern-driven approaches.....	13
1.5 Release characterization.....	15
2. Objectives.....	16
2.1 Investigation of the deagglomeration potentials of ENM agglomerates.....	16
2.2 Investigation of nanoparticle release mechanisms in nanocomposites processing.....	17
2.3 Assessment of real-world situation of ENM releases .....	17
3. Methods .....	17
3.1 Aerosolization and deagglomeration testing of nanopowder particles .....	18
3.2 Automatic drilling and manual sawing treatments on ENM composites .....	19
3.3 Systematic review of ENMs release and exposure studies.....	19
4. Development of an aerosolization and deagglomeration system (publication 1).....	20
5. Comparison of different aerosolization methods (publication 2).....	39
6. Deagglomeration testing of airborne nanoparticles (publication 3).....	62
7. Nanoparticles releases from nanocomposites (publication 4).....	87
8. ENMs releases in industry and research environments (publication 5).....	112
9. Summary of results.....	139
10. Discussion and conclusions .....	141
11. References .....	145
12. List of publications .....	159
13. Acknowledgement .....	162
14. CV .....	164

# 1. INTRODUCTION

## 1.1 Engineered nanomaterials (ENMs) and their applications

ENMs are man-made substances with special functional properties related to diameter, shape and surface chemistry. When the size of the system is reduced to the nano-range certain phenomena become significant, which is not observed in macro-scale structures. For example, the electronic properties of solid materials are altered, exhibiting the so called “quantum size effect” [1]. Other physicochemical properties of materials, such as mechanical, electrical, optical behaviors and chemical reactivity, are also modified compared to those of macroscopic structures. Strength of nano-metals are improved by limiting the dislocation motion from decreased grain size [2]. Mechanical performance of carbon nanotubes/fibers-polymer composites are greatly enhanced by the cross-linking effect of the fillers’ long and hollow structures [3]. The dielectric permittivity and resistivity of nanoparticle-polymer composites depends on the filler particle size and concentration, which can be attributed to changes in matrix amorphous content, porosity and nanoparticle polarizability [4]. Highly dense nanoceramics without large pores in their structures become optically transparent [5]. Increase of surface area to volume or to mass ratio enhances the catalyst reactivity in chemical reactions [6] .

Thanks to these advantageous properties, ENMs have been largely used in various technological applications as aerosols, colloids or powders. Schmid and Riediker [7, 8] initiated comprehensive surveys in Swiss industry on the uses of ENMs, and found that nanoparticles are used in various manufacturing sectors such as cosmetics, surface coatings, paints, textiles, pharmaceutical products, food and food packaging.  $\text{TiO}_2$  and  $\text{ZnO}$  are extensively used in sunscreens to protect the skin from UV damage, by efficiently reflecting light and absorbing the UV content [9]. The same principles apply to self-cleaning surfaces made by  $\text{TiO}_2$  coatings which promote photo-catalytic degradation of organic dirt and photo-induced superhydrophilicity [10]. Silver nanoparticles can provide anti-microbial properties in food packaging and textiles [11, 12].

## 1.2 Hazard

The special physical and chemical properties of ENMs may exert different toxicological effects than their bulk counterparts [13]. Smaller diameters of nanoparticles greatly increase their unit surface area which may relate to stronger biological interactions per mass unit [14, 15]. The

solubility of nanoparticles may also be higher due to their small size profiles or agglomeration tendency, which can alter their toxicity profiles [16]. Furthermore, high aspect ratio nanomaterials, such as nanotubes and fibers, make it more difficult for human bodies to clear them [17, 18]. Particle surface charges were found to modify their biological effects, through altered cellular uptakes or cell apoptosis [19-21]. Toxicity of nanoparticles can be characterized in different dose metrics, such as mass, number and surface area [22]. The mass concentration has been found to be an ineffective indicator for prediction of toxicity. Instead, particle number and surface area have been shown to be better predictors for lung responses for different particle sizes [23, 24]. Agglomeration level of airborne particles influences the deposition efficiency of ENMs in human respiratory tracts, resulting changes in deposited dose per unit mass of exposure. [25]. In general, the deposition fraction increases with decreased particle size, and the highest value locate in nano-range for the main target which is the alveolar region. Once deposited in human lungs, ENMs have been found to be associated with advert effects such as inflammation and reactive oxygen species generation [26-29]. In addition to lung cell toxicity, translocation of nanoparticles across the air-blood barriers throughout systemic circulation into secondary organs, including brain, heart, kidney and liver has been observed [30-35].

### **1.3 Exposure**

Potentials of human exposure to ENMs have been investigated for various industrial processing and activities. These include production including synthesis phase and product collection [36-38]; handling such as weighing, mixing, transferring, sonication [39-43]; spraying [44, 45]; bagging and packaging [46-48]; mechanical treatments of nanocomposites [49-51]. The likeliness of exposure is low if no or minor release of ENMs at source is detected in the first place, or engineering controls and personal protection are well implemented. On the contrary, high release of ENMs from a process without effective control measures resulted in significantly increased immission potentials for the workers directly involved.

### **1.4 Concern-driven risk management approaches**

As the production and uses of ENMs rapidly increase, human risks (worker and consumer) and environmental risks of ENMs have been of concern in the scientific community. An European Union definition of Manufactured Nanomaterials was brought forward which facilitates risk management and governance. The EU definition of ENMs is “any intentionally manufactured

material, containing particles, in an unbound state or as an aggregate or as an agglomerate and where, for 50 % or more of the particles in the number size distribution, one or more external dimensions is in the size range 1 nm to 100 nm.” [52]. The definition is flexible in the number size distribution fraction of 50% particles, and takes into account also carbon nanotubes, graphene flakes and fullerenes with at least one dimension below 1 nm.

Human risk assessment for hazardous chemicals and materials is composed of two elements: exposure and hazard evaluations [53]. Hazard assessment is to evaluate the nature and severity of biological effects associated with ENMs. Occupational exposure assessment determines worker’s contact with ENMs in occupational settings, typically via inhalation or skin deposition of nanoparticle aerosols. Exposure is possible only when release of ENMs occurs and are subsequently transmitted to human receptors. Risk characterizations combine the information derived from these two parts to facilitate decision-making in risk managements and communications (Figure 1). Once the risks are identified, interventional measures could be implemented, including exposure monitoring and controls, workers health surveillance and safety trainings.

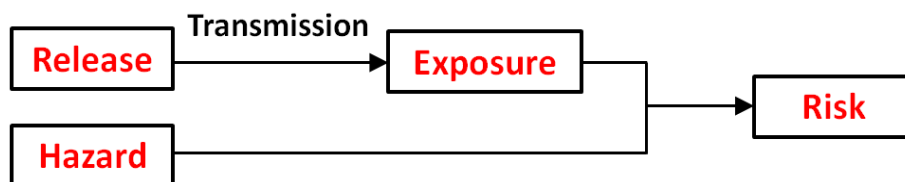


Figure 1 Elements and their relations in risk assessment

For hazard assessment, it is almost impossible to test all types of ENMs in all relevant exposure scenarios. A prominent characteristic of nanomaterials is that during their entire life cycles stages they may change in characteristics, transform and/or interact with the surrounding environments, which can cause e.g., agglomeration or aggregation, surface adsorption of environmental substances or dissolution. In addition, different forms of nanomaterials, such as powder or liquid droplets exposure scenarios may link to distinct forms of nanomaterials. Therefore, priorities should be given to certain ENMs of high concern for potential human toxicities taking into account realistic exposure scenarios.

In order to save unnecessary costs and efforts for assessment of low risk scenarios, a concern-driven approach was especially developed in the EU FP7 MARINA project [54]. This approach

has a tiered structure starting from identifying relevant ENMs in the first step to advanced toxicological testing in the final phase. In tier 1, ENMs of interest are first identified by nanomaterial definition, and then by toxicity-related physicochemical properties as well as by their uses and availabilities for human exposure. In tier 2, defined ENMs of initial concern will go through basic toxicity testing in four toxicity domains: biokinetics, local effects at the point of entry or contact, genotoxicity and short term toxicity (eg. inflammation, cytotoxicity). Tier 3 aims at specific toxicological testing such as in vivo genotoxicity or carcinogenicity, based on the information provided in the first two tiers. For exposure and risk assessment, similar tiered approaches have been also used in development of well structured concern-driven strategies. In a tiered risk assessment, uncertainties both on the toxicity part and the exposure part are assessed. If the remaining uncertainties are high on both, then the next tier would be continued in both directions. If only one of these two part has unaddressed uncertainty, then the tier 2 is conducted only for that part but not for the other. The assessment proceeds along tiers until uncertainty is minimized.

### **1.5 Release characterization**

Determining release mechanisms of hazardous substances is an important step in exposure assessment. In occupational settings, nanoparticles can be released from different forms of materials, namely powder, liquid, and solid matrix that contains nanofillers (e.g., nanocomposites). Nanomaterial powders can be aerosolized during handling and generate airborne particles that pose inhalation exposure risks. The resulting aerosols may consist of primary particles or agglomerates, depending on the process characteristics during the aerosolization (e.g., energy input type and level, duration, material quantity), as well as agglomeration status of the raw materials and deagglomeration of particles in the airborne state. Different types of inter-particle force can be considered, such as van der Waals force [55], electrostatic [56] and capillary force from moisture contents [57]. The shear force inducing deagglomeration could be from the drag of air current on the agglomerates [58]. Nanoparticles can also be released in the form of mist from suspension of low volatile liquids [59], or contained in liquid droplets generated in spraying processes [60]. On the other hand, mechanical treatments destruct nanocomposite matrix and may detach filler particles during the operations. The types of process include drilling, sawing, sanding, abrasion, thermal degradation, UV weathering, and so

on. The process parameters and matrix polymer materials were shown to influence the release of nanoscale particles [61].

Release evaluation is linked to exposure assessment in multiple ways. Characterization of released nanoparticles provide information on material properties such as size, concentration and surface functions, which informs about the hazardous level of released ENMs as well as transmission behaviors which is related to subsequent exposure. It also helps to determine the necessary degree of precaution if exposure and risk levels are uncertain. Release simulation studies use similar conditions (energy type and level, material usage etc.) as those in industrial environments, striving to predict release mechanisms and resulted exposure in real-life. In task-based activities at workplaces, personal exposure may occur in several processes featuring varied release scenarios. Thus, the resulting exposure may be considered as mixed effects from different processes. Take an example of ENMs synthesis, raw materials preparation, furnace operations, product collection and cleaning are all possible activities releasing hazardous nanoparticles. Understanding the release, the subsequent transmission and potential transformation mechanisms in these processes facilitate a decent and comprehensive exposure assessment. On the other hand, a single activity type may trigger different release scenarios, eg. thermal cutting of polymer based nanocomposites may release polymer fume by process heat in addition to matrix materials or filler particles. [62]. In addition, determination of release potential from various industrial processes and ENMs life cycle stages informs policy makers and safety inspectors about the most relevant scenarios that need to be monitored and controlled regarding to worker exposure.

Overall, release characterizations help to understand what the risks might be and how they can be better managed. It is the first step along the risk assessment chain (Figure 1). Release studies facilitate safety design at the source by studying parameters that affect release. As a result, process or material modification can be envisaged towards a lower release possibility.

## **2. OBJECTIVES**

### **2.1 Investigation of the deagglomeration potentials of ENM agglomerates**

Agglomeration and binding strength of aerosol particles influence their transport behavior in the air. Deagglomeration has been shown to occur in human respiratory system when agglomerated

nanoparticles pass through the larynx, where shear forces are induced on the particles due to change of flow direction and speed [63, 64]. Thus, deagglomeration may take place in various industrial activities associated with a range of different energy levels. Once this happens, the aerosol properties are altered, which modifies the subsequent exposure scenario. Environmental condition such as the relative humidity may play a role in this process. The study is to investigate how stable the agglomerates are in the air (how strong the primary particles are bound together), and how humidity conditions influence the deagglomeration process under external energy inputs.

## **2.2 Investigation of nanoparticle release mechanisms in nanocomposites processing**

Incorporated nanofiller particles in nanocomposites may be detached under certain conditions during mechanical treatments, depending on how external energy is applied, the distribution of the fillers in the composite, and destruction level of the matrix. The study aims to determine what the material parameters are that influence release characteristics including particle type, size and concentration. The second goal is to compare the potential differences of the release scenarios from distinct treatment types as well as varied filler types. The derived information is valuable for subsequent exposure assessment, in informing about the possibility of release, potential properties of released particles and relevance of different treatments.

## **2.3 Assessment of real-world situation of ENM releases**

Different industrial treatments and processes feature varied energy applications on ENMs suspensions, powders, raw materials or finalized products. This may release nanoparticle aerosols with largely differed profiles (number/mass concentration, size distribution etc.) into the working environment. The aim of this study is to compare various industrial and laboratory activities associated with ENMs in their potentials to release nanoparticles (likeliness, release rate), and to see whether release characteristics (release rate, aerosol type, size and concentration) can be generalized across different types of treatments (eg. production, intermediate processing and manual handling). The results will be useful in informing about the most relevant activity types for exposure assessment, as well as about materials profiles for risk assessment.

# **3. METHODS**

We compared different types of aerosolization and deagglomeration methods in their performances under varied humidity conditions for nanomaterials with distinct surface properties. A range of aerodynamic shears were applied to the ENM particles in studying their stabilities during their aerosolization and when they become airborne. Online aerosol monitoring equipments were used to measure aerosol properties and offline analysis of particle morphologies were performed using electron microscopes. Laboratory setups were developed for mechanical treatments on nanocomposites in order to investigate relevant release mechanisms. Influences of nanofillers, process type and parameters on release were studied. Lastly we performed a systematic literature review on release scenarios in industrial and research departments. Well developed search strategies and data processing methods were used to ensure a good quality of the review.

### **3.1 Aerosolization and deagglomeration testing of nanopowder particles**

In order to investigate the likeliness of deagglomeration for airborne nanoparticles, an aerosolization system that generates stable aerosols and an effective way of applying deformation energies onto the aerosolized particles are needed. A funnel-based aerosol generator was developed and critical orifices were used to apply varied external shear forces onto aerosols (see also chapter 4) [65]. The aerosolization method resembled a fluidized bed, using only small quantities of materials (min. 200 mg) and was able to generate aerosols with a stable size distribution and number concentration over a sufficiently long period for samplings (min. 30 minutes, max. up to 2 hours, with 250 mg powder). The shear force level was adjusted by tuning the pressure drop across the orifice which was controlled by the air flow rate passing through. The effectiveness of critical orifices on deagglomerating micro-sized [66] and nano-scale particles [67] was shown previously. Conditioned air can be introduced to mix with the main aerosol flow before it goes through the orifice, to modify the relative humidity of the environment. By comparing the particle mean size and total particle generation rate (normalized to total air flow rate) between the shear force conditions and the reference condition (orifice not installed), the tendency to deagglomerate was analyzed for different types of material.

The comparability of aerosol characteristics generated from different aerosolization systems may not be straightforward, due to varied working principles of the methods [68]. A better understanding of how these parameters influence the aerosolization process is needed. Four

aerosol generation and deagglomeration setups, featuring different energy ranges and material usages, were used to test common nanomaterials under basic systemic parameters. Particle number concentration and size distribution were compared across the systems. The robustness of the setups and reproducibility of the results were analyzed. In a further step, the two setups incorporating critical orifices were compared for their performances in deagglomeration testing under varied humidity. How shear force and humidity conditions affected the deagglomeration process of materials with different surface coatings was explored.

### **3.2 Automatic drilling and manual sawing treatments on ENM composites**

Potential release of nanoparticle fillers from mechanical treatments of nanocomposites and subsequent human exposure have been investigated in various studies [69-74]. However, few studies directly compared the possibly different release scenarios from distinct processes, especially between drilling and sawing treatments. Automatic drilling and manual sawing setups were established to test the difference in nanoparticle release from nanocomposites with three different types of nanofillers. Process parameters in the drilling treatment such as drill head dimension and drilling speed were varied to study the influences of these factors. The manual sawing, on the other hand, featured a relatively lower energy input yet potentially different destruction mechanism than the drilling process. Number concentration and mean size of released airborne particles were monitored during the treatments. Morphological analysis was performed to determine whether nanofiller materials were released.

### **3.3 Systematic review of ENMs release and exposure studies**

In addition to simulation studies described previously, real-life data on ENMs release were analyzed from existing scientific literature and reports. A systematic review on studies addressing release and exposure of airborne nanoparticles from occupational settings in the entire life cycle stage of ENMs was conducted. Search terms were determined from frequently used keywords, and the literature searches were performed in comprehensive online databases such as ``Pubmed`` and ``Sciencedirect``. In addition, information was collected from collaborative institutes in their ongoing projects or archived literature. Gathered data were stored in categorized library containing release- and exposure-specific information. The release data were compared across different activities to reveal the degree of process-dependency of ENMs release.

#### **4. DEVELOPMENT OF AN AEROSOLIZATION AND DEAGGLOMERATION SYSTEM**

##### Publication 1

### **A System to Assess the Stability of Airborne Nanoparticle Agglomerates under Aerodynamic Shear**

Yaobo Ding<sup>1</sup>, Michael Riediker<sup>1,2</sup>

<sup>1</sup>*Institute for Work and Health (IST), Universities of Lausanne and Geneva, Route de la Corniche 2, CH-1066 Epalinges, Switzerland*

<sup>2</sup>*SAFENANO, IOM Singapore, Singapore, 048622, Singapore*

*Corresponding author: Michael Riediker, Tel.: +41 21 314 74 53; fax: +41 21 314 74 30.*

*E-mail address: Michael.Riediker@alumni.ethz.ch*

*\*Published in *Journal of Aerosol Science* 2015, 88(0): p. 98-108. Ding, Y. and M. Riediker, A system to assess the stability of airborne nanoparticle agglomerates under aerodynamic shear. [doi:10.1016/j.jaerosci.2015.06.001](https://doi.org/10.1016/j.jaerosci.2015.06.001)*

## **ABSTRACT**

Stability of airborne nanoparticle agglomerates is important for occupational exposure and risk assessment in determining particle size distribution of nanomaterials. In this study, we developed an integrated method to test the stability of aerosols created using different types of nanomaterials. An aerosolization method, that resembles an industrial fluidized bed process, was used to aerosolize dry nanopowders. We produced aerosols with stable particle number concentrations and size distributions, which was important for the characterization of the aerosols' properties. Next, in order to test their potential for deagglomeration, a critical orifice was used to apply a range of shear forces to them. With increasing shear force, the mean particle size of tested aerosols became smaller, whereas the total number of particles generated grew. Moreover, the fraction of particles in the lower size range increased, and the fraction in the upper size range decreased. The reproducibility and repeatability of the results were good. Transmission electron microscopy imaging showed that most of the nanoparticles were still agglomerated after passing through the orifice. However, primary particle geometry was very different. These results are encouraging for the use of our system for routine tests of the deagglomeration potential of nanomaterials. Furthermore, the particle concentrations and small quantities of raw materials used suggested that our system might also be able to serve as an alternative method to test dustiness in existing processes.

## **INTRODUCTION**

Increasing numbers of products based on nanotechnology are leading to an increasing potential for human exposure to nanomaterials in the workplace. Workers can be exposed to nanoparticles during manufacturing processes, use of products, transport, storage or waste treatment [46, 75, 76]. The inhalation of nanomaterials poses potential health risks [77, 78]. Particle sizes and their state of agglomeration determine where they deposit in the lung structure [79] [80]. The size of agglomerates may also influence toxicological mechanisms [81]. Furthermore, nanoparticles deposited in lungs could by-pass their defense system and enter the circulation system, which could adversely affect the cardiovascular system [17, 34]. Information on the particle size distributions of nanomaterials is, therefore, important for assessing the deposition and likelihood of translocation across biological barriers.

The stability of nanomaterial agglomerates is another important material parameter in modeling nanomaterial release and associated human exposure, since it influences the particle size distribution of aerosols during their transport. Most of the industrially important nanomaterials are initially produced in the form of powders. Dust from powders can easily enter the airborne phase as single particles, aggregates, or agglomerates. The size of the agglomerates, however, is often outside the nano-range and can reach from several hundred nanometers to micrometers in diameter [82]. The mechanisms of particle agglomeration, as summarized by Schneider et Jensen. [56], include physical interlock (rough surface, entangled surface shapes, or chain-like, branched structure), electric forces (Van der Waal, conductive/non-conductive), magnetic forces (ferromagnetic, induced magnetic) and soft bridging (sticky surface, liquid film, organic functional groups). Previous studies reported that the deagglomeration of such submicron clusters is dependent on the energy present in the process from which they are released and the turbulence of their transport in the air [83, 84]. Such processes have also been shown to release primary particles or smaller, nano-sized agglomerates [85, 86].

Agglomeration strength can be studied directly, by measuring the binding force between individual particles, or indirectly, by triggering deagglomeration using external forces such as impaction or shear. Binding energy between primary particles was studied using atomic force microscopy [87]. In the inertial impaction method, nanoparticle (NP) agglomerates collided with a substrate at high velocities [85]. By subsequently analyzing transmission electron microscopy (TEM) images of the agglomerates, their degree of fragmentation was determined as a function of their impact velocity. The aerosol generation methods in their study included spark discharge generation and flame synthesis. For silver NPs, the degree of fragmentation increased as collision velocity increased, but decreased with smaller primary particle size. Another fragmentation method is the application of shear-forces in the air by forcing the agglomerate aerosol through a critical orifice. Originally, this effect was described for micrometer-sized particles [66]. Compact particles were effectively separated from each other in the turbulent airflow conditions created by a large drop in pressure. A previous study described the deagglomeration of nano-sized agglomerates [86]. The overpressure used to create different shear forces stayed below or equal to 140 kPa. The mean particle size of the materials tested decreased as the overpressure was increased; this was interpreted as deagglomeration.

Two key components are needed to investigate the stability of NP aerosols with regards to changes in their size and numbers: an aerosolization system, and a means of applying energy to the airborne particles so as to test their stability, as described above. Ideally, the aerosolization system should be able to produce an aerosol with stable particle concentration and size distribution for a reasonably long time. Furthermore, it should only require the use of small amounts of material so that even expensive, novel materials can be tested. Different aerosolization methods exist, such as the continuous drop method [88], the rotating drum method [68, 89], the vortex shaker method [90], the magnetic stirrer setup [86] and the stirred fluidization system [91]. These systems can produce different particle number concentrations by controlling such experimental parameters as the feed rate, rotation speed, or shaking frequency. However, these setups also have some disadvantages. Aerosol stability is a key problem, as the few published time-series graphs for these systems attest [90]. Furthermore, the amount of material needed for the continuous drop method (500 grams, EN15051), the rotating drum method (35 cm<sup>3</sup>, EN15051) [92] and the stirred fluidization method (200 g) makes these tests too expensive to be conducted for some nanomaterials. Recently, a modified rotating drum method based on a downscaled version of the EN 15051 rotating drum was developed, which uses much less powder (6 g) per test [68]. Other aerosolization systems which employ relatively lower amount of raw material include the Venturi dustiness testing device [93] and the low-mass dustiness tester that simulates the powder falling process [94]. The powder quantities used in these two methods are 10 mg and 15 mg, respectively. Finally, the friction in the magnetic stirrer setup can create static charges during aerosolization that have the potential to alter an aerosol's state of agglomeration.

To overcome the shortcomings of the traditional systems to investigate powder aerosolization process, we turned to the fluidized bed system—an aerosolization concept commonly used in modern powder technology and known for its simple, easily controlled operational characteristics [95]. Until now, fluidized bed systems were used mostly with powders composed of micrometer-sized particles. In the present study, a process closely based on the fluidized bed concept was established to create stable aerosols from nanopowders. An orifice-based approach was then used to study the deagglomeration potential of airborne nanomaterials using a wide range of air turbulence levels induced by the pressure drop across the critical orifice. Different

types of materials were tested to investigate the influence of such characteristics as their composition, surface coating, primary particle size, and shape.

## MATERIALS AND METHODS

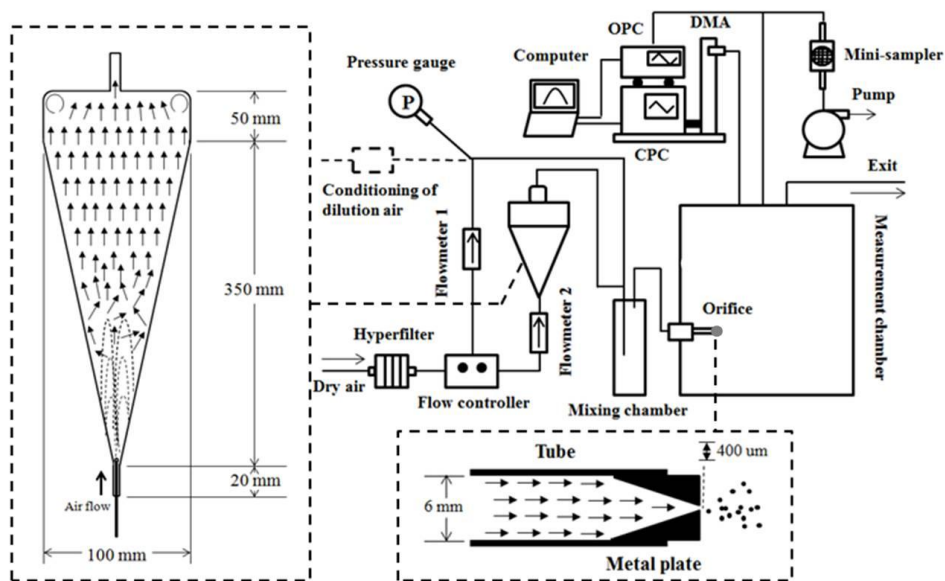


Fig. 1. Schematic diagram of the test system with magnification of the aerosolization device (left part) and the critical orifice (bottom part).

An integrated system was developed, composed of an aerosolization device, transport tubing, a deagglomeration orifice, and a measurement chamber (Fig. 1). A special glass funnel was used to activate dry powders. The relatively thick funnel wall (2–3 mm) was designed to resist pressure differences of up to 400 kPa. Before the start of the test, the funnel was filled with dry powder via the top opening. An airflow is then passed through a nozzle (2.1 mm diameter) at the bottom of the funnel to aerosolize the material and create a single-jet fluidized bed by which aerosols are carried towards the top of the funnel. Nozzles of different diameters can be used to modify the formation of the air jet. During the aerosolization process, the powder accelerates through the center of the lower part of the funnel and then flows back down along the wall. The rate of airflow is between 0.3–1.0 L/min, which creates air speeds from 1.44 to 4.81 m/s at the bottom opening. This airflow generates turbulent movements in the powder and ensures a vigorous aerosolization process. In the top part of the funnel, the airflow becomes laminar, with a Reynolds number from 7.4 (0.3 L/min) to 24.7 (1.0 L/min). In this laminar flow, particles with a

settling velocity lower than the vertical upward airflow velocity will eventually escape the funnel through the top opening. The aerodynamic cut-off diameters, calculated for particles made of different materials, ranged from 2 to 5  $\mu\text{m}$ , with the airflows 0.3 – 1.0 L/min. The calculations were based on the densities of the bulk materials; thus the actual diameters of the particle agglomerates emitted would be slightly larger when effective densities and shape are taken into account. The particles emitted are subsequently transported along carbon-doped conductive tubing (~ 50 cm, Milian S.A.) into a mixing chamber (1 L) and are then diluted with particle-free air to adjust the total volume of airflow. Conditioned air, with different relative humidity, can also be added to the aerosol flow during this phase, in order to study how humidity influences aerosol stability.

The air from the aerosolization system is guided to the deagglomeration orifice, through which the aerosols flow into the measurement chamber. An orifice of 400  $\mu\text{m}$  diameter was used to apply shear forces to the particles. The orifice used in the present study features a transition zone in which the airflow gradually accelerates and concentrates toward the center. Due to the restriction of the orifice, upstream pressure is higher than downstream pressure. Once upstream pressure exceeds twice downstream pressure, the system reaches a condition of choked flow during which the volumic flow rate cannot be increased, even if the upstream pressure is increased. Under this condition, the air velocity at the orifice equals that of sound. In the present study, the pressure in the measurement chamber was kept at one atmosphere by a one-way valve for the overflow of air that was not used by the measurement devices. The pressure difference across the orifice is controlled by managing the upstream pressure. The turbulence level of the airflow inside the critical orifice, which can be indicated by the Reynolds number ( $Re$ ), increases as upstream pressure increases (Hinds 1982, 2-41) [58]. Such a turbulent airflow can already trigger some deagglomeration of loosely bonded agglomerates. Even larger stress is experienced by the aerosol particles when they exit the critical orifice at high velocities, where the turbulent movements and drag forces induced as they encounter the surrounding still air cause further fragmentation of the agglomerates, as reported by [96] who had studied these processes in a system consisting of a transporting tube and an expansion zone with micro-sized  $\text{TiO}_2$  aerosol particles.

The number-size distribution of the aerosols in the measurement chamber (12 L) was assessed using a scanning mobility particle sizer (SMPS, GRIMM, 11.1–1083.3 nm); set to fast mode, each scan takes about 3.5 minutes. The sampling flow rate was set to 0.3 L/min. An optical particle counter (OPC, GRIMM, 0.25–32  $\mu\text{m}$ ) was also used to characterize large particles. The spectrometer scanned once every second and the sampling rate was 1 L/min. Particle morphology was assessed by collecting particles, using a mini-sampler (ECOMESURE, Janvry, France), directly onto TEM grids (200 mesh, copper, Formvar/Carbon) coated with a thin carbon film. The sampling rate was set at 0.3 L/min. Sampling time was 5–15 mins, depending on the aerosol particle number concentration. The TEM grids were subsequently analyzed using a transmission electron microscope (TEM, CM100, H.T. 80kV, Philips, Eindhoven, Netherlands).

The system's total length of transport tubing was kept as short as possible to avoid particle loss. The tube connecting the funnel to the mixing chamber and on to the measurement chamber was about 1 m, and the horizontal portion of the tube was less than 50 cm. The SMPS and the OPC/mini-sampler tubes were each 1 m long. The tubes' inner diameter was 6 mm. The airflow rates used in the tests were 5 L/min or less. The flow Re number at the maximum flow rate was 1172.6, indicating a laminar flow process. Under laminar flow conditions, particle penetration efficiency under gravitational settling calculated for 5  $\mu\text{m}$ , 1  $\mu\text{m}$ , and 0.1  $\mu\text{m}$  diameter  $\text{SiO}_2$  particles are 94%, 99.7%, and 99.9%, respectively (Baron & Willeke 2011, 6-49, 6-50)[97]. For small  $\text{SiO}_2$  particles, the penetration rates under diffusion loss are 90.9%, 96.1%, 98.7%, and 99.4%, for 10 nm, 20 nm, 50 nm, and 100 nm NPs, respectively (Hinds 1982) [58]. These results are very similar for other materials of a variety of densities.

Our experiments used upstream pressure conditions of 100, 200, 300, and 400 kPa in order to apply different shear force levels to the aerosols. A pressure of 100 kPa was used as the reference condition, and the critical orifice was not installed. At this pressure, the aerosol passed through a normal tube outlet into the measurement chamber. Airflow rates of 0.3–1.0 L/min were used to activate the different dry nano-powders in order to achieve similar aerosolization levels as under the reference condition pressure. At high pressures, the volumic flow rate was increased to maintain a constant level of aerosolization. The dilution flow rate was precisely tuned to achieve the required upstream pressure. Prior to tests, filtered clean air (relative humidity < 10%) was used to flush the system until the background particle concentration in the measurement chamber

was below  $10 \text{ p/cm}^3$  (SMPS). Each test used  $250 \pm 10$  mg of powder. The materials tested are listed in Table 1. All the powders were provided by the European Commission's Joint Research Centre in Ispra, Italy, except for  $\text{SiO}_2$  II, which is a commercially available product (AEROSIL R974). Particles of  $\text{ZnO}$  II were coated with a layer of triethoxycaprylylsilane; all other powders were uncoated. The powders were stored in sealed glass bottles before use. Powder weights were measured using an analytical balance (type AL-311,  $\pm 0.1$  mg, American Weigh Scales, Inc.) placed inside a ventilation hood. In the aerosolization process, the activation flow was increased gradually to produce a smooth fluidized bed formation. Dilution flow was introduced subsequently. Immediately after the flows were set, the SMPS and OPC were started simultaneously to monitor the state of the aerosol. Once the particle number and size in the measurement chamber reached a steady state (normally after 30 mins aerosolization), the mini-sampler's pump was started in order to collect airborne samples onto the TEM grids. In this steady state, 10 readings were taken from SMPS scans and from the OPC to calculate averages. A complete test usually lasted 1.5–2 h.

Table 1. Physical and chemical properties of the tested powders.

Material	Ref.	Composition	Primary size, nm	Surface coating	Surface area, $\text{m}^2/\text{g}$	Crystal structure
$\text{SiO}_2$ I	NM200	96.5% $\text{SiO}_2$	20	Hydrophilic	230	Amorphous
$\text{SiO}_2$ II	R974	$\geq 99.8\%$ $\text{SiO}_2$	12	Hydrophobic	$170 \pm 20$	Precipitated
$\text{ZnO}$ I	NM110	$> 99\%$ $\text{ZnO}$	42	Uncoated	13	Zincite (52%) /amorphous (48%)
$\text{ZnO}$ II	NM111	96%–99% $\text{ZnO}$	34	Triethoxycaprylylsilane	16	Zincite (34%) /amorphous (66%)
$\text{Ce(IV)O}_2$ I	NM211	90%–100% $\text{CeO}_2$	10	Uncoated	66	Precipitated
$\text{Ce(IV)O}_2$ II	NM212	99.5% $\text{CeO}_2$	33	Uncoated	28	Precipitated

In order to analyze any changes in size distribution in the aerosols, the relative number size distributions were calculated from the raw SMPS data. This allowed an easier comparison of size spectra with different particle concentration levels. Particle number fractions in different size ranges were calculated to quantify the changes in particle diameter. Particle generation rates under varied pressure conditions were also compared. Analysis of variance (ANOVA) was performed, using Stata software (Stata CorpLP, Texas, USA), to compare the particle size distributions obtained under different pressure conditions.

## RESULTS AND DISCUSSION

### Aerosolization

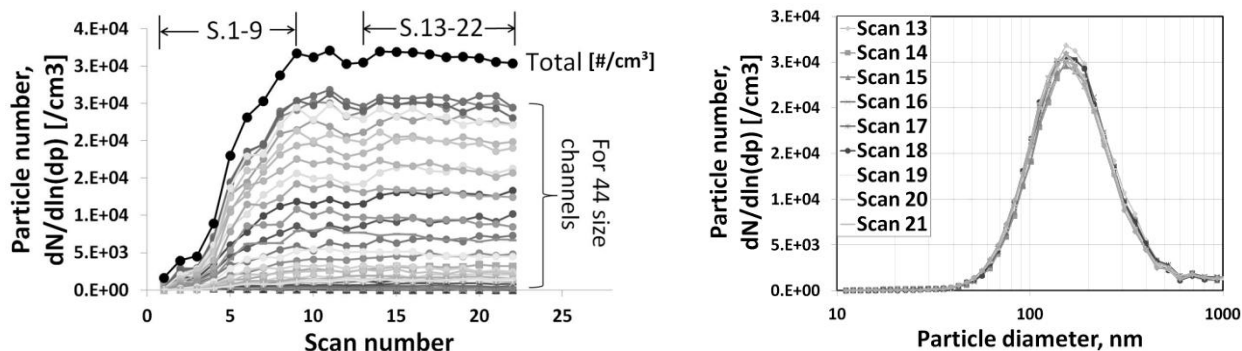


Fig. 2. Left: evolution of particle numbers during the aerosolization process (SMPS, black curve, total number of particles; all curves below are particle numbers in individual size channels). Right: overlay of the particle number size distribution in the steady state.

Firstly, we tested our system's capacity to create and maintain aerosols with stable size distributions and number concentrations over some time. **Fig. 2** (left) shows the evolution through time of total particle number concentration and the individual size channels during a single aerosolization experiment of hydrophobic SiO<sub>2</sub> II powder at atmospheric pressure (without using the critical orifice). Airborne particles were detected as soon as the airflow began. The particle number concentration increased gradually at first and then became relatively stable. The same pattern applied to the particle number concentration in each individual size channel. Fig. 2 (right) shows that the particle number and size distribution did not change significantly once the aerosol entered a steady state. During this period, the variation in the geometric mean size was within +/- 2%. The steady state lasted 0.5–2 h, depending on the type of material and the amount of powder used, and 10 consecutive SMPS scans were selected from this period to calculate the average size and number concentrations. The results show that the system managed to deliver a stable aerosolization process. This stability allows a correct assessment of mean particle sizes from a series of continuous scans, even when the instruments used had relatively long scanning periods, such as the SMPS.

The minimal flow rates required to activate the different types of powders in our experiments ranged from 0.3 L/min to 0.5 L/min. To understand the potential influence of the aerosolization

flow rate on the particle concentration and size distribution generated, an additional series of tests was conducted using a larger range of airflow rates to aerosolize the powders at atmospheric pressure. Flow rates were increased step by step, and each step lasted 1 h. A constant dilution flow was maintained throughout the test to help stabilize the aerosol generated. **Fig. 3** (left) shows the evolution of hydrophobic SiO<sub>2</sub> II particle numbers under six different aerosolization flow rates. Higher flow rates generated more particles. Particle concentrations reached steady state conditions under all six flow rates. The mode sizes measured from the lowest to highest flows were 142.1 nm, 132.8 nm, 129.7 nm, 116.8 nm, 115.6 nm, and 133.8 nm, respectively, with an average size of 128.5 nm and 10.4 nm (8%) standard deviation. At the highest flow rate, an additional side maximum appeared in the particle size distribution in the micrometer size range. The higher flow rate seemed to cause particles with higher settling velocity to exit the funnel into the rest of the system, whereas under low flow rate conditions, these micron-sized particles are effectively kept back. This phenomenon is also shown on **Fig. 3** (right), which compares relative size-number distributions normalized to the total particle number. The shapes of the size distribution spectra were otherwise very similar. These experiments suggested that the system was capable of generating very consistent aerosols at different flow rates, as long as the flow was kept well below the speed that would cause large particles to escape the upper part of the funnel. Within the flow range used in these experiments (0.3–0.9 L/min), particle size distributions were robust, allowing a comparison of data from different tests.

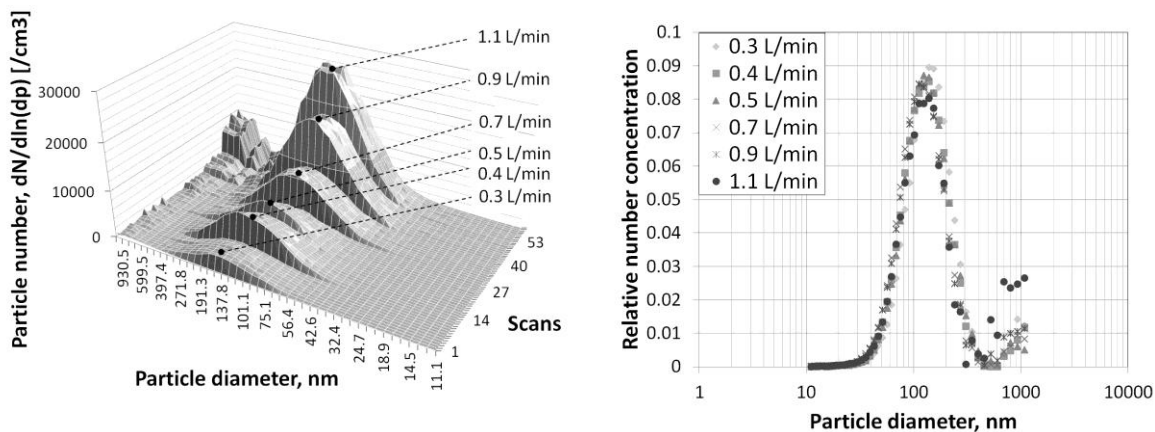


Fig. 3. Left: 3D representation of the size-number distribution at different air flow rates. Right: comparison of relative number concentrations at the same flow rates.

The particle number concentrations generated from the tested materials were compared to those of similar studies, as shown in **Fig. 4**. These systems include the standard rotating drum method [98], the continuous drop method [99], the modified rotating drum method [68], and the vortex shaker method [90, 100]. Lower and upper concentration limits under different experimental parameters in these studies were identified. Different testing conditions were employed in these systems, such as amount of powder used, total air flow and dilution rate and volumes of the different compartments. A comparison of the concentrations obtained for different substances in a given system provides a relative ranking of dustiness. By coincidence, many of these systems show also similar absolute number concentrations for equal substances tested. In all test systems, silica generated high particle number concentrations, followed by cerium oxide, and zinc oxide powders. The same pattern was observed using our system. These results suggest that our approach may also be useful for doing dustiness testing, in particular if only small quantities of novel and costly nanomaterials can be made available for testing purposes.

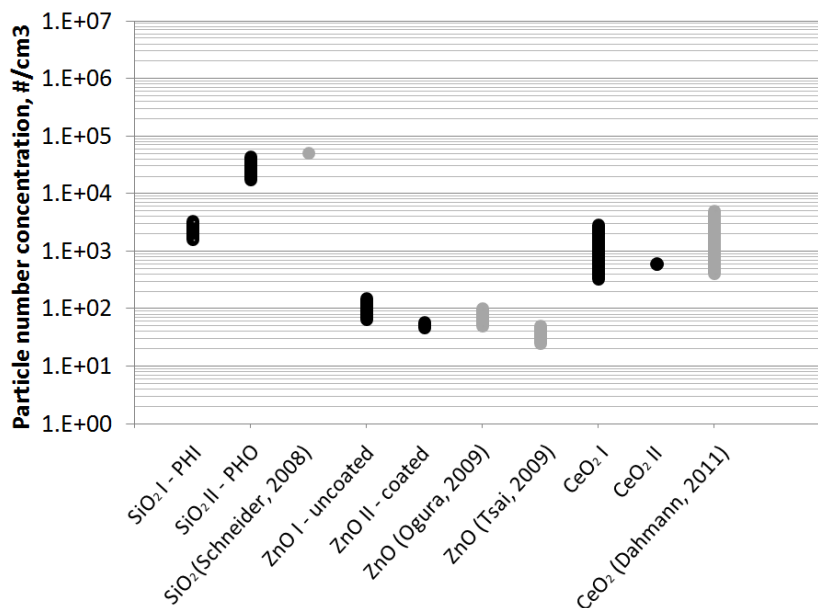


Fig. 4. Comparison of our particle number concentrations (black bars) with those of other aerosolization systems (grey bars), PHI - hydrophilic, PHO - hydrophobic.

### Deagglomeration tests

#### Influence of pressure modifications on mean particle size

The introduction of different pressure conditions had immediate effects on the geometric mean size of the aerosols. The results are shown in **Fig. 5** for different materials. Firstly, significant reductions in mean particle size were observed for most of the materials tested as pressures increased. The exception was type II SiO<sub>2</sub> with a hydrophobic surface coating. In contrast, all other aerosols, including type I hydrophilic SiO<sub>2</sub>, showed a drop of 25%–40% in their original mean sizes. Secondly, deviations were seen between the same materials with different surface coatings or original primary particle sizes: the two types of SiO<sub>2</sub> aerosol exhibited almost a three-fold difference in mean particle size, as the blue curves show. After testing, the deviation still existed. For the two types of Ce(IV)O<sub>2</sub>, the difference in particle size was smaller but still distinguishable. Averagely 25% difference was recorded between this two materials for the four pressure condition. In comparison, the two ZnO powders generated similar results whether they were coated or uncoated. Thirdly, the effects of the three highest pressures were similar or, in other words, the effect became smaller as the pressure rose. This is shown in the graph by the flatter slopes between 200–400 kPa.

Theoretically, the drag force that a moving particle experiences from the surrounding air is proportional to its diameter, meaning smaller particles experience less resistance. This might explain the ineffectiveness of the critical orifice on the hydrophobic SiO<sub>2</sub> aerosols and the reduced effects of the highest pressures on the other materials. Moreover, smaller agglomerates are more likely to be composed of tightly packed primary particles, in comparison to large ones that are loosely bonded internally. Hence, it is more difficult to break smaller agglomerates up into smaller particles. The deviation in mean particle size for the same types of material can be due to different primary particle diameters/shapes, surface areas, and coating types. For example, the Ce(IV)O<sub>2</sub> and SiO<sub>2</sub> aerosols composed of larger-sized primary particles had larger agglomerate sizes. The two types of ZnO had similar primary particle diameters and their agglomerate sizes are also closely comparable. Additionally, the coating type seemed to contribute to the size difference of the SiO<sub>2</sub> aerosols. In the experiments, the hydrophilic powder was much fluffier than its hydrophobic counterpart. It was also more difficult to aerosolize and sometimes required a higher flow rate in order to achieve stable aerosolization. Obvious differences in the appearances of the ZnO powders were not observed, however. The agglomerate size of different materials was also influenced by their elemental composition, as

this determines the Hamaker constant in van der Waals interaction [55]. In summary, these results suggest that different nanomaterials have different lower particle or particle aggregate size limits below which they tend not to deagglomerate further under normal conditions where extreme energy processes are not present.

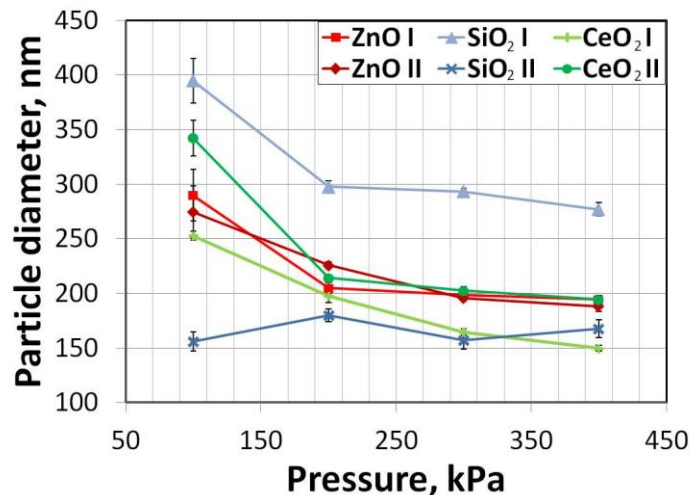


Fig. 5. Influence of pressure on geometric mean diameter for different materials (data from the SMPS).

### Influence of pressure modifications on particle number size distribution

Following the changes in GMD seen in the aerosols, the number size distribution spectra were compared in order to reveal the potential effects on different size ranges, as shown in **Fig. 6** (left) for ZnO I (uncoated) as an example. The mode size was largely shifted to the smaller size range. The particle number fractions in the upper size range decreased, and those in the lower size range increased (shown by the zoom-in windows). Furthermore, the variation in the particle fraction in each size channel was reduced, as indicated by the shortened error bars. The only exception was hydrophobic SiO<sub>2</sub> aerosol which did not experience any noticeable change in the mode size. For other materials with different surface coatings (results not shown), the same patterns of reduced mean particle size and enhanced stability were registered. However, the difference in effect between the three highest pressure levels were not obvious, despite using the ANOVA method to statistically evaluate the significance of those pressure changes on the size spectra. The results were positive for all the materials when comparing the reference and overpressure conditions. The effects of pressure over a wider range of sizes based on the data from the optical particle counter (OPC) were also compared. Generally, the particle number fraction in the lower end of

the size range increased as pressure increased. For aerosols with relatively larger particle sizes, such as hydrophilic SiO<sub>2</sub>, the OPC provided a good size resolution for presenting potential modifications.

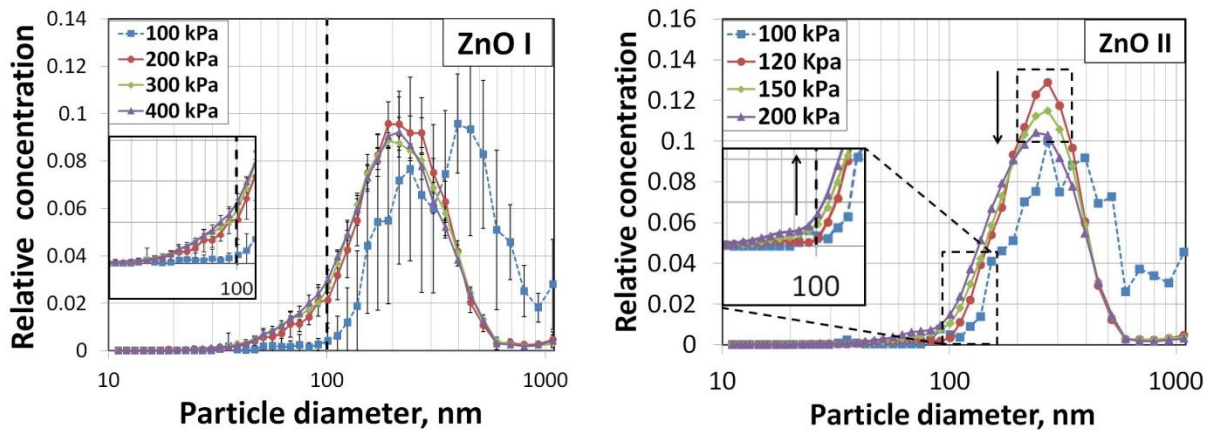


Fig. 6. Comparison of particle size distribution under different pressure conditions (from SMPS), left: 100-400 kPa, right: 100-200 kPa.

In a similar study [86], the reduction in mean particle size was also observed when pressures up to 240 kPa are applied in the critical orifice. However, in their study, the aerosols had larger mean sizes both before and after testing, as well as broader spectra resulting from a different aerosolization process. Another recent study investigated deagglomeration of micronized lactose particles by using nozzles with different diameters [101]. The greatest reduction in mean particle size was from 5.6  $\mu\text{m}$  to 3.2  $\mu\text{m}$ . In comparison, the present study worked with smaller particles under higher pressures. These conditions allowed the study of NP behavior in a lower size range and their airborne stability within extreme energy processes.

As the different shear forces applied produced similar results, more closely defined pressure steps were tested in order to understand the point where effects started. The results for coated ZnO II are shown in **Fig. 6** (right). It shows the same general pattern of size reduction as pressure rises. At 120 kPa, a well-distributed size spectrum with a narrow peak was already created, as the red curve shows. With continuously increasing pressures, the peak lowered and moved gradually to the left. The particle number fraction below 100 nm continued to grow during this process. Results suggested that the critical orifice can already start to affect certain materials at low-shear

force levels, indicating their loosely bonded agglomerate structure (see section on morphological characterization).

### Influence of pressure modifications on particle number concentration

The consequences of pressure increases on particle generation rates are shown in **Fig. 7**. This rate corresponds to the aerosol concentration divided by the total airflow. Particle generation is greatly enhanced under higher pressure conditions. The influences of pressure varied across different types of material. The two ZnO powders and the type II Ce(IV)O<sub>2</sub> showed the most significant increases, with 70- to 80-fold increases under the three highest pressures. Type I SiO<sub>2</sub> showed only minor augmentation (about six-fold). The generation rates of the ZnO powders under the reference pressure were below 250 units on the graph. The increases in ZnO particle numbers corresponded well to the reductions in their mean particle size and fitted with the idea that the deagglomeration of larger particles might have been due to external forces. The result suggested that potential particle loss in the critical orifice is negligible for the tested powders. Chen et al. investigated the particle loss mechanism inside a critical orifice [102] and found that this process mainly occurred downstream of the orifice. They attributed this to large turbulence in the air stream in that region. However, in their study, the critical orifice exit led into another tube, while in our system the critical orifice led directly into the wide measurement chamber. Thus particle losses were minimized by the open space after the orifice.

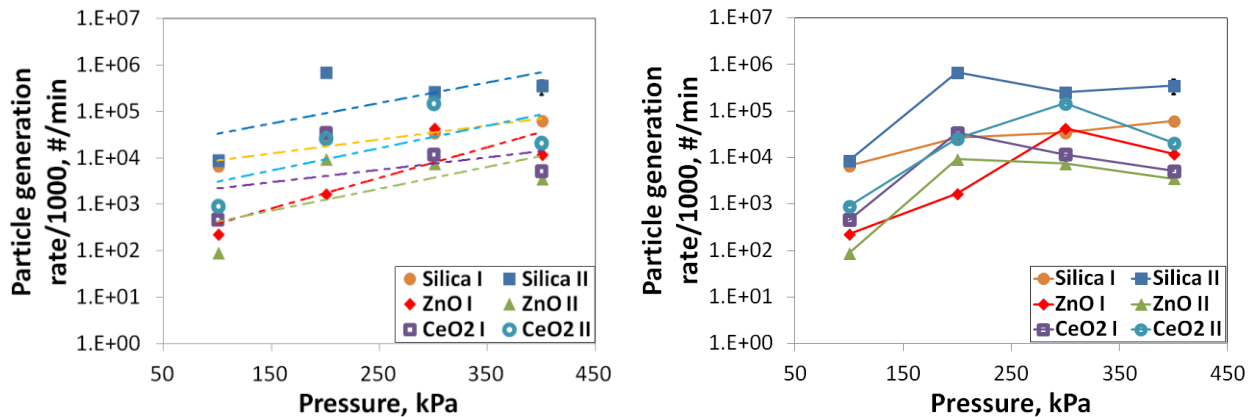


Fig. 7. Particle generation rates for different materials under increasing pressures, left: figure used in the published article, right: modified version not included in the publication.

### Influence of pressure modifications on particle number fractions in different size ranges

The influences of the pressure modifications on the particle number fractions of the different materials were also calculated (see **Fig. 8**) by grouping the particles into three size ranges: <100 nm, 100–350 nm, and >350 nm. The 100 nm cut-off represents the diameter of nanoparticles in according to the definition of nanoparticles. The aerodynamic behavior of particles changes to being mostly influenced by either inertia or Brownian motion at a size of approximately 350 nm. Particle numbers in each of the three size ranges were summed and subsequently normalized to the total particle number. At elevated pressures, most of the materials showed increased particle number fractions in the <100 nm size range. The results seemed to be powder-dependent. The two ZnO powders showed a seven-fold change in their particle number fractions, from 2%, to 14% under the highest pressure. The two CeO<sub>2</sub> powders showed a three- to five-fold increase. In contrast, SiO<sub>2</sub> aerosols were not much affected. In the >350 nm size range, the particle number fractions were reduced under higher pressures. The values were three to five times lower for ZnO and CeO<sub>2</sub>, but for SiO<sub>2</sub> particles only a slight reduction of number counts was seen. For the 100–350 nm size range, most of the materials showed little change in the number fraction except for the type I hydrophilic SiO<sub>2</sub>, which saw an increase in numbers. These modifications in particle number fractions suggested that it was mostly the larger agglomerates which broke up into NPs.

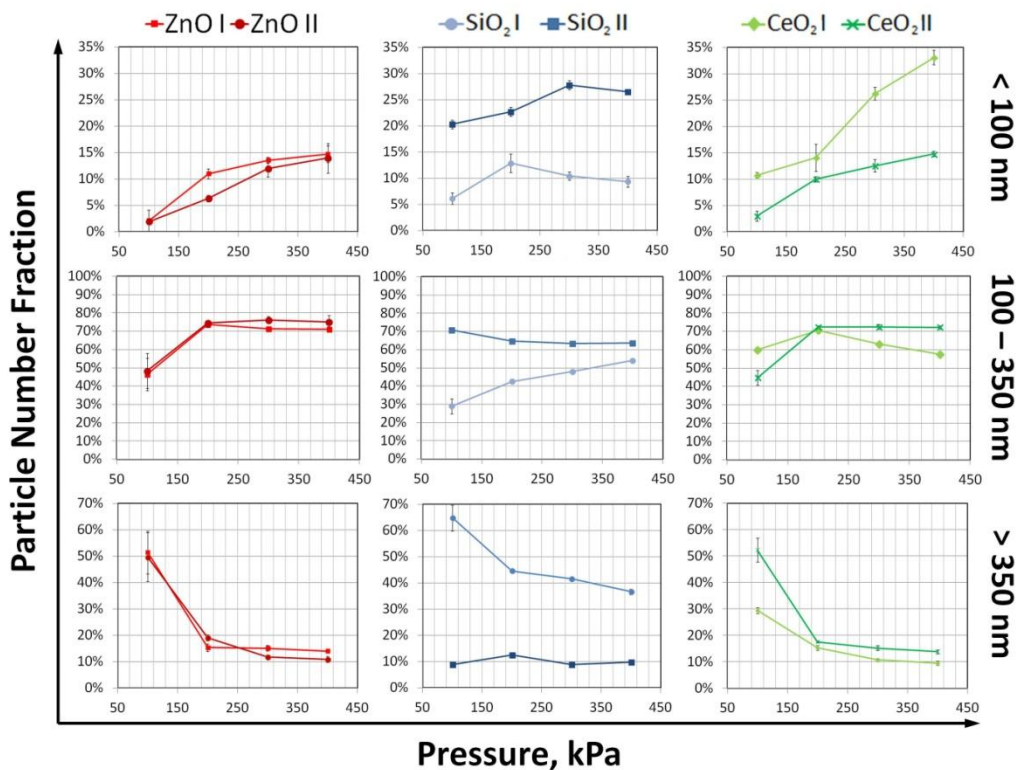


Fig. 8. Comparison of pressure influences on particle number fractions for different materials (from SMPS, 10.8–1083.1 nm).

### Repeatability & Reproducibility

Replicate tests were conducted under different shear force conditions for all the materials tested in order to examine the reproducibility of the results. For any single aerosolization, the absolute particle number concentration at steady state could vary by up to several-fold under the same experimental conditions. However, the relative number concentrations (normalized to total particle number) were highly reproducible. The size distribution spectra, measured in replicate tests, overlap tightly. The variations of the mean particle size were within 5% under different pressure conditions. The p values obtained in the statistical analysis (ANOVA for geometric mean sizes in replicate tests) were 0.522, 0.141, and 0.502 for SiO<sub>2</sub> II under 100 kPa, CeO<sub>2</sub> II under 300 kPa and ZnO I under 400 kPa, respectively. These results indicate that the variations in particle concentration in the different experiments did not significantly alter the particle size distribution.

### Morphology analysis

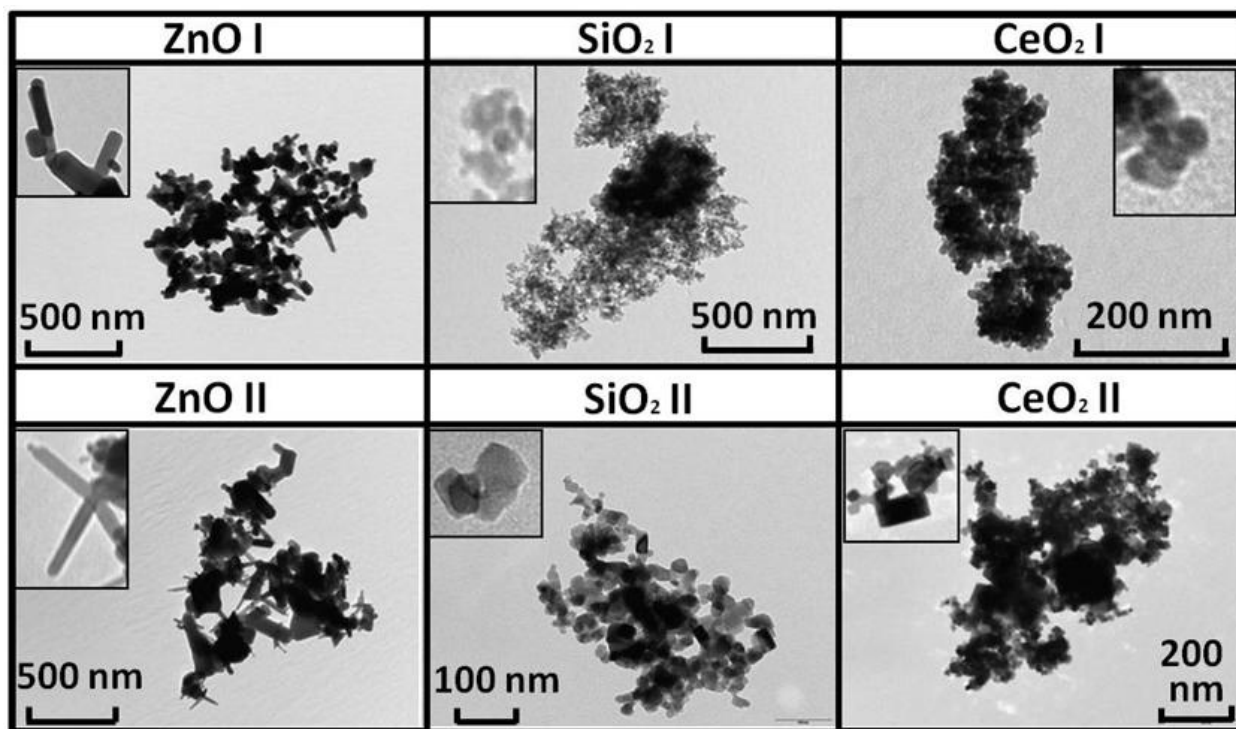


Figure 9. TEM images of airborne samples for different materials (condition: 100 kPa). Insert: 10-fold magnification compared to main image.

The airborne samples collected onto TEM-grids were assessed for primary particle shape and agglomerate structure. **Figure 9** shows the different agglomerate morphologies of the materials tested. The two types of ZnO were composed of rod-like particles. The CeO<sub>2</sub> II particles appeared as square blocks, whereas the CeO<sub>2</sub> I and the two types of SiO<sub>2</sub> particles had round shapes with smooth edges. The ZnO agglomerates showed porous, loose structures, whereas the other two materials showed denser agglomerations of primary particles. The comparison of TEM images confirmed that average agglomerate sizes were smaller at higher pressure conditions, as shown in **Fig. 10**. The denser structure of the hydrophobic SiO<sub>2</sub> agglomerates shown on the TEM images may also explain why the mean particle size for this material remained relatively stable despite varied pressure conditions, whereas the porous ZnO agglomerates seemed to rapidly collapse under external forces, which is in agreement with observed reductions in particle size and increases in particle number. Further studies are needed to assess whether this was because of the primary particle shapes or other particle properties.

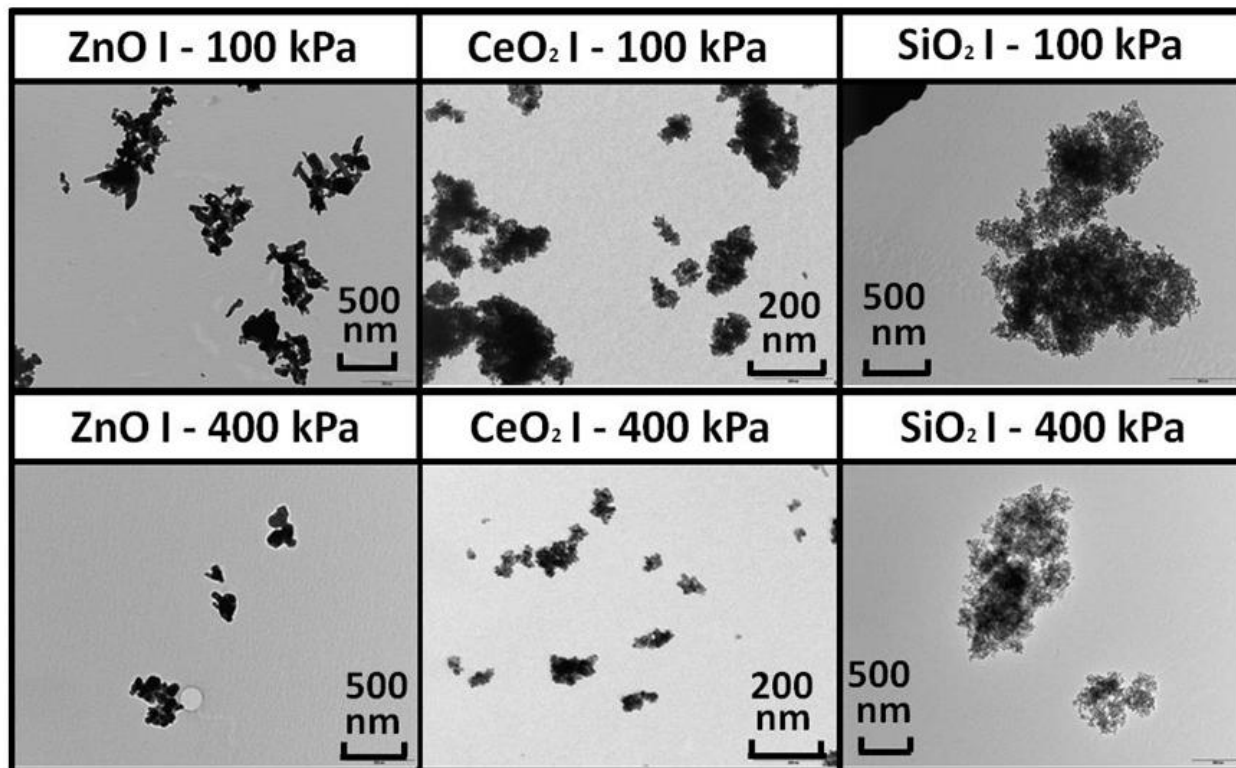


Fig. 10. Comparison of airborne samples under different pressure conditions.

## CONCLUSIONS

In this article, we describe a robust system for the aerosolization of nanomaterial powders and the subsequent characterization of their agglomerate sizes. We also assess how stable their agglomerates are by varying energy with pressure drops affecting the aerosols across a critical orifice. The system allows us to create aerosols that are very stable over time, which is important for the correct characterization of the aerosols created in this study, but which could also prove useful for other purposes where a well-controlled aerosol environment is needed, for example in toxicological studies. The comparison of the present study's particle concentrations with published dustiness data for similar powders suggests that the system also has the potential to be used as a dustiness testing system requiring only small quantities of powder (200 mg/test in our setup). This could prove to be a useful alternative to the standard rotating drum method (CEN EN15051) and the continuous drop methods, which both require relatively large amounts of powder. Using our system, the pressure drop across the critical orifice, used to test the stability of the aerosol, can be finely controlled. The air in our system is accelerated to sonic speed—the highest possible speed in such a system. These high levels of shear force correspond to the range of energy input that might be expected in most industrial and laboratory processes. The reductions in particle size and the increased particle number counts under elevated pressure-drop conditions, suggest that some of the NP agglomerates break apart in the air. We propose the use of this system for the routine testing of nanomaterials in order to obtain a ranking of their deagglomeration potentials. This will be useful for exposure and risk assessments on nanosafety issues. Moreover, our system not only enables a study of the influence of environmental conditions, such as relative humidity, but also of particles with different surface functionalities.

Acknowledgements: The authors are grateful for the financial support for this study from the EU FP7 project on Managing Risks of Nanomaterials (grant agreement no: 263215). They also wish to thank the University of Lausanne for the use of its Electron Microscopy Facility for TEM characterizations.

**\*Citations in this article are compiled in the complete reference list at the end of this report.**

## 5. COMPARISON OF DIFFERENT AEROSOLIZATION METHODS

Publication 2

### **Dustiness and Deagglomeration Testing—Interlaboratory Comparison of Systems for Nanoparticle Powders**

Yaobo Ding<sup>1</sup>, Burkhard Stahlmecke<sup>2</sup>, Araceli Sánchez Jiménez<sup>3</sup>, Ilse L. Tuinman<sup>4</sup>, Heinz Kaminski<sup>2</sup>, Thomas A.J. Kuhlbusch<sup>2</sup>, Martie van Tongeren<sup>3</sup>, Michael Riediker<sup>1,5</sup>

<sup>1</sup> *Institute for Work and Health (IST), Universities of Lausanne and Geneva, Route de la Corniche 2,*

*CH-1066 Epalinges, Switzerland*

<sup>2</sup> *Institute of Energy and Environmental Technology (IUTA), Air Quality & Sustainable Nanotechnology Unit, Bliersheimer Straße 58-60, 47229, Duisburg, Germany*

<sup>3</sup> *Centre for Human Exposure Science, Institute of Occupational Medicine (IOM), Research Avenue North, Edinburgh EH14 4AP, United Kingdom*

<sup>4</sup> *TNO, Lange Kleiweg 137, Rijswijk, The Netherlands*

<sup>5</sup> *IOM Singapore, 30 Raffles Place, 17-00 Chevron House, Singapore 048622, Singapore*

*Corresponding author: Michael Riediker; Tel.: +41 21 314 74 53; Fax: +41 21 314 74 30; E-mail address: Michael.Riediker@alumni.ethz.ch*

*\*Published in *Aerosol Science and Technology*, 49:12, 1222-1231.*

[DOI:10.1080/02786826.2015.1114999](https://doi.org/10.1080/02786826.2015.1114999)

## **ABSTRACT**

Different types of aerosolization and deagglomeration testing systems exist for studying the properties of nanomaterial powders and their aerosols. However, results are dependent on the specific methods used. In order to have well-characterized aerosols, we require a better understanding of how system parameters and testing conditions influence the properties of the aerosols generated. In the present study, four experimental setups delivering different aerosolization energies were used to test the resultant aerosols of two distinct nanomaterials (hydrophobic and hydrophilic TiO<sub>2</sub>). The reproducibility of results within each system was good. However, the number concentrations and size distributions of the aerosols created varied across the four systems; for number concentrations e.g. from 10<sup>3</sup> to 10<sup>6</sup> #/cm<sup>3</sup>. Moreover, distinct differences were also observed between the two materials with different surface coatings. The paper discusses how system characteristics and other pertinent conditions modify the test results. We propose using air velocity as a suitable proxy for estimating energy input levels in aerosolization systems. The information derived from this work will be especially useful for establishing standard operating procedures for testing nanopowders, as well as for estimating their release rates under different energy input conditions, which is relevant for occupational exposure.

Keywords: aerosolization, dustiness, deagglomeration, nanoparticle, interlaboratory

## **INTRODUCTION**

Engineered nanomaterials in powder form are widely used in modern technologies, such as in paint additives [103], catalysts [104], nanocomposites [105], functional ceramics [106], and superconducting materials [107]. Particles accidentally aerosolized during production, handling and storage of nanopowders in occupational settings may pose exposure risks to workers [38, 42, 46, 108]. Nanoparticles have been shown to cause adverse health effects in human bodies via inhalation and subsequent translocation to secondary organs [17, 34]. Therefore, risks associated with exposure to engineered nanomaterials must be managed. A better understanding of how nanopowders behave during aerosolization is needed in order to establish proper safety control strategies in workplaces.

Dustiness, defined as the tendency of a powder material to generate airborne particles under an external energy input, has been tested by different systems to simulate powder handling processes in occupational settings. These experiments, which characterize airborne particle concentrations and size distributions, facilitate possible scenario predictions in exposure assessments. European Standard 15051, for measuring the dustiness of bulk materials, describes two reference testing procedures: the rotating drum method (EN 15051, part 2) and the continuous drop method (EN 15051, part 3) [109]. However, these systems required large amounts of test materials which are not suitable for nanomaterials due to their costs and potential risks. A downscaled, modified test system has been developed combining continuous drop and a significantly smaller rotating drum, and this permits the use of smaller quantities of test materials [68]. Systems based on a vortex shaker, also offering the possibility of testing smaller quantities, have recently been studied in view of their application for dustiness characterization [90]. Furthermore, Boundy et al. (2006) established an air jet dispersion method for testing the dustiness of pharmaceutical powders. The basic principle involves injecting powder through an orifice into a glass jar for subsequent characterization. It is noteworthy that these dustiness testing methods are different from deagglomeration tests, in that quantitative measurements of particle release are given (particle numbers or mass per unit nanopowder). Deagglomeration tests investigate the stability of nanoparticle agglomerates using different types of aerosolization and post-treatments on aerosolized particles subject to a range of energy levels. These tests provide qualitative results, but not quantitative ones, on how different forces trigger deagglomeration. Critical orifices have been used in these processes as means of applying high levels of shear forces [65, 67, 101].

Whether tests based on different aerosolization processes deliver comparable results is, however, unknown. Indeed, measurements are influenced by the diverse parameters used in each aerosolization system. These include the system's intrinsic properties (e.g., associated energy levels; how that energy is applied, via shear force, impaction aerosolization, or dilution flow rates; compartment dimensions), environmental conditions (e.g. relative humidity), material characteristics (e.g., quantities tested and dustiness), and types of sampling device. Stronger deagglomeration processes may create airborne particles with a smaller mean size whereas less vigorous treatments may release larger particle agglomerates. Higher flow rates can dilute

aerosols into lower concentrations. Raw material moisture content affects cohesive forces binding primary particles in powder agglomerates, and the dust generation rate is inversely proportional to this factor [110]. Furthermore, measurement devices which may themselves encourage deagglomeration during measurements (such as the Electrical Low Pressure Impactor) should be used with caution. **Table S1** (Supporting Information, SI) lists examples of the TiO<sub>2</sub> nanopowder aerosol properties measured using different systems. Aerosol concentrations ranged from 100 #/cm<sup>3</sup> using a standard rotating drum method, to 10<sup>6</sup> #/cm<sup>3</sup> using the vortex shaker method. The mode size of generated aerosols also differed from several hundred nanometers to a few microns.

The characterization of airborne nanoparticles generated from powders in occupational exposure assessment should, therefore, take into account the specific testing procedures. How different process characteristics influence measurements must be better understood. In the above aerosolization and deagglomeration methods, there was no common means of estimating associated energy levels. It is difficult to directly compare real-life exposure scenarios with the testing methods established to date, just as it is to predict aerosol properties resulting from a specific process and the subsequent exposure mechanism. A common method for comparing energy ranges across different systems is needed.

In the present study, four aerosolization and deagglomeration systems were used to test hydrophobic and hydrophilic TiO<sub>2</sub> nanopowders. These systems provide relatively low (compared to treatments using critical orifices) but easily distinguishable energy input levels. We explored how system characteristics and test conditions modified aerosol characteristics such as concentration and size distribution. We also assessed if air velocity may be useful for estimating energy inputs in aerosolization systems. For this, a basic comparison of the systems presented was needed to facilitate ranking them for deagglomeration based on their methods. While some of the methods allow testing the stability of airborne agglomerates, in this paper we only assessed the deagglomeration occurring during the aerosolization of the powder particles.

## **MATERIALS AND TEST SETUPS**

### **Materials**

Two nanomaterials in powder form were tested: hydrophobic titanium dioxide (NM103) and hydrophilic titanium dioxide (NM104) from the repository at the European Commission Joint Research Center (JRC–IHCP in Ispra). They had been stored in vials of 500 mg or 100 g (depending on the test setup) in an inert atmosphere. **Table 1** summarizes the main material characteristics [111]. The selection of these two materials as test powders was based on the rationale that the different surface coatings allow studying their effects on powder aerosolization and deagglomeration processes. The profiles of generated aerosols (size and concentration) are expected to differ due to distinct agglomeration levels caused by varied surface properties. Moreover, titanium dioxides are widely used in industrial sectors and have raised a high concern for human hazard risks [112].

Table 1. Physical and chemical properties of the tested materials

Name	Titanium dioxide (NM103)	Titanium dioxide (NM104)
Composition	89% TiO <sub>2</sub> , 6.2% Al <sub>2</sub> O <sub>3</sub>	89.8% TiO <sub>2</sub> , 6.2% Al <sub>2</sub> O <sub>3</sub>
Primary particle size (XRD), nm	20	20
Surface modification	Hydrophobic (PHO)	Hydrophilic (PHI)
Specific area, m <sup>2</sup> /g	60	60
Crystal structure	rutile	rutile
Moisture content*	1.61%	2.02%

\*Information from the manufacturer.

### Test setups

Four different systems were used, featuring different types of aerosolization processes using a variety of energy inputs, and allowing a comparison of aerosol characteristics (particle number and size distribution) under different experimental conditions. Each system was developed or installed by one of the four partners and tested for the comparison study, using the above-described materials. **Figure 11** shows schematic diagrams of the four measurement setups.

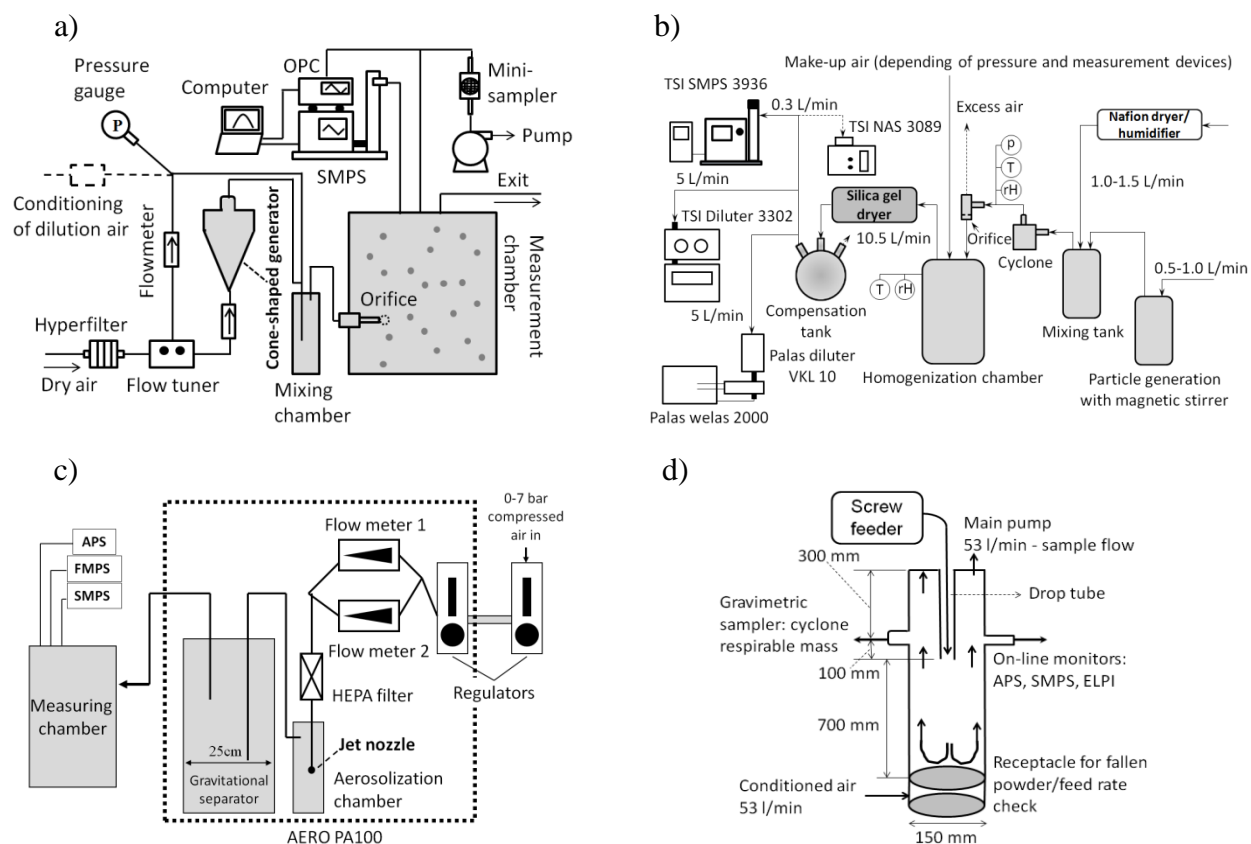


Figure 11. Aerosolization systems tested: a) fluidization funnel; b) magnetic stirrer; c) air jet aerosolizer; and d) continuous drop.

### 2.2.1 System I—Fluidization Funnel

A system based on fluidization was developed for continuous aerosolization of dry powders in small quantities (**Figure 11a**) [65]. Aerosolization is achieved inside a pressure-resistant glass funnel. Filtered dry air is blown in from the bottom opening, activating the powder body. The aerosol created is diluted by another flow in a mixing chamber. Conditioned air with a different relative humidity can be introduced at this point to study its influence. A relative humidity (RH) range from 2% to 90% can be controlled. Subsequently, the aerosol is transported into a large drum (12 L) from which online measurements and sample collection take place. A critical orifice can be installed in the chamber to study the stability of aerosol agglomerates but was not used in this study. Details of the sampling equipment are given in **Table S2 (SI)**. To avoid particle losses, anti-static conductive tubes are used for particle transport between compartments. The measurement chamber is electrically grounded.

The system was initially flushed with filtered dry air to create a clean background ( $< 10 \text{ \#/cm}^3$ ). Powder quantities for each test were  $250 \pm 10 \text{ mg}$ . The aerosolization flow was set at 0.3–0.5 L/min to maintain constant particle generation. The critical orifice was not installed for this study, and aerosol particles passed through a normal tube outlet into the measurement chamber. Particle concentration usually became stable after 20 min of aerosolization. Measurements continued for at least 30 min after this period. Relative humidity (RH) inside the system was  $2 \pm 0.2\%$ , and the temperature was  $20^\circ\text{C}$ . Two replicate tests were performed for each type of material.

### 2.2.2 System II—Magnetic Stirrer

A test rig using a magnetic stirrer in a pressurized beaker to activate powder materials is shown in **Figure 11b** [67]. A dry powder is aerosolized under constant carrier flow, and the aerosol generated is introduced into a mixing chamber for conditioning their RH (up to 90% RH possible, validated up to 70% RH). After conditioning, the aerosol passes a pre-separator (cyclone) to remove agglomerates above approximately  $1.5 \text{ \mu m}$  (cut-off diameter). Finally, the aerosol is introduced into a homogenization chamber (volume 10 L) either via normal tubing (zero overpressure) or via an orifice under various differential pressure conditions. The critical orifice was not installed in this study, which simulated the basic case of aerosolization for this setup. Anti-static conductive materials and tubes are used in the system to minimize particle losses. Airborne particles are characterized using online instrumentation sampling from the homogenization chamber (see **Table S2, SI**). Furthermore, they could be sampled on suitable substrates by using an electrostatic precipitator for subsequent SEM analysis.

The powder volume tested in each experiment was  $20 \text{ cm}^3$ . The background particle concentration inside the test system was recorded with a few measurement scans before the experiment. The magnetic stirrer's rotation speed (1000-1250 rpm, stirrer length: 30 mm) inside the beaker (250 mL high pressure glass bottle, Schott Duran glass bottle after DIN EN 1595) was controlled to produce constant powder agitation. Depending on the powder used, steel balls were occasionally used to assist the aerosolization process. The volume flow into the beaker was 0.5–1.0 L/min. The total flow volume needed by the measurement devices was about 10 L/min, thus an additional air flow was passed into the homogenization chamber to provide sufficient sampling flow. Sensors for temperature, humidity, and pressure were used to monitor

experimental conditions. RH was below 2% in the tests. Measurements took approximately 30–45 min depending on the powder type. Two replicate tests were conducted for each type of material.

### 2.2.3 System III—Air Jet

The third system consisted of a commercial aerosolizer (Aero PA100, Model NA002, Particle Measuring Systems, United States) (**Figure 11c**). It generates aerosols from powder materials by applying high velocity air jets to the powder surface. A pressurized source of clean, dry air is connected and regulated at the input. The flow rate is controlled and monitored by two parallel flow meters. After passing through a HEPA filter, the air is driven through a nozzle with three small holes to create high velocity jets for aerosolization. Aerosol generation strongly depends on the flow rate and how close the jet nozzle is to the powder surface. The aerosol passes through a gravitational separator (10 L), where large particle agglomerates are separated from the aerosol as a function of particle diameter and density. The aerosol is finally characterized by sampling from a measuring chamber. Details of characterization equipment are given in **Table S2 (SI)**.

In this experiment, the aerosolization process used a 5 cm nozzle-to-powder distance. The aerosolizer was set at a constant 5 L/min flow rate and was applied for 700 seconds. Note that although the airflow was continuous, aerosol concentrations transported into the measuring chamber were not. Aerosol concentrations first increased, reached a maximum level, and subsequently dropped back to zero as the powder was consumed. Each experiment used 500 mg of powder. The measuring chamber was ventilated after each run until the particle concentration was below  $10 \text{ \#/cm}^3$  as measured using a CPC. During all runs, RH in the measuring chamber was  $26 \pm 2\%$  and the temperature was  $17 \pm 1^\circ\text{C}$ . Two replicate tests were carried out for each type of material.

### 2.2.4 System IV—Continuous Drop

The continuous drop method, often used as a reference tool for testing the dustiness of dry powders, was also used in this study [92]. The aerosolization process is shown in **Figure 11d**.

The powder to be tested is placed in a screw feeder that drops the powder into the drop chamber at a constant feed rate. The dropping powder meets an upward air flow of 53 L/min (0.05 m/s) introduced from the cylinder chamber floor, creating turbulence in the particle surroundings. The aerosol generated is sampled above the drop tube. Relative humidity and temperature are adjusted by introducing conditioned air into the system.

The feed rate (2.8 g/min) was adjusted and measured before each experiment. The cyclone and drop cylinder were flushed by running clean air through them at 20°C and at 50% RH for 10 min. Next, the feeder was run continuously for 1 min, before measurements started which lasted 5 min. Details of characterization equipment are given in **Table S2 (SI)**. Two replicate tests were carried out for each type of material.

### **Characterization Methods**

Scanning mobility particle sizer (SMPS), optical particle counter (OPC) and aerodynamic particle sizer (APS) were used to measure particle number concentration and size distribution. The instruments used in the different setups are summarized in **Table S2 (SI)**. An inter-comparison of the SMPS settings used in the test methods is given by **Table S3 (SI)**. It is noteworthy that the equivalent diameters determined by these different devices are not the same, due to different measurement techniques used. This should be considered when constructing and interpreting the size distributions. The SMPS determines the electrical mobility of airborne particles. The OPC characterizes particle diameter by their optical properties and the light scattering principle. The APS classifies the particles according to the aerodynamic diameter.

### **Estimation of Energy Input**

Although the four measurement systems shared certain similarities, they differed in several aspects, shown in **Table 2**. For example, aerosolization energies differed significantly between systems. As an indirect parameter of energy, the relative velocity between the aerosolization air flow and the powder particles was used to compare the different systems' energy levels. The funnel setup used 0.3–0.5 L/min air flow to aerosolize the powder, creating an air velocity of 1.32–2.20 m/s at the funnel's bottom hole (2.5 mm in diameter). The rotating magnetic stirrer (a solid stick 3 cm long) in the pressurized beaker had a maximum linear velocity of 1.57–1.96 m/s

at both ends (assumed to be the aerosolization air flow speed), as calculated based on a speed of 1,000–1,250 rpm. In the air jet system, the powder was kept 5 cm from the air nozzle delivering a 5 L/min flow rate. The air speed measured at 5 cm away from the nozzle (simulating the scenario when the flow reaches the powder surface) was 14 m/s. In the continuous drop method, particle settling velocity was calculated as the relative speed to air. For particles with a diameter of 10  $\mu\text{m}$ , the Stokes’s law applies for determining particle settling velocities [58]. For particles with a diameter of 100  $\mu\text{m}$ , with a Reynolds number larger than 1.0, a modified equation is used to calculate the settling velocity [58]. Settling velocities were 0.003 m/s and 0.88 m/s for 10  $\mu\text{m}$  and 100  $\mu\text{m}$  particles, respectively. Particles smaller than 10  $\mu\text{m}$  have even slower settling speeds.

Based on these calculations, **Table 2** provides a rough (low, medium, or high) ranking of the energy input levels in the aerosolization methods used. Other system characteristics that could potentially alter the properties of generated aerosols are also listed.

Table 2. General comparison of test setups

System	Material quantity	Flow rate, L/min	Relative humidity	Aerosolization mechanism	Relative velocity (energy level), m/s
Funnel	250 $\pm$ 10 mg	1.5–2	2 $\pm$ 0.2%	Blowing	1.32–2.20 (medium)
Stirrer	20 cm <sup>3</sup> (5–8 g)	2	< 2%	Mechanical stirring	0–1.96 (low-medium)
Air jet	500 $\pm$ 10 mg	5	26 $\pm$ 2%	Blowing	14 (high)
Drop	2.8 g/min	53	50%	Air friction	0.003–0.88 (low)

\*Energy level can be varied within systems, but only the lowest possible values were used in this work.

## 2.4 Data analysis

Number concentrations in the size range below 1  $\mu\text{m}$ , as well as the mode diameters in the aerosols generated, were compared across the different systems. Broader size distribution spectrums were plotted by combining SMPS and OPC (or APS) data (effective density used: air jet and drop systems, 1 g/cm<sup>3</sup>. refractive index used: Funnel, 1.59; Stirrer, 2.56). The data units from the optical particle counters were converted into dN/dlogDp [# /cm<sup>3</sup>], in order to compare

size channels with the different widths used in the other devices. Particle size distributions from replicate tests were compared to estimate each system’s robustness. Spectrums were normalized to the total particle number in the size range considered (dependent on the specific system). This allowed a better comparison of the size distributions in different concentrations. The mode size(s) of aerosols is also plotted against the velocity of the aerosolization flows in the different systems, facilitating the analysis of this parameter’s potential influence on aerosol properties. The size distributions of aerosols with different surface coatings are also plotted.

## RESULTS AND DISCUSSION

### Particle Number Concentration and Mode Diameter

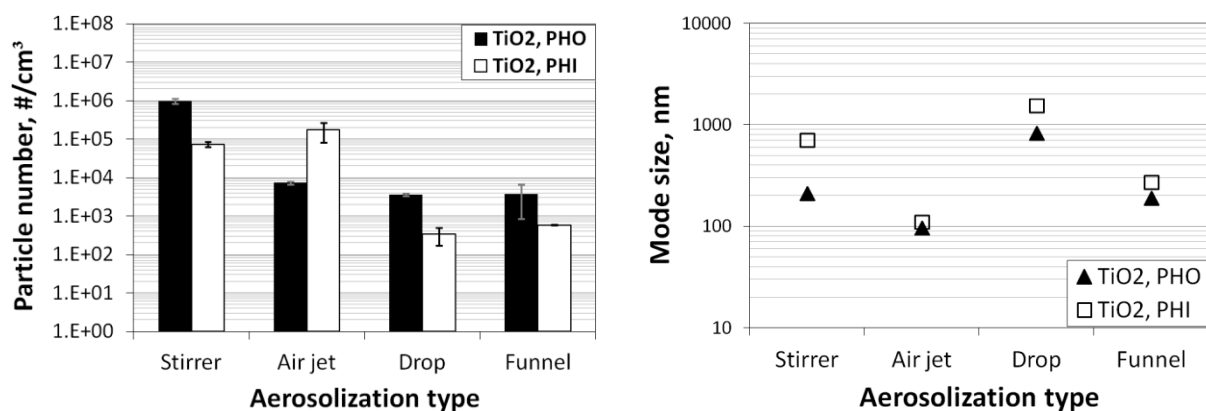


Figure 2. Comparison of total particle number (34-965 nm) and mode diameter

A comparison of number concentrations in the aerosols generated from the different systems is shown in **Figure 2** (left). The SMPS and APS/OPC data were used, and total particle numbers were compared for a common same size covered by all the systems. Particle numbers varied across a large range, from about 200 #/cm<sup>3</sup> to 100,000 #/cm<sup>3</sup>. The funnel and drop setups produced lower concentrations in the aerosols of both materials compared to the other two methods. Hydrophobic powder aerosols showed higher particle concentrations than hydrophilic powder aerosols in three methods, but not with the air jet system—it produced higher numbers of hydrophilic particles. In all four systems, the differences in particle numbers for the different materials were about one order of magnitude.

The mode diameter of the aerosols generated is also shown in **Figure 2** (right). The results varied greatly: from about 100 nm to above 1  $\mu\text{m}$ . The largest mode diameters resulted from the continuous drop method; the smallest mode diameter came from the air jet setup. The hydrophilic particles usually had a larger mode size than the hydrophobic particles, however the diameters for the two materials were similar in the air jet system. It is noteworthy that a second mode was observed in the size distribution of the hydrophobic aerosol generated in the drop method. This is discussed in the following sections.

Particle number concentrations in experimentally-generated aerosols have a close relationship to the system characteristics and testing conditions. The amount of raw materials used indicates how many particles are available to be aerosolized. Energy input may affect the level of deagglomeration of the powder particles. High energy processes are more likely to thoroughly break-up the powder agglomerates, thus generating aerosols with a high particle number concentration. Furthermore, the volume flow rate also modifies particle number. For the same amount of available particles, a higher flow rate dilutes the aerosol into a lower number per unit volume. In order to study deagglomeration processes, it would be key to maintain the airborne particle concentration within a range that is above the detection limit of the measurement instruments, but also not sufficiently high as to promote immediate secondary effects (e.g., re-agglomeration in the airborne state). The systems used in this study worked in suitable concentration ranges, which allowed a comparison of the deagglomeration effects in the different setups.

The system parameters and testing conditions varied between the experiments. The associated energy levels were highest for the air jet system, as calculated in the method section, and this might be responsible for the high particle generation of the hydrophilic powder, in spite of low material consumption (500 mg). On the other hand, for the drop method, although the quantity of material used was high (~2.8 g), the particle number was low due to the relatively small energy input for aerosolization. In comparison, the stirrer system seemed to somehow balance these factors. The funnel setup, with low material use (250 mg) and a moderate aerosolization energy, worked in low concentration ranges under the given aerosolization flows. Similarly, the vortex shaker method has generated concentrations in 300–2,000  $\#/\text{cm}^3$  range using only 0.25–1  $\text{cm}^3$

TiO<sub>2</sub> powders [100]. The air flow rate was 5–20 times higher in the drop system than in the other systems. This may have contributed to the low number concentration observed. In general, the high particle concentrations obtained in our experiments were comparable to those for ultrafine TiO<sub>2</sub> in the combined single drop-rotating drum method (up to 10<sup>6</sup> #/cm<sup>3</sup>) [68].

Aerosolization time is another factor influencing particle number concentration. This is especially true for systems showing decreasing particle generation over time [99]. In the air jet experiments, particle concentrations reached maximum values after a few minutes of aerosolization. Particle numbers then gradually decreased to background levels. Similar patterns have been observed: brief initial bursts, decaying rates during rotation, and then constant rates [68]. The difference in the air jet method was that material quantities used were small, thus powder was rapidly consumed, and then concentrations dropped to a very low level. In comparison, the funnel system was shown to be able to maintain stable concentrations over longer time periods (>30 min) [65]. This was also the case for the stirrer system in the present work.

### **Effect of Air Velocity on Aerosol Diameter**

The energy inputs during different aerosolization processes were ranked based on the relative velocity of activation air flow as described above. A comparison of the air velocity-aerosol size relationship is given in **Figure 3**. The both mode sizes measured by the SMPS in the drop system are included. Particle diameters were shown to be inversely proportional to the velocity of aerosolization flows. Higher air speeds generated smaller mode sizes. Particle sizes decreased rapidly in the velocity range up to 1 m/s, but size reduction slowed down at higher speeds. Similar patterns were seen for both materials. The hydrophilic particles experienced larger decreases in mode size as air speed increased than did the hydrophobic particles.

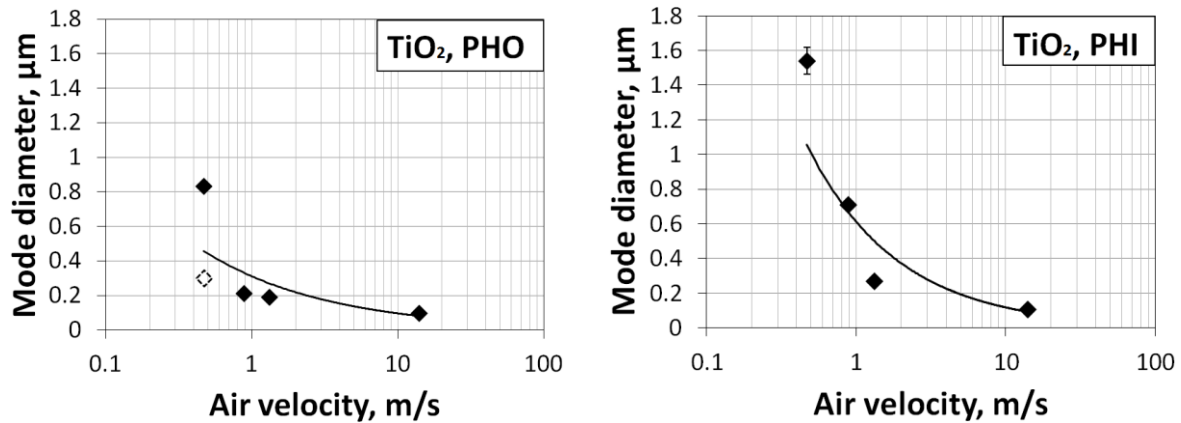


Figure 3. Influence of aerosolization flow velocity on mode diameter of generated aerosols (fitted curves are added to show the general patterns; white dot on left graph represents secondary mode diameter for the drop method)

The mode diameter of aerosol particles was earlier reported to be associated with the energy level during powder aerosolization: the size of airborne particle agglomerates was smaller under higher shear forces [65, 67]. This was explained by drag from the air current, which acted as a major deagglomerating force in these processes. The drag force is proportional to the velocity and diameter of the particle [58]:

$$F_D = \frac{3\pi\eta vD}{C} \quad (1)$$

where:  $\eta$ , air viscosity;  $v$ , particle velocity relative to air;  $D$ , dynamic shape factor;  $C$ , slip correction factor.

The shape factor is constant for a given particle, and it was set equal to 1 for simplicity matters. The Cunningham slip effect becomes significant when particle size is below 10  $\mu\text{m}$ . Drag forces differ for particle agglomerates with different diameters. The values calculated against particle size at the average velocities in the systems tested are shown in **Figure 4**. For 1  $\mu\text{m}$  particles, forces ranged from 0.06–2.05 nN.

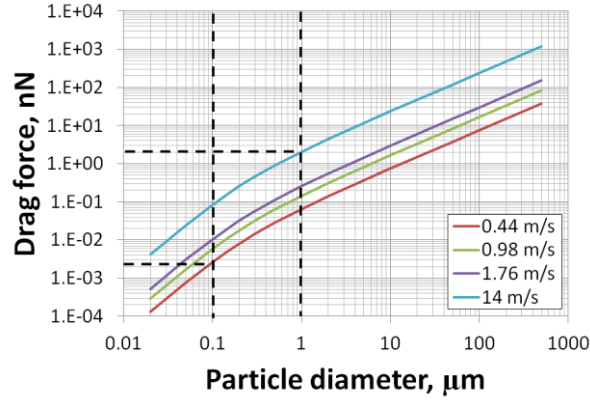


Figure 4. Drag force–particle size relationship for the various relative velocities in the tests

The dominant mechanism by which uncharged particles form agglomerates when stored as powders is direct contact [113], bonding individual particles by van der Waals (VDW) force.

This interparticle force can be calculated as below [55]

$$F = -\frac{A}{D_1} F_y(x), \quad y = \frac{D_2}{D_1}, \quad x = \frac{r}{D_1} \quad (2)$$

where: A, Hamaker constant;  $D_1$ , diameter of the smaller particle;  $D_2$ , diameter of the larger particle; r, distance between the two particles.

For two spherical particles of the same diameter ( $y=1$ ), when  $x \ll 1$ , then approximately

$$F_1(x) = -\frac{1}{24} \frac{1}{x^2} \quad (3)$$

The contact distances of two primary particles can be viewed as the material's VDW radius. At this distance, separation between the particles reaches an equilibrium where the interfacial potential is minimal [114]. For titanium, the value is 0.215 nm [115]. The diameter of primary particles in our tests was 20 nm ( $D_1 = D_2$ ). The Hamaker constant A for  $\text{TiO}_2$ – $\text{TiO}_2$  (rutile) interaction in the air is  $15.3 \times 10^{-20}$  J [116]. The result of VDW force interaction was

$$F_{\text{VDW}} = 2.64 \text{ nN} \quad \text{for } r = 0.215 \text{ nm, } D = 20 \text{ nm}$$

In comparison, the drag forces created in our different test setups were in the range of  $2 \times 10^{-3} \sim 2$  nN for particle diameters of 0.1–1  $\mu\text{m}$  (**Figure 4**). Although the drag comprises small forces, up to three orders of magnitude lower than the calculated VDW force, it can still affect the deagglomeration process. In a study using numerical simulation to investigate the dispersion of  $\text{TiO}_2$  nanoparticle aggregates under shear flow, it was found that the aggregates started to deagglomerate when the ratio of fluid force to the interparticle force was over 0.001 [117]. Thus, the shear force ingredients created in our experiments may be responsible for the different mode

diameters of the aerosols generated. Higher air velocities induce stronger drag on the particle agglomerates, which leads to higher deagglomeration efficiencies by overcoming interparticle binding forces. As a follow-up, we have carried out further work on quantifying the effects of air speed by incorporating critical orifices in two of the systems, which expands on the present study into a consideration of a much broader energy range.

## Particle Size Distribution

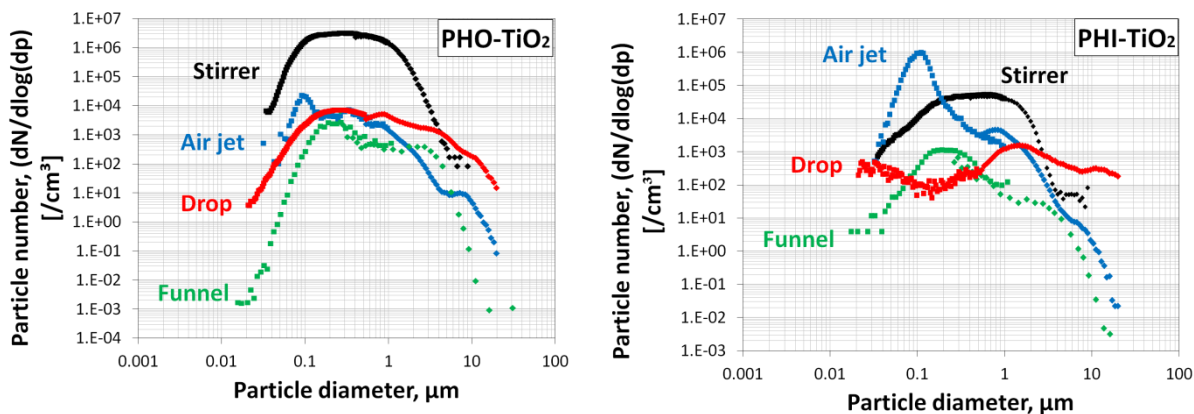


Figure 5. Comparison of full particle number size distributions for the different systems

Particle number size distributions from the aerosols of different systems, including SMPS and OPC (or APS) data, are compared in **Figure 5**. The peaks in the size distributions were located in different size ranges. However, the deviations seemed to be smaller for the hydrophobic aerosols than for their hydrophilic counterparts. Comparing the two powders by system, higher peaks were generally shown for the hydrophobic particles than for the hydrophilic particles, except for the air jet system. The peaks created using the air jet and the funnel methods were sharper; they were relatively broader for the other two systems. Two particle size modes were observed for the hydrophobic aerosol in the continuous drop system (**Figure 5** left): one above 1 μm and another around 300 nm (measured by SMPS). Small variations were noted when combining data points obtained using different measurement equipments. However, this was only to be expected because of their different operating principles.

The varied shapes of the size distribution spectrums can be attributed to the different deagglomeration levels in the test setups. At low energy input, powder particles were partially deagglomerated, generating aerosols with a large mode size. Using large amounts of materials

may alter local interactions between the air flow and the powder particles, which may lead to the reduced dispersibility of the powder agglomerates. How agglomerate size in powder fluidizations depends on parameters including gas velocity and energy input has been described previously [118, 119]. In contrast, higher drag forces created in the air jet system broke agglomerates down to the sizes for which associated drags become comparable to the interparticle binding force (as discussed in previous sections). Furthermore, the funnel setup—which resembles a fluidized bed—features another deagglomeration mechanism: collisions between flowing particles [113, 120]. These conditions promoted sharper peaks in the size distribution of the aerosols generated. The two modes in the particle size spectrum observed in the drop system may be due to the low energy input. Indeed, a particle size distribution in powders is usually bimodal [121, 122]. Primary particles form submicron and micro-sized agglomerates. Small particles are readily aerosolized, but big particles need more energy to be deagglomerated. The mode size measured in the 200–300 nm range may be directly due to small, easily aerosolized particles, whereas the mode in the 1–2  $\mu\text{m}$  range was the result of particles broken down from larger powder agglomerates under low shear forces. Other investigators of  $\text{TiO}_2$  have observed similar bimodal behavior in submicron and micron ranges when using rotating drum methods, as shown in **Table S1 (SI)**. Energy input into those systems was considered low, since the rotation speeds used were 4 rpm [98] and 11 rpm [68]. This process shares some similarities with the drop method, as amounts of powder are raised to a certain height and fall back down. Moreover, Dahmann and Monz (2011) showed that nanopowders tested in their continuous drop experiments typically had bimodal distributions. In comparison, monodispersed size distributions have been more common in high energy processes, such as vortex shaker systems [90, 100].

## **Reproducibility**

The results obtained in replicate tests from different systems are summarized in **Table S4 (SI)**. Variations in absolute number concentrations were generally small, but some cases with several-fold differences were also observed. Overall the results were still within the same order of magnitude. Total particle number concentrations were calculated for the size range below 1  $\mu\text{m}$ , with the exception of the drop method, which had larger mode sizes for its aerosolized particles. The mode diameters from replicate tests were very similar ( $\text{SD} < 8.3\%$ ). **Figure S1 (SI)** compares the size distribution spectrums, at relative scales, for hydrophilic  $\text{TiO}_2$ . The particle

fractions in certain size ranges varied slightly. A relatively larger difference in peak heights was seen using the drop method. In general, the reproducibility of the aerosols generated by the four systems was good, facilitating a robust comparison of the different methods.

### **Effects of Material Surface Coatings**

Relative particle number distributions were compared for the two materials with different surface coatings (**Figure S2, SI**). In general, the mode diameters were larger for the hydrophilic TiO<sub>2</sub> than for hydrophobic. The differences between the two materials were more significant in the stirrer (RH ~2%) and the drop systems (RH ~50%) than that in the air jet (RH ~26%) and the funnel systems (RH ~2%), even though the RH in the stirrer system was very low. This can possibly be explained by the shear forces during aerosolization. The differences were small for the two systems with the highest air velocities and significant for the two systems with the lowest velocities. In the drop system, a bi-modal size spectrum was observed for the hydrophobic TiO<sub>2</sub>, which exhibited a high particle fraction in 200–300 nm range.

Particles with hydrophilic surfaces absorb water more easily than particles with hydrophobic coatings. Both environmental humidity and the raw powder's moisture content can contribute to the formation of water menisci between individual particles. In mid-range RH (40%–70%), it has been shown that the pull-off force (maximum attractive force between particles) on a hydrophilic surface increased with the increasing humidity [123]. On mica surfaces, this force was several times larger in the capillary regime than in the pure VDW regime. This might explain the differences in mode sizes and number concentrations between our two aerosols, both in the drop system with 50% RH, and in the dry stirrer and funnel systems. However, with higher energy inputs, the difference in particle size was smaller, as seen in the air jet system. The drag force level created using this method may overcome the additional capillary adhesion from the water layer, thus triggering deagglomeration. In this case, the effect of a hydrophilic surface is compromised by a sufficiently high shear force.

### **CONCLUSIONS**

The present study tested TiO<sub>2</sub> nanomaterial powders with different surface coatings (one hydrophilic and one hydrophobic) using four different aerosolization and deagglomeration

systems. These generated stable aerosols for measurement, and the results obtained in each system showed good reproducibility. However, significant variations in aerosol properties, such as number concentration and size distribution, were observed in the different setups. The hydrophilic aerosol of TiO<sub>2</sub> tended to have a larger particle size than its hydrophobic counterpart. However, processes associated with high energy input levels seem to reduce the influence of surface properties on particle size distributions. Finally, the particle size was shown to be inversely related to the velocity of the aerosolization air flows.

The test setups used very different air flow rates, raw material quantities, aerosolization mechanisms, and associated energy levels. The varied results from the same materials indicate that the characterization of nanoparticle release should take into account specific testing protocols. The data obtained from each of the different systems offers suggestions as to which scenarios they could model most appropriately and how SOPs should be adapted with regard to specific tests. For example, the drop method could be used to determine a material's propensity to be aerosolized (dustiness) in low energy processes, thanks to its ability to measure the mass fraction of samples that become airborne. In contrast, the three other methods are more useful and valuable for the study of agglomerate stability in high energy processes. They are also useful for the determination of particle size distributions in powder characterizations.

The relative velocity of aerosolization air flow was used for a rough comparison of system energies to study if aerosol properties are affected by this parameter. More precise estimations of energy input level would take into account specific aerosolization method (the way external energies are applied). This aspect can be further explored in future experiments. In the present work, the significant influence of air velocity on aerosol particle diameter indicates that this parameter might be a good indicator for the energy levels associated with a variety of industrial processes. It is especially applicable to the handling of nanomaterial powders in occupational settings, where air velocities can be easily assessed from workers' operational activities and behaviors. For example, air speeds when handling powders in a laboratory can be estimated from fume hood flow patterns and other process parameters such as transfer distances, pouring heights, or mixing rates. The "micro-environment" surrounding powder particles during filling and packaging at manufacturing sites involves air current movements, assessed using local conditions

(e.g., ventilation or wind speed) and workers' operational procedures. The values calculated can then be compared with those from laboratory testing methods, in order to predict aerosol properties that might result from such scenarios. This is especially useful when field measurement data are lacking, but the risk level is considered high and in need of assessment. As a further step, this metric could be used to rank the potential for nanoparticle release in different industrial activities and processes.

## **ACKNOWLEDGEMENT**

The research leading to these results has received funding from the European Research Council under the European Union's Seventh Framework Programme (FP/2007-2013)/ERC Grant Agreement n.263215.

## Supplemental Information (SI)

Table S2. Summary of particle numbers and mode size of TiO<sub>2</sub> aerosols generated using different systems

Method	Particle number, #/cm <sup>3</sup>	Mode size
Rotating drum*	100–250	356–391 and 835–898 nm
Single-drop/rotating drum**	10 <sup>3</sup> –10 <sup>6</sup>	200nm, 1–2 μm
Vortex shaker***	300–2,000	>100 nm

\*[98]. \*\*[68]. \*\*\*[100].

Table S2. List of devices used for aerosol characterizations

System	Equipment	Manufacturer/Type	Size range
Funnel	Scanning mobility particle sizer (SMPS)	GRIMM, 5.403	11.1–1083.3 nm
	Optical particle counter (OPC)	GRIMM	0.25–32 μm
Stirrer	Scanning mobility particle sizer (SMPS)	TSI, Model 3936	34–1000 nm
	WELAS (OPC)	Palas, Model 2100	0.4–9.3 μm
Air jet	Scanning mobility particle sizer (SMPS)	NANEUM, NP S500	5.15–971.0 nm
	Aerodynamic particle sizer (APS)	TSI, Model 3321	0.523–20.5 μm
Drop	Scanning mobility particle sizer (SMPS)	TSI, Model 3936	20.5–523.3 nm
	Aerodynamic particle sizer (APS)	TSI, Model 3321	0.523–20.5 μm

Table S3. Inter-comparison of the SMPS settings used in the test systems

	Sampling/sheath flow rate, lpm	Time per scan	Impactor	Charge correction	Diffusion loss correction
Funnel	0.3/3.0	≈ 3 min	Yes (d <sub>50</sub> =1082 nm)	Standard multiple charge correction	Yes
Stirrer	0.3/2.0	150 s	No	Manual multiple charge correction	Yes
Air jet	0.2/3.5	120 s (60 s clearance time)	No	Not required (unipolar corona charger)	No
Drop	1.0/3.0	120 s	Yes	No	No

Table S4. Particle number concentrations and mean diameters in replicate tests

Material	Hydrophobic TiO <sub>2</sub>		Hydrophilic TiO <sub>2</sub>		Size range
	Number, #/cm <sup>3</sup>	Mode size, nm	Number, #/cm <sup>3</sup>	Mode size, nm	
Funnel	1,747	191.1	612	271.8	11.1–1,083.3 nm
	5,926	191.1	599	271.8	
Stirrer	891,782	209.1	81,840	710.5	34.0–1000.0 nm
	1,080,532	216.7	67,968	710.5	
Air jet	6,819	103.7	108,976	110.0	5.15–971.0 nm
	7,775	92.2	234,735	110.0	
Drop	4,500	835.0 (241.4)	1,351	1,486.0	0.0205–20.5 μm
	4,841	835.0 (299.6)	869	1,596.0	

Figure S1. Reproducibility of particle size distribution in replicate tests on hydrophilic TiO<sub>2</sub>

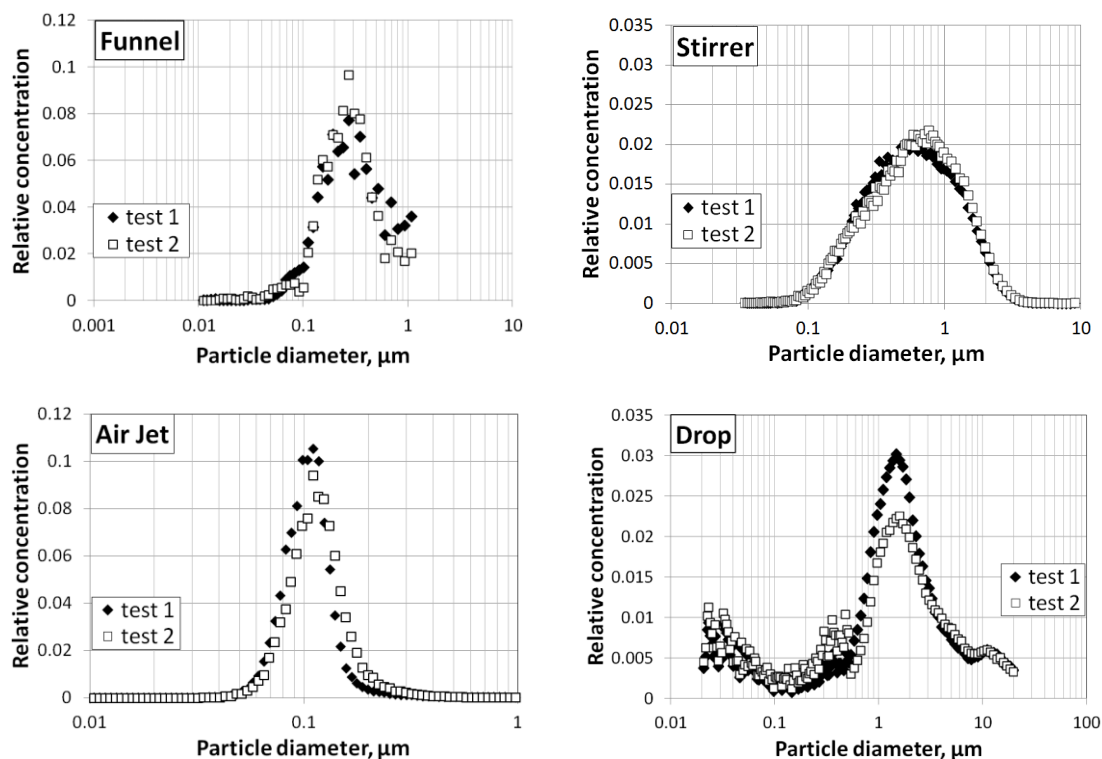
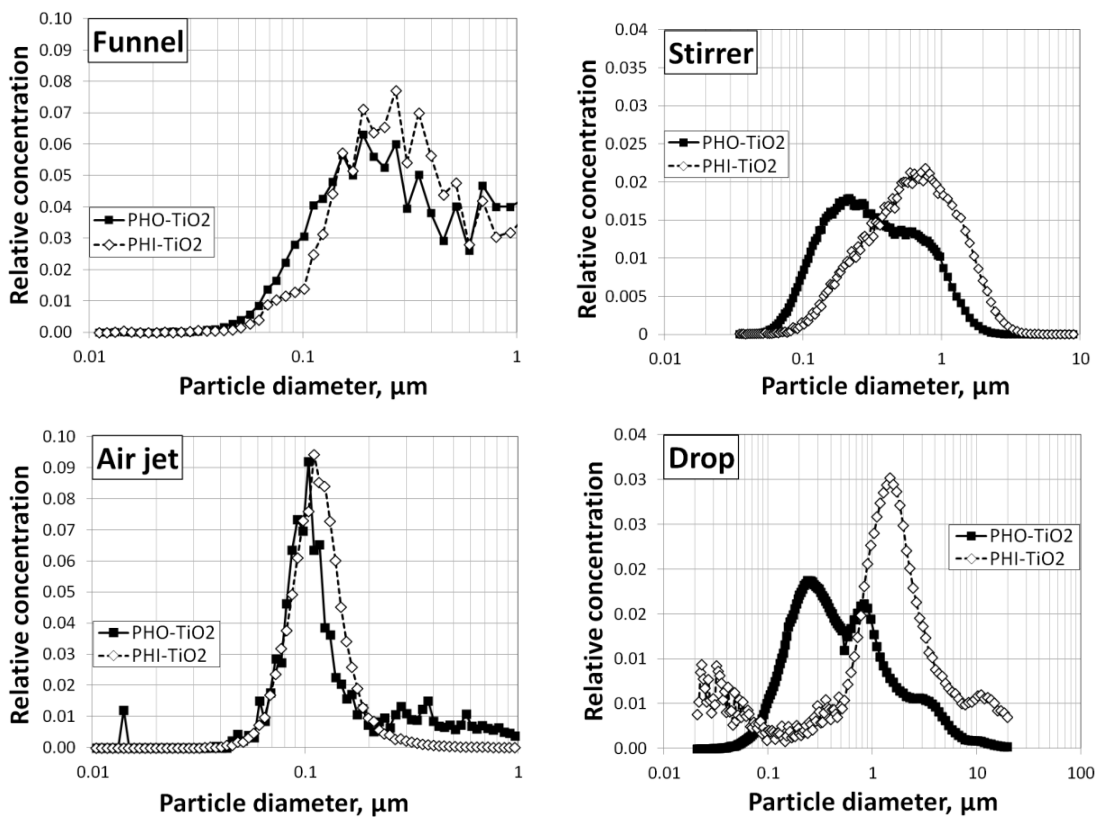


Figure S2. Comparison of size distribution for hydrophobic and hydrophilic TiO<sub>2</sub> aerosols



\*Citations in this article are compiled in the complete reference list at the end of this report.

## 6. DEAGGLOMERATION TESTING OF AIRBORNE NANOPARTICLES

### Publication 3

Deagglomeration testing of airborne nanoparticle agglomerates – stability analysis under varied aerodynamic shear and relative humidity conditions

Yaobo Ding<sup>1</sup>, Burkhard Stahlmecke<sup>2</sup>, Heinz Kaminski<sup>2</sup>, Yunhong Jiang<sup>3</sup>, Thomas A.J. Kuhlbusch<sup>2</sup>, Michael Riediker<sup>1,4</sup>

<sup>1</sup>*Institute for Work and Health (IST), Universities of Lausanne and Geneva, Route de la Corniche 2, CH-1066 Epalinges, Switzerland*

<sup>2</sup>*Institut für Energie- und Umwelttechnik (IUTA), Bliersheimer Straße 58-60, 47229, Duisburg, Germany*

<sup>3</sup>*Institute of Particle Science and Engineering, University of Leeds, LS2 9JT Leeds, UK*

<sup>4</sup>*SAFENANO, IOM Singapore, 30 Raffles Place, #17-00 Chevron House, Singapore, 048622, Singapore*

*Corresponding author: Michael Riediker; Tel.: +41 21 314 74 53; Fax: +41 21 314 74 30; E-mail address: Michael.Riediker@alumni.ethz.ch*

#### Abstract

Occupational exposure to nanomaterial aerosols poses potential health risks to workers at nanotechnology workplaces. Understanding the mechanical stability of airborne nanoparticles under varied environmental conditions is important for estimating aerosol size distribution which influences their distribution in the air and also their effects on the human body. In this study, two aerosolization and deagglomeration systems were used to investigate the deagglomeration potentials of nanopowder aerosols with different surface hydrophilicity under a broad range of relative humidity. Critical orifices were employed to apply shear forces induced by pressure drop onto airborne agglomerates. The applied pressure drops were associated with decreased mean particle size and increased particle numbers. Augmenting humidity increased particle size and reduced number concentration. Hydrophilic aerosols were more sensitive to the humidity changes than their hydrophobic counterparts. However, the testing systems also had an influence on the observations. The results suggest that the applied energies were able to overcome inter-particle binding force and trigger deagglomeration processes. The humid environment, on the other hand, facilitated agglomeration behaviors and reduced deagglomeration. It suggests that describing humidity of workplace air may be relevant when assessing human exposure to nanomaterial aerosols.

## Introduction

Engineered nanomaterials (ENMs) are widely used in various industrial sectors [8]. However, human exposure to aerosols of ENM powders have been shown at nanotechnology workplaces, in a variety of laboratory activities as well as industrial processes, such as synthesis, handling and cleaning [124, 125]. Distinct properties of released airborne ENMs (e.g., number concentration and size distribution) were identified in these scenarios; this may be associated with process characteristics such as energy input level. Different profiles of aerosol particles modify their transport and exposure routes, such as deposition in lungs [25]. Once inhaled, ENMs can pose various adverse effects in human bodies, such as inflammation [16], generation of oxidative stress [126], DNA damage [127], and translocation to secondary organs (thus potentially alter their functionalities) [32, 35]. The biological effects of ENM aerosols are closely related to their physicochemical characteristics such as particle number, size and surface area and functionality [19, 128, 129]. Therefore, health risks of airborne ENMs exist, and it is important to understand their properties when released into the environment in order to assess the risk level associated as well as for developing efficient methods for release and exposure preventions.

Understanding the mechanical stability of airborne particle agglomerates is very important for correctly estimating their size profiles. Aerosol particles often exist as agglomerates held together by different types of inter-particle forces [56]. It is probable that agglomerated particles break up into smaller agglomerates or even primary particles, when subject to larger dispersion forces during release, transport or along the exposure routes, and during inhalation through the mouth and the throat [63, 64]. Deagglomeration may modify the size distribution of aerosol particles, which in turn can lead to their altered biological interaction behaviors. Thus, it is beneficial to study the deagglomeration potential of airborne nanoparticles under a range of energy inputs and environmental conditions, in simulating broad real-life exposure scenarios.

Aerodynamic deagglomeration processes have been studied using various systems, such as an orifice or a nozzle, capillary tubes, stationary plate, mixer disperser, and fluidized bed [130]. Aerosol particles are accelerated through an orifice which creates shear flow; this condition induces turbulence and shear forces on the particles, and promotes their collisions [65-67, 101]. Capillary tubes deagglomerate airborne particles by velocity gradient from sheath flow and by

impaction at the tube inlet [131]. Mixer disperser and fluidized bed induce similar turbulent conditions resembling above processes [118, 132, 133]. Stationary plates break particles by impaction on their surface, in addition to acceleration mechanism from a nozzle [85, 134, 135]. These methods feature a range of energy inputs and have been used for achieving different aerosol dispersion levels.

Relative humidity (RH) is known to have an influence on aerosol properties. The most prominent effect is to facilitate moisture condensation on particle surface or inside agglomerate capillaries, enhancing their agglomeration by capillary force [136]. This process modifies the size distribution of aerosols, and may change their behaviors in deagglomeration processes. Numerous studies have investigated RH effects on dispersion of micro-sized pharmaceutical powder particles [137-139], however, few studies had looked at deagglomeration behaviors of nanoparticles, especially for aerosols created from industrial powders which are associated with occupational risks. Due to a different water condensation mechanism for nanoscale particles, they may be more sensitive for humidity changes than their macroscopic counterparts [136, 140].

In the present work, we used two aerosolization and deagglomeration systems that are based on the orifice method to study the deagglomeration potential of nanopowder aerosols under a range of RH conditions. Identically sized titanium dioxide nanopowders with two different surface hydrophilicities were tested to study the humidity effects. A broad range of energy inputs were applied to the airborne particles in order to provide a comprehensive understanding of the deagglomeration process.

## **Materials and Methods**

### **Materials**

The tested nanomaterials were obtained from the repository at the European Commission Joint Research Center (JRC–IHCP in Ispra): hydrophobic (NM103) and hydrophilic (NM104) nanoscale TiO<sub>2</sub>. The primary particle size is 20 nm (determined by x-ray diffraction), with a specific surface area 60 m<sup>2</sup>/g. The crystal structure is rutile.

### **Test systems**

The setups used in this study were previously described in detail [65, 67, 141]. Both methods used critical orifices to apply shear force onto aerosol particles, but differed in their approach to create the aerosol from a powder. The detailed schematics of the two systems are available in the supplemental information (SI, Figure S1).

The funnel-based aerosol generator [65] uses the fluidized bed system concept, in which a steady air flow passes through the bottom opening of a funnel filled with powder and thereby continuously activates the dry powder. The aerosol generation can be maintained for long periods (> 30 minutes) at stable particle number concentration and size distribution. The aerosol is led into a mixing chamber and conditioned to target humidity by mixing the dry aerosolization flow (~2% relative humidity) with humid air (RH>90%). The aerosol then passes through a critical orifice into a large collection volume from which several sampling lines collect particles for characterizations. Devices used to characterize the aerosol in this study included a scanning mobility particle sizer (SMPS, GRIMM, particle number size distribution and total count in the range of 11.1–1083.3 nm), an optical particle counter (GRIMM, number size distribution and counts in the range of 0.25-32  $\mu\text{m}$ ), and a mini-sampler (ECOMESURE, Janvry, France) that collects airborne particles by impaction directly onto TEM grids (200 mesh, copper, Formvar/Carbon).

The second system is based on aerosolizations by a magnetic stirrer in a pressurized beaker [67]. The generated aerosol is then mixed with humidified air. The aerosol is subsequently introduced into a cyclone to remove particles above appr. 1.5  $\mu\text{m}$ . The aerosol then passes a critical orifice and is subsequently measured by online and offline equipments. Make-up air is added beforehand to satisfy the total flow rate needed for characterizations. A SMPS (34-1000 nm, electrical mobility, TSI) and a Palas WELAS (0.4-17  $\mu\text{m}$ ; optical diameter) are used to measure particle number and size distribution. The airborne particles are collected on flat single-crystalline silicon substrates with an area of 1 x 1 cm, by a Nano Aerosol Sampler (TSI, Model No. 3089) with a home-made unipolar charger unit upfront. The samples were subsequently analyzed by a high resolution scanning electron microscope (JEOL 7500F).

The test conditions are listed in **Table 1**. The RH ( $\pm 5\%$ ) and the pressure drops ( $\pm 2\%$ ) were well maintained during the experiments. The pressure drop level is proportional to the total air flow volume passing the orifice. During the test, the aerosolization flow was kept constant, in order to

avoid changes of aerosol profiles due to different aerosolization levels. Only the dilution flow rate was tuned to modify the total flow. The aerosol particles are accelerated in the orifice, and the total volumic flow rate determines the air speed (thus basically the particle velocity). The air velocity increases with flow rate until a critical condition (choked orifice) is reached when the upstream pressure is appr. two times higher than the downstream pressure. This is the 100 kPa pressure drop in our study (since the downstream atmosphere was at ambient pressure). The particles experience shear stress in the orifice and subsequently strong resistance by the ambient air when ejected out of the orifice. The sheath flow and the drag from the air molecules are mainly responsible for potential deagglomeration. The drag force is proportional to the relative velocity between the particle and the medium as well as to particle diameter [58]. Thus, larger pressure drops apply higher energy inputs on the particles, leading to potentially more significant deagglomeration.

**Table 1 Experimental conditions tested in the two systems**

	Pressure drop, kPa				Relative humidity, %			
	0	50	100	150	0	25	50	75
Funnel	0	50	100	150	0	25	50	75
Stirrer	0	50	100	150	0	30	50	70

### Data analysis

Particle number size distributions, geometric mean sizes and total numbers under different pressure drop and humidity conditions are compared to show the influences of these two parameters. The spectra were normalized with respect to total particle number concentrations. Furthermore, Particle fraction in three size ranges (<100, 100-350, 350-1000 nm) were compared with regard to different conditions. Particle number concentration in individual size channels were summed respectively in the three ranges, and divided by the total number. The <100 nm fraction represents nanoscale particles. The 100 to 350 nm range represents those small particles

that are outside the nanoscale but with aerodynamic behavior still mostly dominated by Brownian motion, while the particle fraction  $>350$  nm is dominated mostly by inertia.

Statistical analysis was performed, wherever sufficient number of experimental replicates was available, on particle number and mean size obtained under different pressure drop and humidity conditions. Analysis of variance (ANOVA) and the comparison of geometric mean sizes measured under different conditions were calculated with Stata (Stata CorpLP, Texas, USA). A p value below 0.05 was considered significant. Spearman rank correlation (coefficient  $r_s$ ) was used to analyze the correlations of changes in mean particle size to test parameters. In addition, regression analysis was performed for changes of particle number in individual size channels under varied humidity and pressure drop conditions.

## Results

### Comparison of systems and powders under basic (non-orifice) test conditions

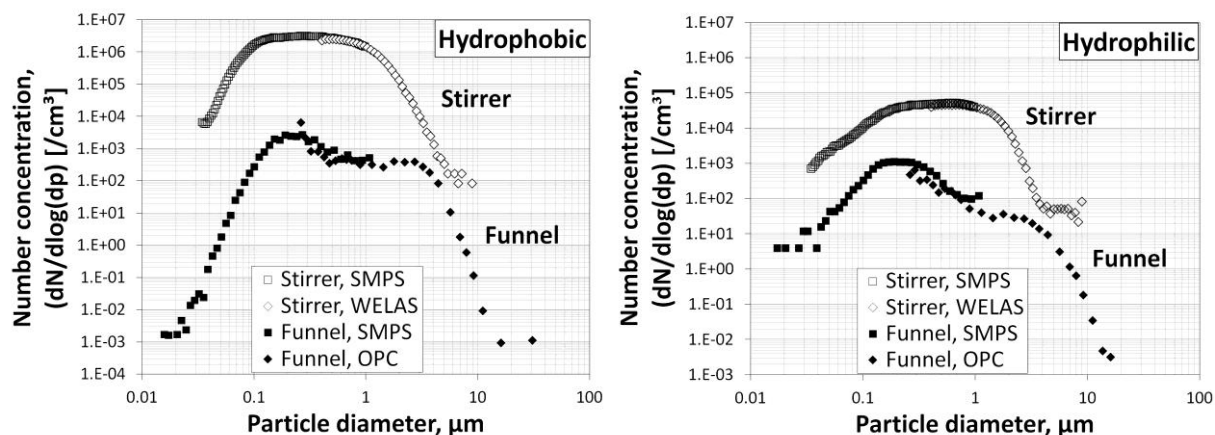


Figure 1 particle number size distribution of the aerosols generated from the two types of nanopowders, left: hydrophobic  $\text{TiO}_2$ , right: hydrophilic  $\text{TiO}_2$  (no orifice,  $\text{RH}=0\%$ ).

A comparison on the particle size distributions of aerosols generated from the two test setups under basic conditions (without orifices,  $0\%$  RH) is shown in **Figure 1**. In general, the size spectra from the stirrer system were broader than those from the funnel system. The higher peaks created in the stirrer system indicated higher total particle concentrations. The hydrophobic powder generated higher aerosol concentrations than the hydrophilic powder did, and also

smaller mode diameter. The data measured by the SMPS and by the optical counters were in general consistent (demonstrated by the smooth transition on the curves). The two systems featured different aerosolization mechanisms, quantity of raw materials used (250 mg v.s. 5-8 g) and air flow rate; these may be responsible for the varied aerosol profiles created. Different aerosolization means have been shown to result in distinct aerosol properties [88], and this may lead to varied deagglomeration behaviors of the aerosol particles.

### Effects of pressure drop and humidity on particle number size distribution

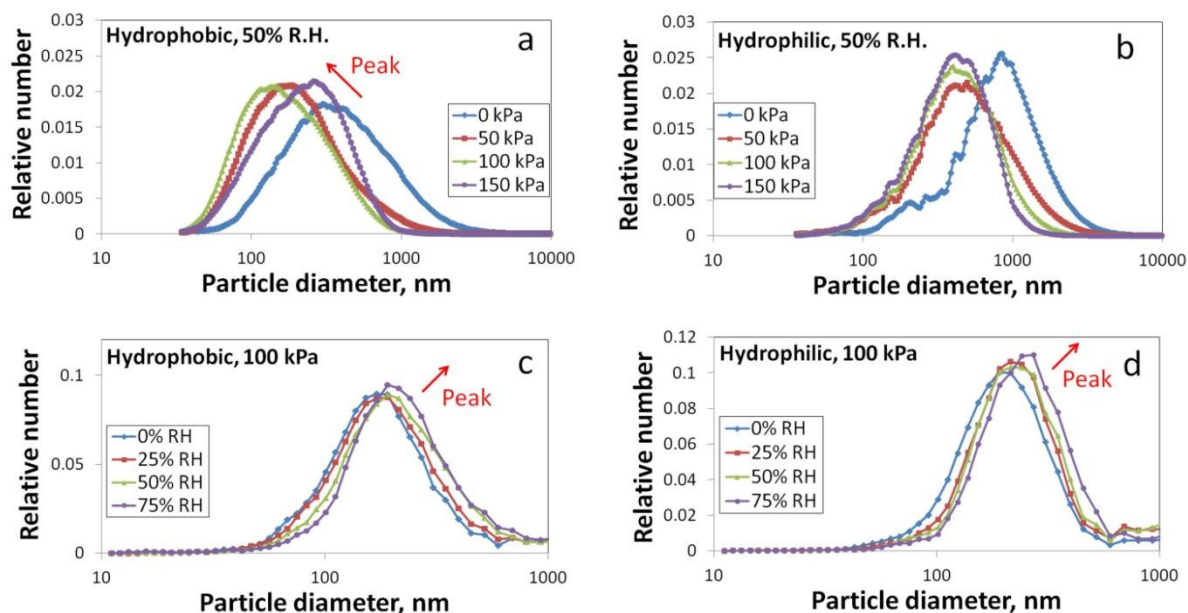


Figure 2 Comparison of particle size distributions (a,b: pressure drop effects at 50% RH, stirrer; c,d: humidity effects at 100 kPa pressure drop, funnel)

The influences of pressure drop and humidity on aerosol size distribution are shown in **Figure 2**. The highest pressure drop (100 kPa) and mid-range relative humidity (50%) are taken as examples. Higher pressure drops shifted the spectrums to the smaller size range (**Figure 2 c,d**). The effects seemed to be more evident for the hydrophilic particles (NM104) than for the hydrophobic ones (NM103), as abnormal behaviors were observed at 150 kPa for the latter (**Figure 2c**). On the other hand, increasing humidity resulted in larger mode sizes for both materials (**Figure 2 c,d**). Moreover, the peaks became higher under humid atmosphere. The decreased mode size and higher peaks indicates the deagglomeration events triggered by pressure drop. The larger modes suggests that moisture content facilitated agglomeration among particles.

### **Influence of pressure drop and humidity on particle mean size and number concentration**

The changes of mean diameter and total particle concentration under varied pressure drop and humidity conditions are shown in **Figure 3**. In general, particle sizes decreased with increasing pressure drop, but the number concentration was less consistently linked to pressure drop. The particle number experienced significant augmentations up to 15 folds in almost all cases compared to the reference condition (**Figure 3 e-h**), with larger variations in the stirrer system. Comparing the two systems, the stirrer resulted in larger mean particle size than the funnel did. Pressure influences seemed to be equally significant for both materials. On the other hand, humid conditions increased mean particle diameter and greatly decreased particle number. Its influences seemed to be more prominent for hydrophilic aerosol particles than for their hydrophobic counterparts (**Figure 3 i-l**). It was noted that at atmospheric pressure the RH condition did not significantly modify the particle size of the hydrophobic aerosols created in the funnel system (**Figure 3i**). These findings suggest that the pressure drops created turbulent conditions in the air flow, which promoted particle collisions. This facilitated agglomeration by moisture content condensate on particles surfaces. The size changes seen in the funnel system may not be as obvious as those in the stirrer system, thus statistical analysis was performed for **Figure 3 a,b,i,j**. All the correlations of these size changes in relation to the two variables were statistically significant, only except for one condition (hydrophobic TiO<sub>2</sub> at 0 kPa, **Figure 3i-diamonds**). The complete results are available in the supplemental information (Table S1).

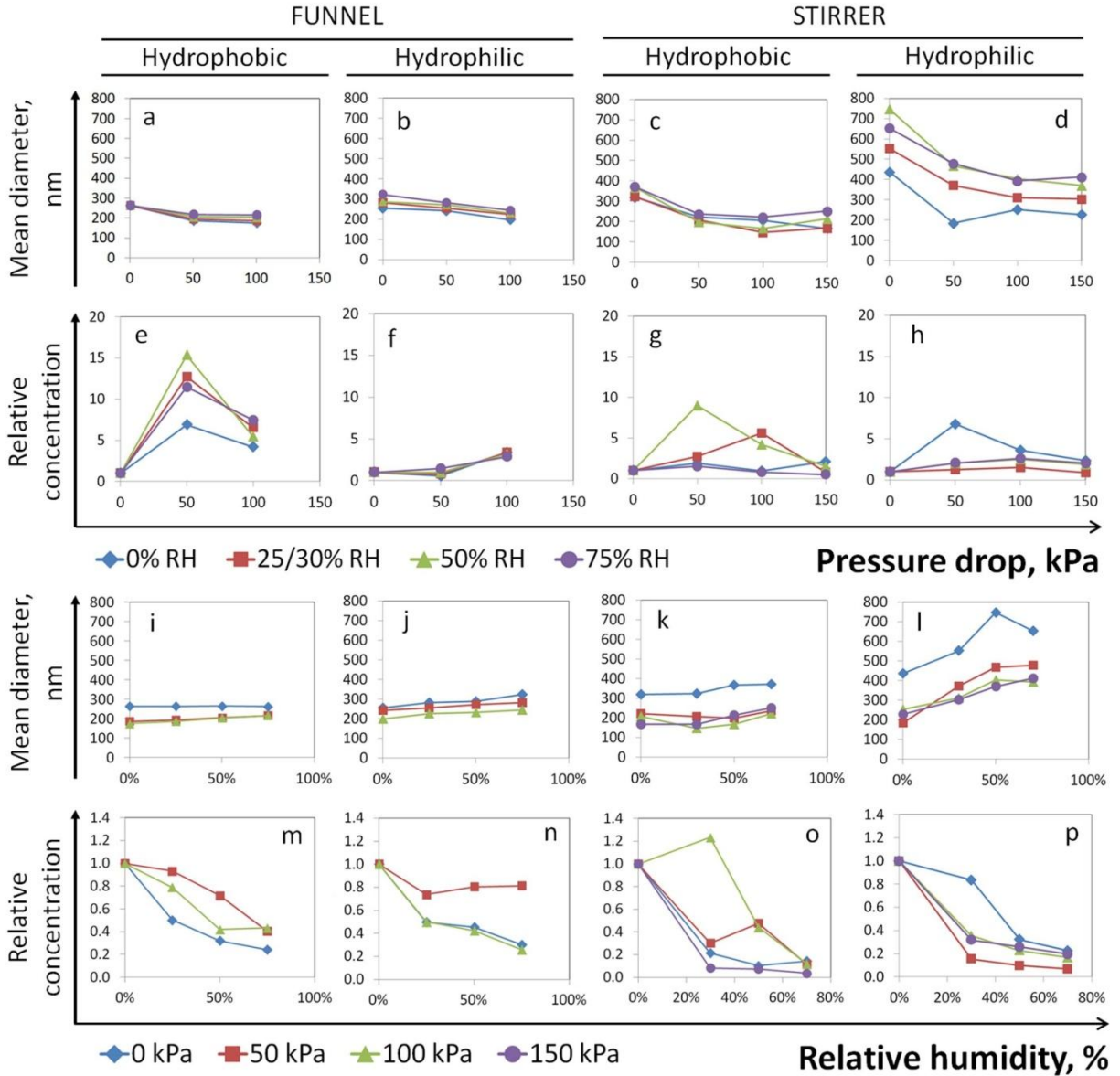


Figure 3 Effects of pressure drop and relative humidity on particle mean diameter and total number concentration of hydrophobic (NM103) and hydrophilic (NM104) TiO<sub>2</sub> aerosols. Total particle number concentrations are in relative scales, compared to the reference conditions (0% RH / 0 kPa).

### Influence of humidity and pressure drop on aerosol properties

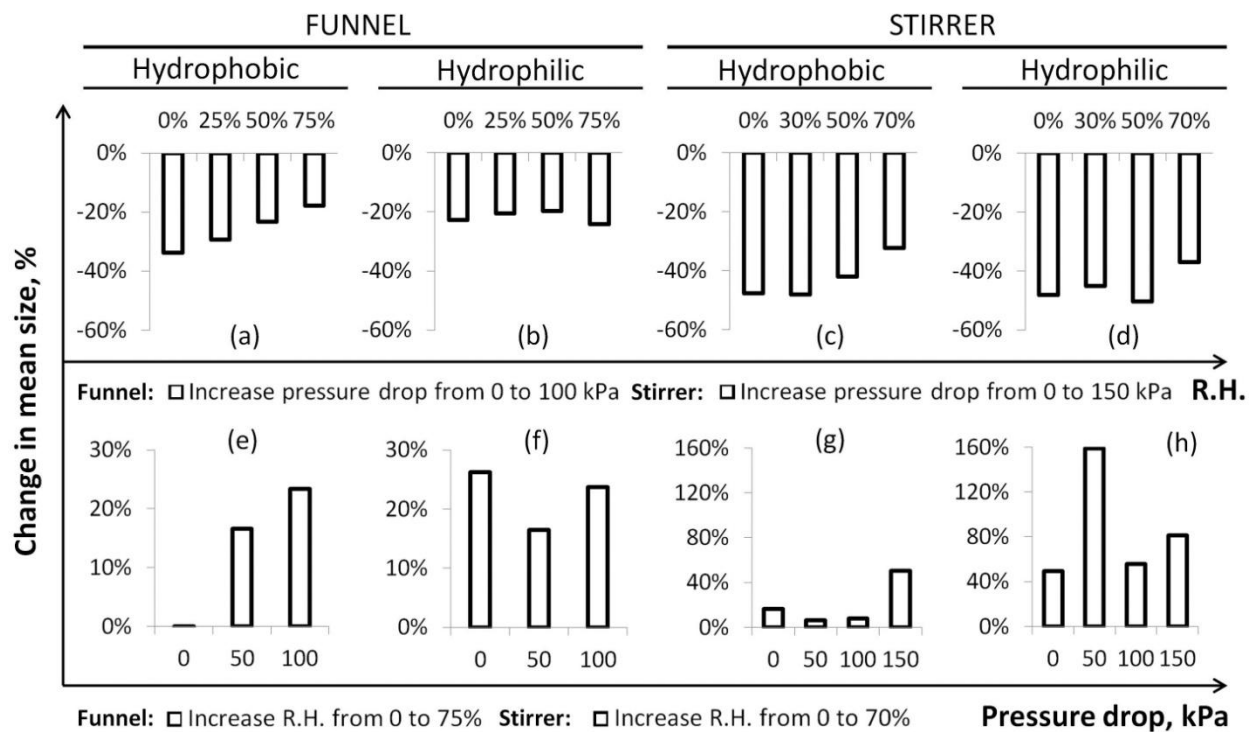


Figure 4 Influence of pressure drop and relative humidity on mean particle size. The results show the increase (+) or reduce (-)

How humidity influenced the effects of pressure drop on aerosol profiles is shown in **Figure 4**. For the hydrophobic aerosols, the decrease of particle size with pressure drop was reduced under higher humidity (**Figure 4a**). For the hydrophilic aerosols, the degree of reduction in particle size with pressure drop seemed to be independent of humidity (**Figure 4b**). Comparing to the funnel system, the stirrer system induced more significant reductions in particle size (**Figure 4c,d**). How pressure drop influenced the effects of humidity on aerosol profiles is shown in **Figure 4** (e-h). For the hydrophobic aerosols in the funnel system, the effects of humidity only showed up when pressure drops were applied. (**Figure 4e**). The overall humidity effects became stronger when increasing pressure drop. For hydrophilic aerosols, the effects of humidity remained similar under different pressure drops (**Figure 4f**). In the stirrer system, comparing the two materials the hydrophilic particles experienced larger changes by humidity than their hydrophobic counterparts (**Figure 4g,h**). The data presented here compare the particle size changes observed under the lowest and the highest values of the two variables: 0 - 100 (150) kPa and 0% - 70 (75)%. A more detailed analysis using the values within these ranges, such as from 0 to 50 kPa

or from 50% to 75%, is available in Figure S2 (SI). The analysis shows that for smaller particles generated in the funnel system, to achieve the same degree of size reduction, higher pressure drop was required for the hydrophilic particles than for the hydrophobic ones; for larger particles generated in the stirrer system, most of the effect was already observed in 0-50 kPa pressure drop range for both two materials.

### **Effects of pressure drop and humidity on particle fractions in different size ranges**

The influences of pressure drop and humidity on particle number fractions are presented jointly in 3D in **Figure 5**. The particle fraction below 100 nm increased significantly with the pressure drop but decreased with the relative humidity (inserts a-d). In contrast, number fraction in > 350 nm size range responded conversely to the pressure drop and humidity (inserts i-l). The particle fractions between these two size ranges registered minor increases with pressure drop and decreases with humidity (inserts e-h). It is noteworthy that increases induced by pressure drop in <100 nm range were more significant at lower humidity, such as 0% or 30% (inserts a-d: red dotted curves). Comparing the two materials, the hydrophobic aerosols consisted of up to 40% particles below 100 nm (inserts a,c), whereas their hydrophilic counterparts had only 10-25% in this size range (inserts b,d). In comparison, the hydrophilic aerosols had much higher fractions in >350 nm range (max. 80% v.s. max. 50%). The hydrophobic particles experienced larger changes in the size range below 100 nm (comparing inserts a,c to b,d), while the hydrophilic ones did so above 350 nm (comparing inserts i,k to j,l). Comparing the two systems, hydrophobic aerosols in the stirrer setup were still composed of about 60% particle in >350 nm range at the highest pressure drop (insert l, circled), whereas they had only around 20% in the funnel setup (insert j, circled). In general, the stirrer system generated large particles in higher fractions and nanoscale particles in lower fractions than the funnel did. This may primarily contribute to their different responses to the test variables. The results were in line with the observations on modifications of the mean particle size by pressure drop and humidity.

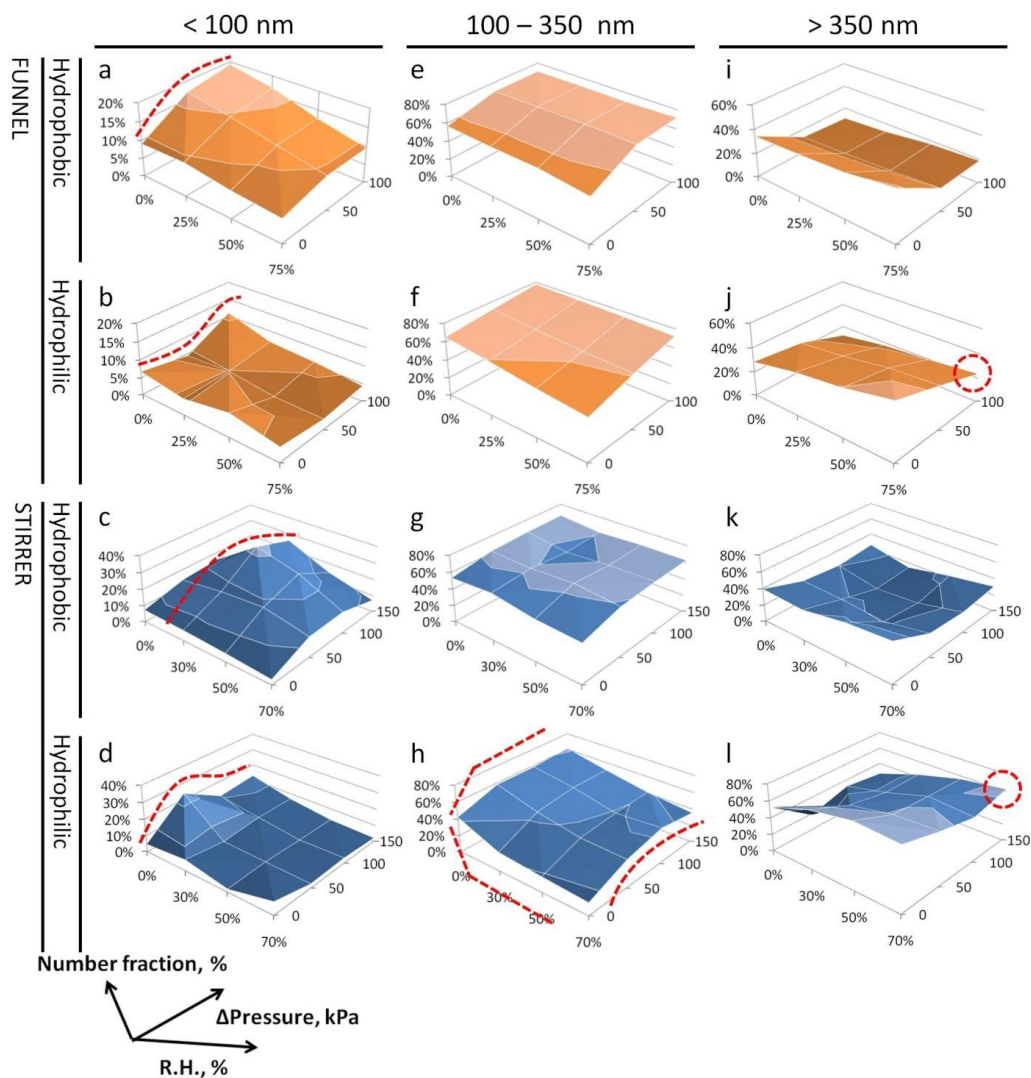


Figure 5 Effects of pressure drops on particle number fractions in three different size ranges (<100 nm, 100-350 nm, >350 nm) for the hydrophobic (NM103) and hydrophilic (NM104) TiO<sub>2</sub> aerosols.

Particles with different size profiles may respond differently to humidity changes. Influences of pressure drop and humidity on particle number in each size channels were analyzed by regression analysis, in order to investigate which size ranges were the most sensitive to these two variables (**Figure 6**). The results are presented under exemplary conditions, such as 100 kPa and 0% RH. As humidity increased, the most reduction in particle number (relative change with respect to the total) was seen in the size range below 100 nm, peaking in 40-80 nm. (**Figure 6**, left). The responses decreased for larger particles. For the effect of pressure drop, particle

numbers in the size range below 271.8 nm was increased (positive values), while those above this size decreased (negative values) (**Figure 6**, right). The numbers of nano-sized particles and of those close to 1  $\mu\text{m}$  were affected the most. Moreover, the most sensitive particle size with respect to pressure change was larger under higher humidity (Figure S3, SI). The results suggest that the humid conditions tended to reduce nanoscale particles, while its effect was less significant for larger particles. For the pressure drop condition, it seemed to facilitate the generation of particles around or below 100 nm, however, the moisture content somehow prevented this process by acting as a glue as discussed previously.

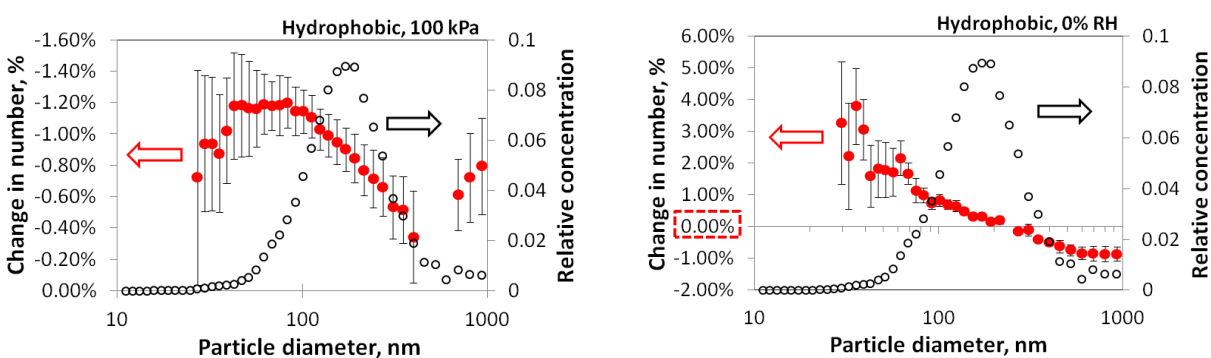


Figure 6 Changes of particle number in individual size channels (SMPS) by increasing relative humidity (left) and by increasing pressure drop (right). Particle size distributions at 0% RH (open circles) are also presented for comparison purposes. Only statistically significant values are plotted ( $p < 0.05$ ). Error bars represent 95% confident intervals. Data are from the funnel system on the hydrophobic  $\text{TiO}_2$ .

### Morphological analysis of airborne nanoparticles

Morphological analysis of aerosol particles generated in the funnel system is shown in **Figure 7**. The images are presented in micro-scale for overall distribution of particles on the filter, as well as in nano-scale to show morphologies of individual agglomerates and primary particles. Comparing the two materials, NM104 generated larger agglomerates than NM103 did. The agglomerates of the hydrophobic  $\text{TiO}_2$  were generally smaller than 1  $\mu\text{m}$ , while those of hydrophilic  $\text{TiO}_2$  can reach sizes up to several microns. The primary particles typically had spherical or rod-like shapes. The hydrophobic coatings were not visible under the microscope.

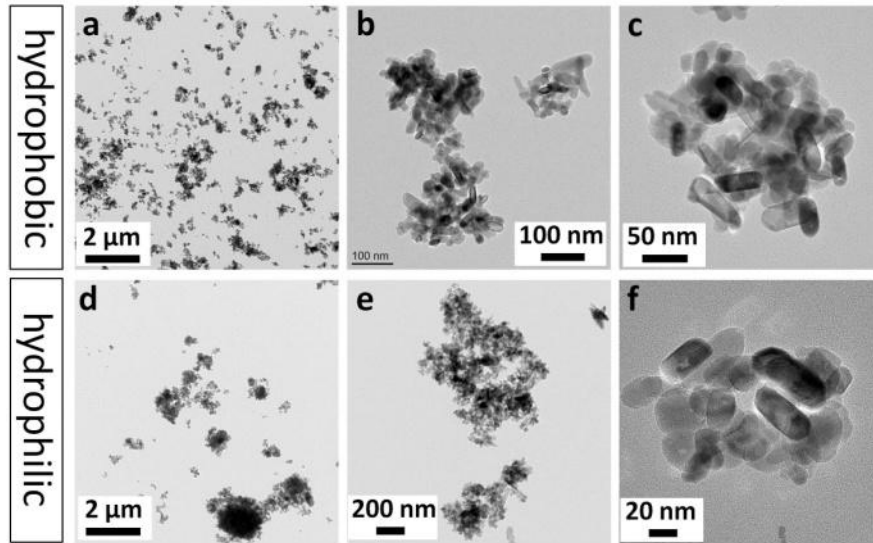


Figure 7 TEM analysis of particle morphology in the funnel system for the hydrophobic (NM103) and hydrophilic (NM104) TiO<sub>2</sub> aerosols (conditions: 0 kPa/0%).

The airborne particle morphologies observed in the stirrer system is shown in **Figure 8**. The results obtained under the lowest and the highest pressure drops and humidity were compared. Particle size seemed to be smaller and deposition was denser, when treated by higher pressure drop, both at low and high humidity (**Figure 8**: comparing a to b, c to d). In contrast, higher humidity resulted in much lower particle density on the grid, both at low and high pressure drops (**Figure 8**: comparing e to f, g to h). Comparing the two materials, NM104 (hydrophobic) had significantly lower particle generation than NM103 (hydrophilic) (**Figure 8**: comparing d to h). The particle agglomerates were densely packed and had irregular shapes. Chain-like structures and very larger agglomerates were sometimes observed when treated with no pressure drop (**Figure 8** a,c,e,f), whereas the highest pressure drop mostly resulted in spherical particle agglomerates (**Figure 8** b,d,g,h). The microscopic observations on the effects of the two variables regarding particle number concentration and mean size were in line with the online measurement results.

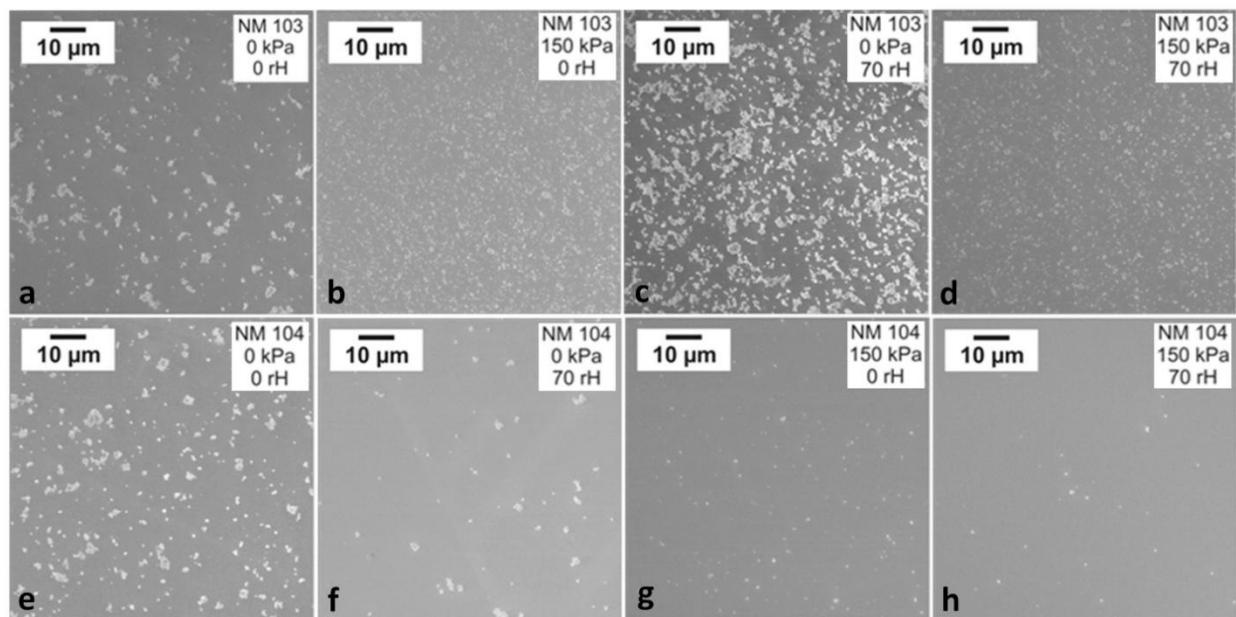


Figure 8 SEM observations on particle morphology in the stirrer system

## Discussion

The increased particle number concentration and decreased mean size, as well as changes in fractions for large and nanoscale particles suggest that the rapid transfer through the orifice induced by the pressure drop caused a deagglomeration process. Higher speeds induced larger drag forces on the particles, being responsible for the reduction of particle size. The air flow velocity stops increasing above the critical condition, and this may be responsible for the decreased effect of pressure drop at 150 kPa. The degree of drag is not much changed when further increasing upstream pressure above choked condition. Moreover, the drag force is proportional to particle diameter; this may explain its more significant effects on the aerosols with a larger mean size, such as those generated from the hydrophilic powder (NM104) and from the stirrer system. The less correlated number concentration can be due to different powder pre-treatment, such as powder storage [142] or filling into the aerosolizers. The variation of absolute particle generation in these two systems can vary up to several folds but will stay usually well within the same order of magnitude. Thus most of the changes seen in our study were attributable to the modifications of pressure and humidity. These observations are consistent with the findings from previous studies using orifices to break nanoparticle agglomerates. Ding and

Riediker tested pressure drops up to 300 kPa with different types of materials and found that deagglomeration mostly occurred below 100 kPa [65]. Significant deagglomeration took place already at minor increases of the upstream pressure (as low as 20 kPa) and the pressure-number curves suggested a non-linear dependency of the deagglomeration from the applied shear force. This behavior was also seen for the hydrophobic aerosols in our study (**Figure 3** a,c: reduced effect from 0-50 to 50-100 kPa). Stahlmecke et al. [67] also observed good negative correlations between pressure drop (up to 140 kPa) and nano-aerosol mean particle sizes. Sosnowski et al. demonstrated deagglomeration of micro-sized pharmaceutical powder particles using a converging nozzle [101]. These studies were all conducted in relatively dry environments (RH<15%).

Relative humidity showed an opposing effect by increasing particle size and decreasing particle number. This suggests that the air moisture content promoted agglomeration between primary particles. In this process, two mechanisms can be considered: 1. A thin layer of water molecules condenses on the particle surface with increasing humidity, and particles are subsequently bonded upon collisions by the water content on their surface; new agglomerates are created; 2. Moisture condenses directly in capillaries inside the particles (capillary condensation), thus strengthening the original agglomeration. The capillary force can be related to RH by the following equation [136]:

$$F = 4\pi\gamma cR^* \left(1 - \frac{D}{\sqrt{\frac{V}{\pi R} + D^2}}\right)$$

where:  $\gamma$ , surface tension of the liquid interface;  $c$ , factor related to the contact angle;  $R$ , radius of particle;  $R^*$ , for two identical spheres  $R^* = R/2$ ;  $D$ , contact distance of two particles;  $V$ , volume of water meniscus.

Increasing ambient humidity would lead to formation of larger meniscus volume ( $V$ ) between contacting particles, which in turn results in stronger attractive force. This may explain the continuous increase of particle size and reduction of particle number, as well as the less significant effects of the pressure drop observed at high RH level. The hydrophilic surfaces facilitate faster water condensation with smaller contact angle at the liquid interface, resulting in an augmentation of the capillary force; this may be responsible for the different responses of the

two tested materials to humidity changes: at high RH, even treated with the largest pressure drop the hydrophilic aerosol particles remained still in much larger sizes than their hydrophobic counterparts. Capillary force was shown to vary with relative humidity, being monotonic increase or decrease, peaking at certain RH, step-wise increase or independent of RH, depending on the particle properties such diameter, shape, surface hydrophilicity and roughness. [136, 143].

Deagglomeration can occur when the dispersion force, which is related to the drag force in our case, is comparable to the interparticle binding force. In a simulation study, researchers found that nanoparticle aggregates started to deform even when the dispersion force under shear flow reached 0.1% of the interparticle force [117]. In our study, the dominant mechanisms for particle agglomeration were van der Waals (VDW) force and capillary force. The VDW interaction is normally much less significant than the capillary attraction and would be partly screened if moisture content is present [140]. Thus, only the capillary force is considered in our study as the main interaction mechanism between particles. The exact capillary force range in our study would be complex to calculate because of many undefined parameters, however, for a rough estimate one could refer to the values given in other studies for similar conditions, such as 10-30 nN for 30 nm spheres at 0° contact angle, 90-180 nN between a nanoscopic AFM tip and a silicon wafer [136], 0-80 nN between a 100 nm spherical particle and a flat surface at 0-100% RH [140]. On the other hand, as a driving force for dispersion, the drag is calculated using the following equation (Hinds 1982):

$$F_D = \frac{3\pi\eta v D}{C}$$

where:  $\eta$ , air viscosity;  $v$ , relative velocity;  $D$ , particle diameter;  $C$ , slip correction factor; assuming a dynamic shape factor of 1.

In our work, the maximum flow speed can reach that of the sound ( $\approx 340$  m/s, 20°C) under choked flow condition at 100 kPa pressure drop. This would result in a drag force level up to 50 nN for 0.1-1  $\mu\text{m}$  particles. This range may provide dispersion forces which are comparable with the estimated capillary interaction. This suggests that with the energy input range we applied in our experiments, deagglomeration can take place not only with dry particles but also under humid conditions. This may support our finding that although humidity helped to facilitate

agglomeration, the pressure drop still played an observable role in reducing the mean particle size at high RH.

The fact that a low pressure drop showed significant effects for hydrophobic particles indicate that the agglomeration force was mostly likely dominated by weaker van der Waals interactions between relatively dry particles. For hydrophilic particles, prominent influences were seen only when a high pressure drop was reached, which suggests that particle interaction in this case may have been strengthened with moisture condensation. The only difference between the two materials is their surface hydrophilicity. The stronger pressure effects seen in the stirrer than in the funnel maybe be caused by the larger particles generated in the former system; a stronger drag is expected for a larger particle diameter. The bigger particles might be also responsible for the result that significant pressure drop effects on the hydrophilic particles started at lower values in the stirrer system (0-50 kPa) than in the funnel system (50-100 kPa). Drag force is proportional to particle size as shown in Figure S5 [58]. As the size increases, the dispersion force may become high enough at a certain point, which overcomes the capillary interaction and trigger particle deagglomeration. Thus, a lower pressure drop might be able to exert prominent effects on the large particles generated from the stirrer. The enhanced humidity effects at higher pressure drops for the hydrophobic particles may be due to the fact that more collision events triggered by turbulent flow promoted agglomeration by the water content absorbed on particles surface (even though the absorption can be weak depending on how hygroscopic the surface is). Another possible explanation is that smaller particles generated under higher pressure drops were more sensitive to humidity changes [140]. For hydrophilic particles, agglomeration by capillary force may already exist due to the moisture content in the raw powders (resulting in different aerosol properties from the two materials when tested even in completely dry environment, as shown in **Figure 1**). This may explain their less responsive behaviors to the increasing humidity when treated by pressure drop (**Figure 4b**).

## Conclusions

In this study, we observed significant effects of pressure drop and relative humidity on aerosol particle properties. Pressure drops generally decreased particle size, and increased total particle

number. Elevating relative humidity generally led to increased particle size and decreased total particle number. The humidity influence on the hydrophilic aerosols (NM104) was very evident in both systems. In contrast, the two systems differed when testing the hydrophobic material (NM103): the effects were significant (though weaker than for NM104) in the funnel system, while they were less clear in the stirrer system. This might be due to the different particle size spectra generated in the two systems (normally smaller in the funnel system). Humidity conditions may affect small particles more than big particles. For particle number counts, the effects of pressure drop and humidity were not very clear, which can be attributed to the inter-test variability of absolute particle number concentrations in the aerosolization tests (up to an order of magnitude). The increased number and decreased size suggested particle agglomeration under humid conditions and deagglomeration under external energy inputs. The shear force from the drag of ambient air induced by critical orifices was responsible for the deagglomeration of particles. The bridging effect of absorbed surface water content and resulting capillary forces promoted airborne particle agglomeration. Mean particle size increased continuously with humidity, which indicates lower deagglomeration levels by the pressure drops, whereas the applied shear forces altered aerosols' responses to humidity, possibly by modifying their size profiles.

The results suggest that aerosol properties, including particle size and surface hydrophilicity, play a relevant role for the deagglomeration potentials under varied relative humidity. In occupational exposure scenarios, it is possible that aerosolized nanopowder particles can be further deagglomerated when the energy input reaches a certain level. Particle deagglomeration started to take place at low shear forces, which applies to common nanomaterials handling activities in occupational settings. It will be important to know if humidifying workplace environments can contribute to reduce numbers of small particles, thereby alleviating workers' exposure risk.

## **Acknowledgement**

This study received the financial support from the EU FP7 project on Managing Risks of Nanomaterials (MARINA, grant agreement no: 263215). The authors gratefully thank Dr. Guillaume Suarez (IST) and Mr. Gregory Plateel (IST) for their excellent laboratory supports. The authors also wish to thank Dr. Pascal Wild for his assistance in statistical analysis.

**\*Citations in this article are compiled in the complete reference list at the end of this report.**

## Supplemental Information (SI)

Figure S1 Schematic diagrams of the funnel (top) and the stirrer systems (bottom) used for the deagglomeration tests

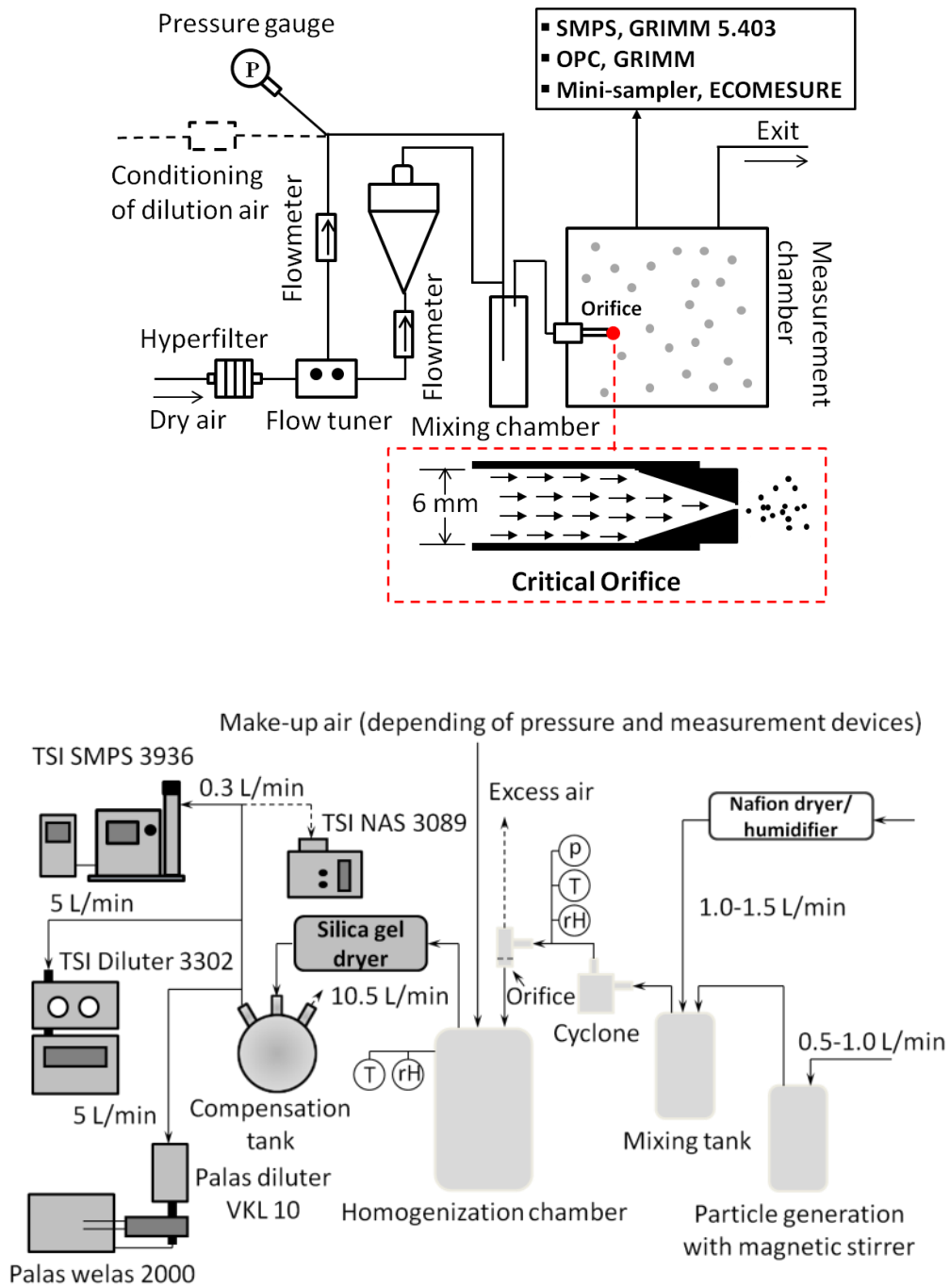


Table S1 Correlations of mean particle size with the four RH and the three pressure drop conditions shown in

Figure 3 a,b,i,j.

RH/ $\Delta$ P	Hydrophobic TiO <sub>2</sub>		Hydrophilic TiO <sub>2</sub>	
	r <sub>s</sub>	p	r <sub>s</sub>	p
0	-0.9418	<0.0001	-0.9383	<0.0001
25%	-0.942	<0.0001	-0.6913	0.0004
50%	-0.942	<0.0001	-0.8727	<0.0001
75%	-0.8425	<0.0001	-0.9304	<0.0001
0 kPa	-0.0664	0.7322	0.8638	<0.0001
50 kPa	0.9684	<0.0001	0.9055	<0.0001
100 kPa	0.8633	<0.0001	0.9463	<0.0001

r<sub>s</sub>: Spearman's coefficient, positive correlation (+) and negative correlation (-), p: statistical significance.

Figure S2 Influence of pressure drop and relative humidity on mean particle size. The results show the increase (+) or reduce (-). The effects were much more significant by increasing pressure drop from 0 to 50 kPa than from 50 to 100 kPa (a: comparing blue to red rectangles). Particle sizes were reduced more by increasing pressure drop from 50 to 100 kPa than from 0 to 50 kPa (b: comparing blue to red rectangles). The pressure drop effects were the most predominant in 0-50 kPa range, for both material types (c,d: comparing blue to red or purple rectangles).

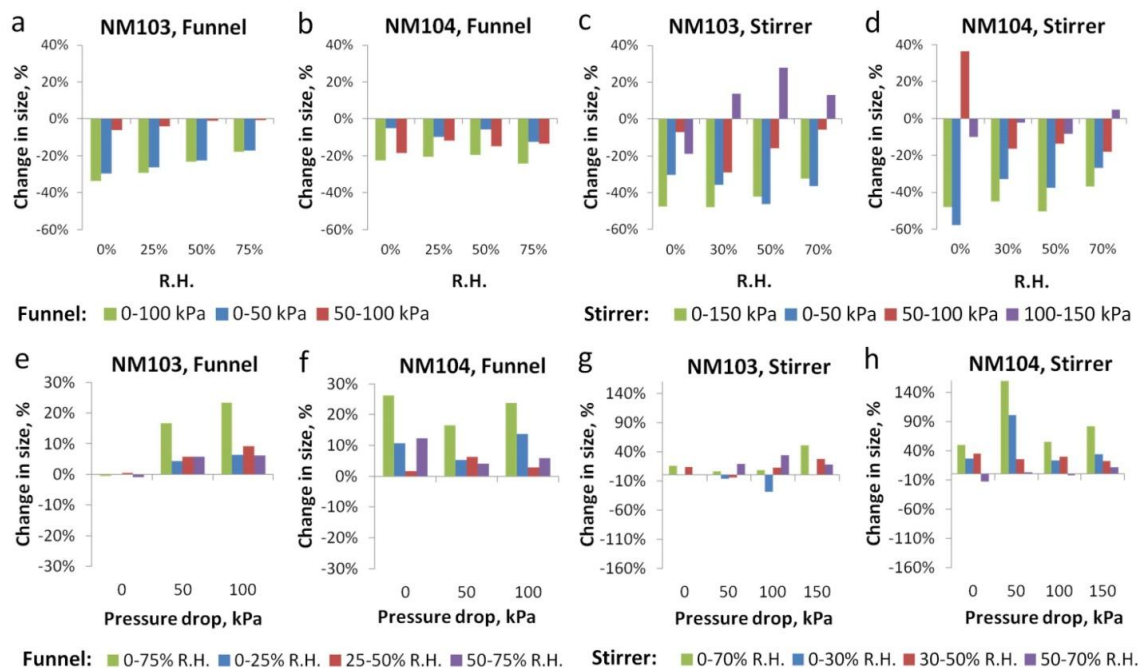


Figure S3 Comparison of changes in particle number in individual size channels (SMPS) by increasing pressure drop (left) and by increasing humidity (right). Only statistically significant values are plotted ( $p < 0.05$ ). Error bars represent 95% confident intervals. Data are from the funnel system for the hydrophobic (NM103) and hydrophilic (NM104)  $\text{TiO}_2$  aerosols.

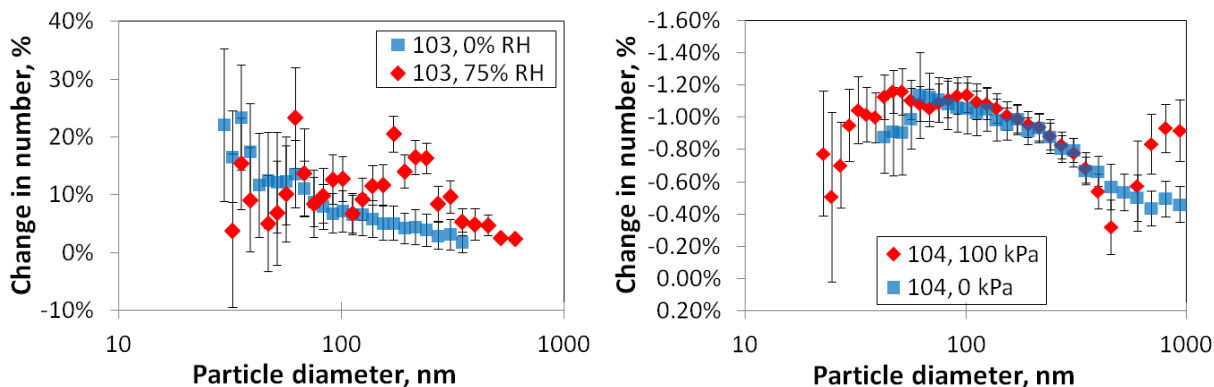


Figure S4 SEM observations on particle morphology in the stirrer system.

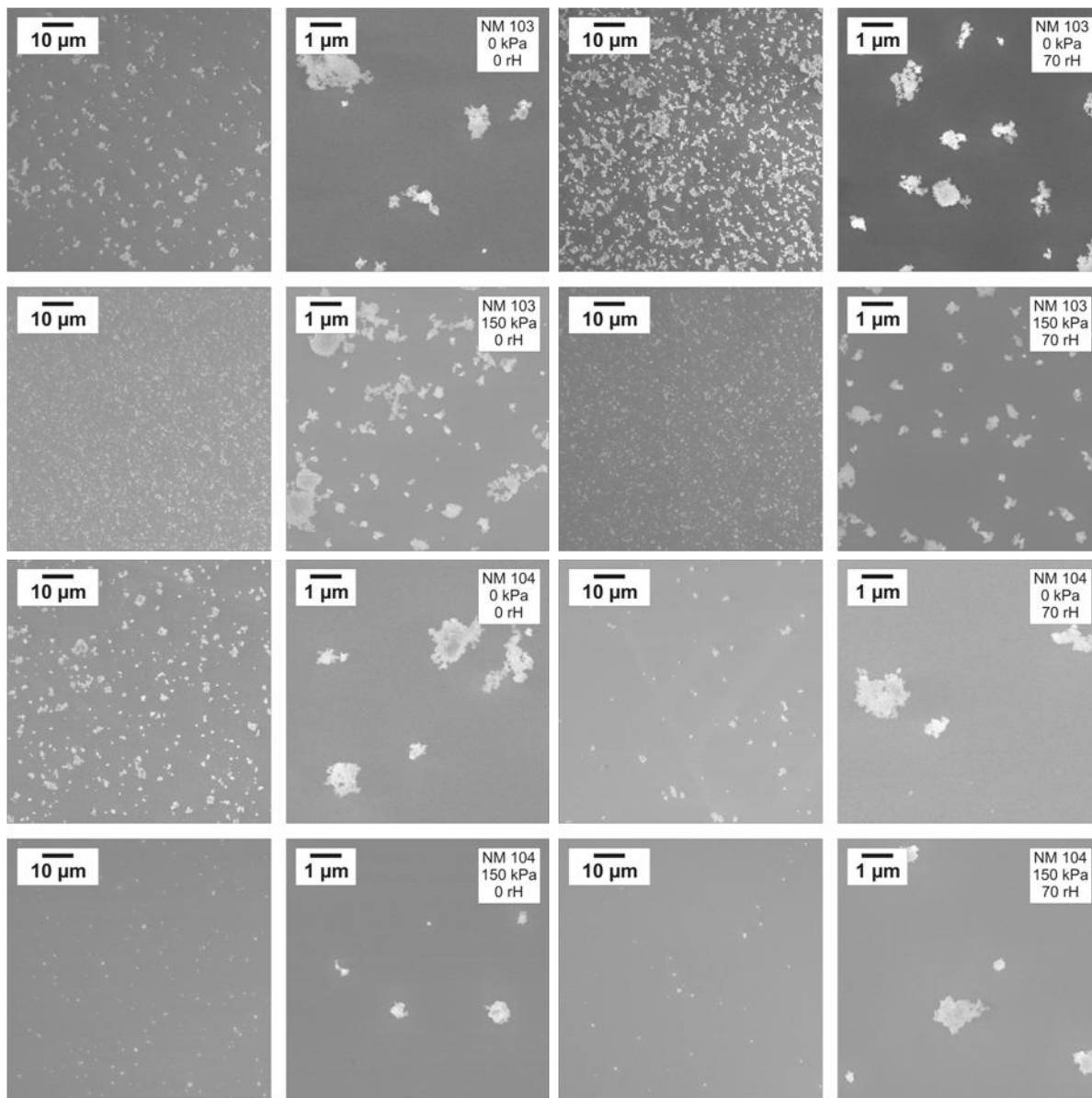
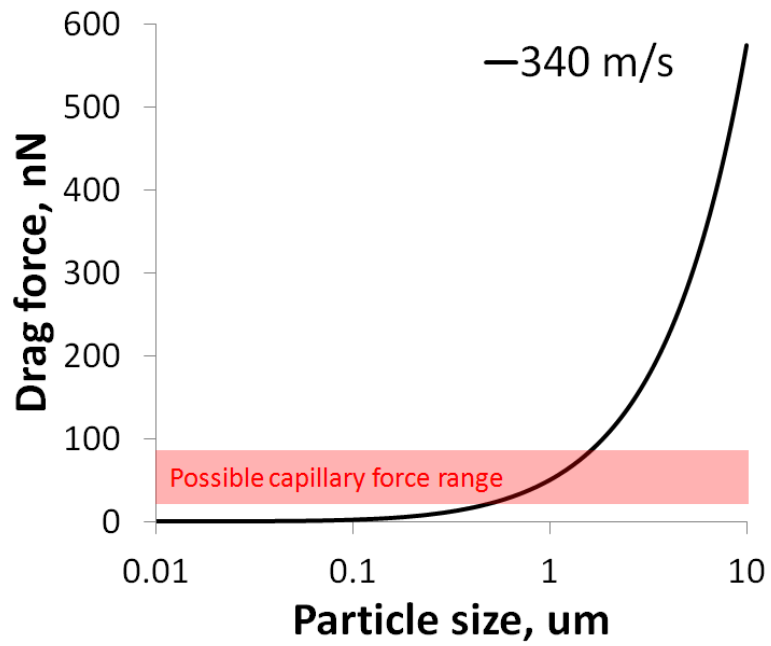


Figure S5 Dependence of aerodynamic drag on particle size at 340 m/s relative velocity.



## 7. NANOPARTICLE RELEASE FROM NANOCOMPOSITES

Publication 4

### Nano-object release during machining of polymer-based nanocomposites depends on process factors and the type of nanofiller

Yaobo Ding<sup>1</sup>, Wendel Wohlleben<sup>2\*</sup>, Mael Boland<sup>2,3</sup>, Klaus Vilsmeier<sup>2</sup>, Michael Riediker<sup>1,4\*</sup>

<sup>1</sup>*Institute for Work and Health (IST), University of Lausanne and Geneva, Lausanne, Switzerland*

<sup>2</sup>*Dept. Material Physics, BASF SE, Advanced Materials Research, Ludwigshafen, Germany*

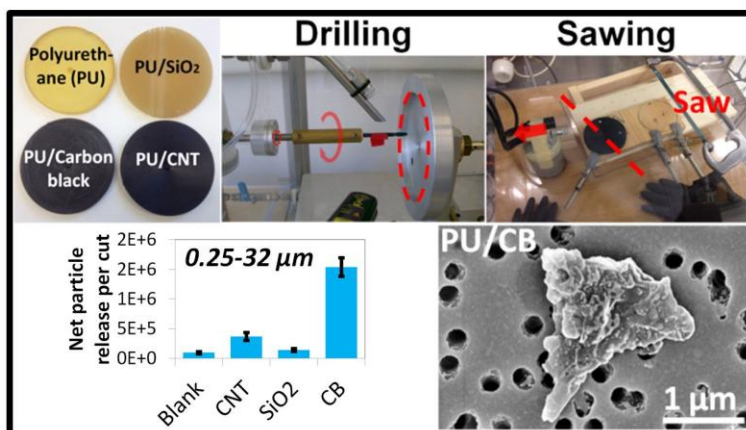
<sup>3</sup>*CNRS-Chimie ParisTech, Université Paris 6, Paris, France*

<sup>4</sup>*SAFENANO, IOM Singapore, Singapore*

\*Corresponding author: [Wendel.Wohlleben@basf.com](mailto:Wendel.Wohlleben@basf.com)

\*Corresponding author: [Michael.Riediker@hospvd.ch](mailto:Michael.Riediker@hospvd.ch)

Graphical abstract:



\*Submitted.

## **ABSTRACT**

We tested the likelihood of nanomaterial release from composites when treating them with two different mechanical processes, automated drilling and manual sawing. Polyurethane (PU) polymer discs (1 cm thickness and 11 cm diameter) were created using different nanomaterial fillers: multiwall carbon nanotubes (MWCNT), carbon black (CB), silicon dioxide (SiO<sub>2</sub>), and an unfilled PU control. Drilling generated far more submicron range particles than did sawing. In the drilling tests, different nanofillers did not result in significantly different particle number concentrations or sizes, except for the PU/MWCNT samples, which produced larger particles than control samples. Higher drilling speed and larger drill bit size were associated with higher particle counts. Differences between composites were observed during sawing: PU/CB released higher number concentrations of micro-sized particles compared to reference samples. All the nanofiller reinforced composites generated greater numbers of nanoscale particles, among them individual nanoparticle agglomerates were observed from treating the PU/SiO<sub>2</sub> samples. Furthermore, polymer fumes were released due to the process heat. For both drilling and sawing, the majority of the aerosolized particles were polymer matrix materials containing nanofillers (or protruding from their surface). Results suggest that: 1. processes associated with higher energy inputs are more likely to result in higher particle release; 2. nanofillers may alter release processes; and 3. other types of released particles, such as the polymer fumes from high-temperature processes, must also be considered in occupational exposure and risk assessments.

Keywords: nanoparticle, nanomaterial composite, drilling, sawing, release, occupational exposure, risk

## **INTRODUCTION**

Engineered nanomaterial (ENM) fillers, such as carbon nanotubes (CNTs), carbon nanofibers, carbon black (CB), silicon dioxide (SiO<sub>2</sub>), titanium dioxide (TiO<sub>2</sub>), or nanoclay, have all been added to different polymer matrices to manufacture nanocomposites with improved material properties [144-146]. During research and development, as well as during the industrial processing of such materials, filler particles can be released, leading to subsequent human exposure [124, 125]. When inhaled, ENMs may cause unwanted toxic effects on humans. In rats, multiwall carbon nanotubes (MWCNTs) were shown to have pathogenic effects similar to those

of asbestos [147]. SiO<sub>2</sub> nanoparticles were found to cause cytotoxicity in human bronchoalveolar cells [148]. In mice, lung exposure to CB nanoparticles led to a considerable increase in DNA single-strand breakages [15]. To date, nanomaterials are still associated with considerable uncertainties related to their hazard and exposure potential [149]. Understanding release and characterizing the released particles will help address important knowledge gaps.

It has been proposed that particle release from nanocomposites is affected by various process parameters and material properties, such as the type of treatment, environmental conditions (e.g., temperature, humidity), matrix properties (e.g., brittleness, degradation potential), and filler type, physical form (e.g., fiber length, orientation), content, and dispersion [150-152]. Comparing different processes and associated release patterns is especially interesting from an occupational hygiene viewpoint. Previous investigations have determined levels of nanoparticle release during different mechanical and chemical processes. Dry machining of polymer-alumina-CNT composites in a laboratory simulation study led to considerable release of nano-sized and fine particles and fibers [61, 153]. A greater release of nanoparticles was also recorded from the friction of mechanical shocks and abrasion processes on composite surfaces [154]. By studying the mechanical properties and crushing behavior of composites, Sachse et al. demonstrated that nano-sized and ultrafine particles were emitted from polymer composites reinforced with nano- and microsilica, as well as with nanoclay fillers. However, other studies found no significant release from nanocomposites, in comparison to the control materials, and in certain cases the generation of airborne particles was even lower. During the thermal cutting of polystyrene (PS) foam, over 99% of the filler particles were found to be embedded in submicron aerosol particles [62]. An investigation of nanoclay polymer composites during drilling showed that integrating nanofillers into the base polymer decreased particle concentrations [155]. During the sanding of thermoplastic polyurethane (PU)/CNT composites, no free nanofillers were observed, and it was concluded that more than 97 wt% of the filler materials were still embedded in the polymer matrix [69]. However, despite the efforts made so far, conclusive predictions about particle release, whether from specific nanocomposites or specific processes, remain difficult to make.

In this study, we drilled and sawed cross-linked PU-based composites reinforced with three types of organic and inorganic nanofillers. Drilling is a process associated with high-speed mechanical shear forces to produce a hole; sawing is considered a relatively low-speed process with a limited

contact area with the material [156]. To the best of our knowledge, there have been few investigations comparing particle release scenarios in these two processes. PU is a matrix material rarely studied in release tests. In the present study, release tests for these two processes were set up, validated, and used to examine how process parameters influenced the particle number concentration, size range, and particle morphology of the aerosols released.

## MATERIALS AND METHODS

### Materials

The materials tested were polymer composites reinforced using different organic or inorganic nanomaterial fillers. The base polymer was partially cross-linked PU synthesized using a prepolymer process handled by our project partner, Nanocyl. **Table 1** lists the four types of material tested. Pure PU samples were used as negative controls. The visual appearance of the samples, as well as the transmission electron microscope (TEM) characterizations of the morphologies and the distribution of the filler particles in the matrix, is shown in the supporting information (Figure S1).

Table 1. Summary of the types of composite materials tested

Matrix	PU	PU	PU	PU
Filler	(control)	SiO <sub>2</sub>	MWCNT	CB
Type and producer	Cross-linked	Fumed silica (ABCR)	NC7000 [157]	Vulcan XC72
Content (w/w), %	1571 0.09	0.09	0.09	(Cabot) 0.09

\*Sample dimensions: 11 cm  $\Phi$  x 1.0 cm thickness, disc.

### Test setups

#### Automatically controlled drilling system

Drilling tests were done inside a transparent plastic chamber (154 L volume, Figure S2, left) in order to separate the drilling process from the outside atmosphere. The sample was fixed to a rotatable round plate that allowed the drilling position to be changed between drilling tests. Only the drill bit was inside the chamber. The pressure of the bit on the composite material was controlled by a spring pulling the sample towards the drill bit (drill force: 17 N). An infrared

thermometer with an effective sensing zone of 1 cm<sup>2</sup> was used to continuously monitor temperature changes during drilling. The sampling ports for particle measurements were pointed towards the drill hole. A DISCmini (Matter Aerosol, Switzerland) was used for measuring particle number concentration and mean diameter in the 10–300 nm size range. In addition, gold filters (0.2 μm pore size, Φ25 mm, APC) were used to collect airborne particles for subsequent analysis using a scanning electron microscope (SEM). The sampling flow rate was 5 L/min. Filtered air was used to flush the chamber before each test until the background particle concentration was below 200 #/cm<sup>3</sup> (DISCmini). Five drilling tests were conducted, one after the other, for each sample type. In order to clean out the residual particles from the previous drilling tests, the chamber was flushed using a 30 L/min air flow for at least 15 min. Each drilling test lasted about 1 min. Different drilling speeds and drill bit sizes were used (**Table 2**).

Table 2. Drilling test parameters

		Drilling speed, rpm		
		1200 (S3)	1550 (S5)	1880 (S7)
Drill bit	4	-	All	SiO <sub>2</sub>
size, mm	8	MWCNT	MWCNT	All

\*Entire range of drilling speeds: 900–2,900 rpm from settings (S) 1-10.

### Manual sawing setup

A laboratory glove box (284.9 L volume) was used to enclose the sawing experiment (Figure S2, right). Samples were tightly fixed to a wooden support. The saw was operated via the box's rubber gloves. The enclosure was flushed with high flow rates of filtered air (50 L/min) until the background particle concentration was below 20 #/L. Sampling ports were placed about 10 cm from the cutting position to the side of the main sawing axis. Sampling was done using a DISCmini, a filter sample holder (2 L/min inflow) equipped with a gold-coated track-etched filter (0.8 μm pore size), a sample collector for transmission electron microscopy (TEM, grid sampler, Ecomesure), and an optical particle counter (OPC, 1 L/min inflow, GRIMM). The OPC

measures particle number and size distributions from 250 nm to 32  $\mu\text{m}$ . A thermometer (Celsimeter<sup>®</sup>, K-thermocouple:  $-50^{\circ}\text{C} \sim +1000^{\circ}\text{C}$ , Spirig, Switzerland) was used for measuring the temperature of the manual saw's blade (blade dimension:  $300 \times 12.5$  mm, HSS-high speed steel, technocraft<sup>®</sup>). Four to five cuts were conducted in each test. Sawing began in the center of the sample, and the distance between sawing positions during the test was about 2 mm. The length of the cut was thus kept approximately the same. The material was not completely sawn through in order to avoid touching the wooden support. Each sawing session lasted about 5–7 min. During this period, the air supply to the enclosure was set at 6 L/min to replace the air drawn for sampling needs. After each cut, sampling continued for 10 min. Between cuts, the chamber was flushed at a flow rate of 50 L/min filtered air for about 15–20 min to clean out residual particles.

### **Data analysis**

To estimate the number of particles released per drilling event, we first averaged the peak particle concentrations generated after each drilling test. The peak concentration was determined from the fitted curve of moving averages over 50 seconds (Figure S3). The total particle release from a single drilling event was then estimated by assuming that: a) the chamber was a well-mixed environment in which homogeneous particle concentrations were present at the end of a drilling event; and b) that all released particles in the size range analyzed by the DISCmini were still airborne during this peak period of the drilling event. The particle loss during the drilling event (ca. 1 min) was not taken into account since the sampling flow rate was low. The total number of released particles counted was thus determined by integrating the average concentration over the chamber volume. The total number of background particles was determined based on average background concentration during the 15–30 min before each test. The net release was then calculated by subtracting background particles from the total number of released particles. The analysis of variance (ANOVA) of the average number and mean size of the particles from different samples was performed using Stata software (Stata CorpLP, Texas, USA). P-values  $<0.05$  were considered statistically significant.

## **RESULTS**

## Release scenarios in the drilling tests

### *Influences of types of nanoparticle filler and drilling parameters*

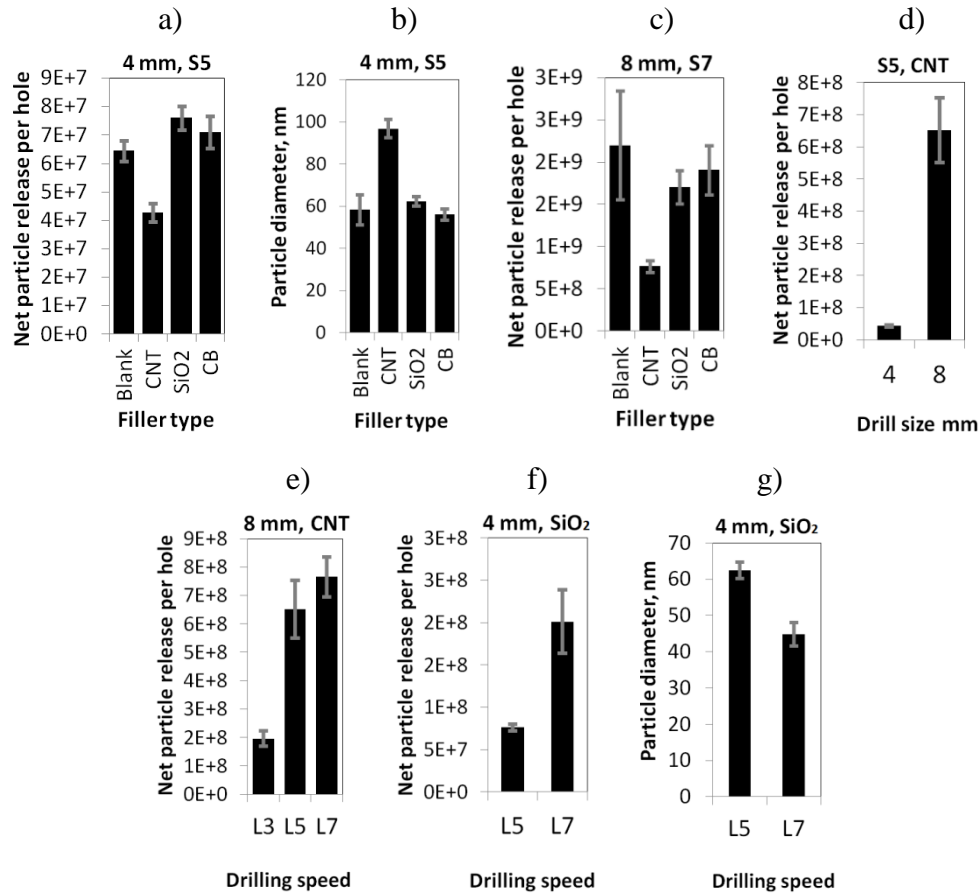


Figure 1. Influence of types of nanomaterial filler, drill speed setting (S5 or S7), and bit diameter (4 mm or 8 mm) on the net release of particles and their mean diameter (size range: 0–300 nm). The statistical analysis: a)  $p=0.0056$  (group),  $p=0.013$  (PU-PU/CNT pair),  $p>0.1$  (other pairs); b)  $p<0.001$  (group),  $p<0.001$  (PU-PU/CNT pair),  $p>0.1$  (other pairs).

The net particle release numbers and particle sizes under the various test conditions are compared in **Figure 1**. The PU/CNT sample released the lowest number of particles compared to the other samples, with both the small and big drill bits and at different drilling speeds (**Figure 1** a,c). In general, the number of particles released increased with the larger drill bit size and the faster drilling speed (about two orders of magnitude higher). However, the relative order between the different types of nanomaterial filler remained unchanged. The SiO<sub>2</sub>- and CB-reinforced composites released similar numbers of particles to the blank sample. The total

number of particles generated by drilling a single hole through the sample ranged from  $4.3 \times 10^7$  to  $2.2 \times 10^9$  #/cm<sup>3</sup> using the two sets of experimental conditions. The mean diameter of the released PU/CNT particles was around 100 nm, which was the largest from among the samples (**Figure 1b**). Particle generation soared from  $4.3 \times 10^7$  to  $65.2 \times 10^7$  #/cm<sup>3</sup> (about 15.2 times higher) when using the bigger drill bit (**Figure 1d**). Particle release with a big drill bit continued to increase with higher drilling speeds (**Figure 1e**), and the pattern was similar using a small drill bit (**Figure 1f**). The variations in results were larger (shown by the error bars) when using high drilling speeds or the big drill bit. Higher drilling speed resulted in a slightly lower average particle sizes (**Figure 1g**). During the experiment, the local temperature on the drilling sites remained below 70°C (**Figure S6**), and thus below the temperature at which the polymer matrix or thermal degradation products can evaporate and recondense into aerosol particles.

### *Morphological analysis*

Released airborne particles were collected and analyzed by SEM, as shown in **Figure 2**. All the particles collected had the visual appearance of polymer matrix materials. The diameters of pieces of drilled-out material were usually in the order of a few micrometers. Different geometries were observed for the various composite types, such as irregular thin flakes for the PU/CNT samples or lumps of materials for the other samples. **Figure 2** (e–h) shows close-up images of the surface morphologies of the three filler samples. Numerous bright spots appeared on the PU/CNT and PU/CB composites; their size and apparent higher electron density can be attributed to protrusions of nanofiller on the particle surface. For PU/CNT samples, elongated features were clearly visible at the surface (**Figure 2g**); these matched the known diameter and length of the specific CNTs used. In contrast, a cluster of hollow structures was observed on the PU/SiO<sub>2</sub> sample (**Figure 2h**). Most of the released particles were matrix materials with protrusions of nanofiller particles at the surface. The particle coverage on the surface of the aerosol filters remained relatively sparse, resulting in a considerable statistical uncertainty from the microscope observations. Thus, although no individual primary nanoparticles were observed during the drilling experiments, their occurrence cannot be completely excluded.

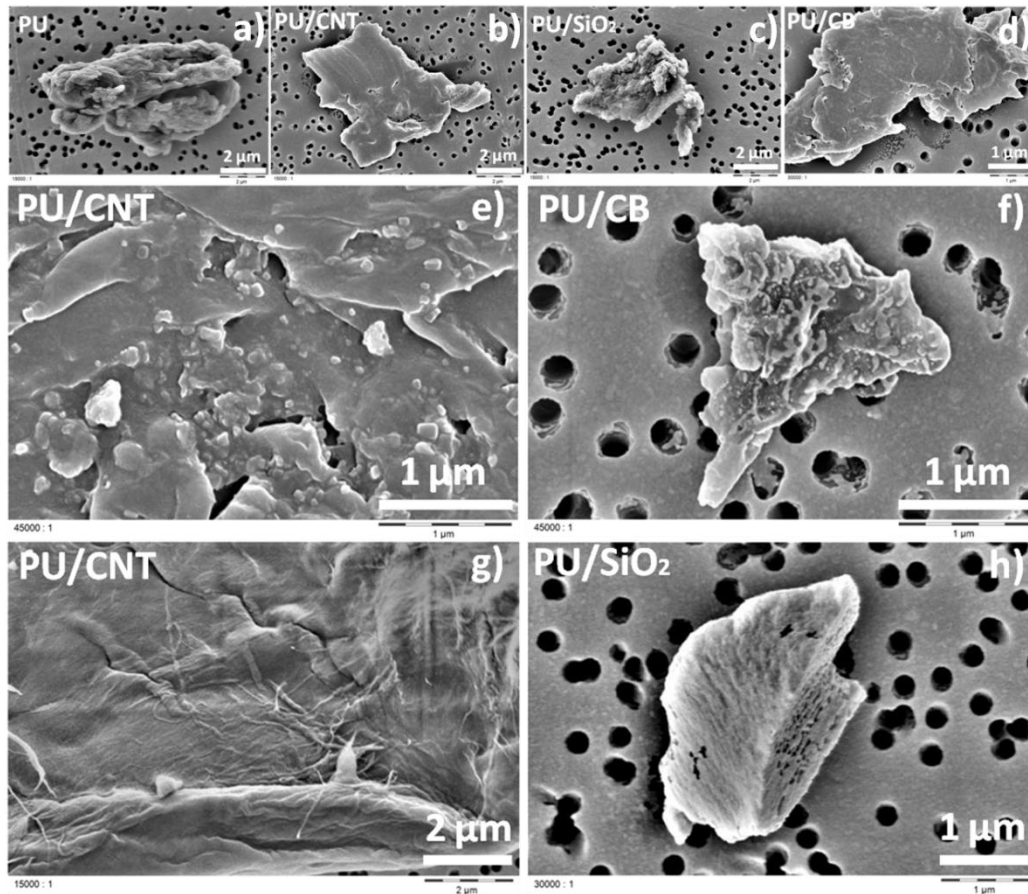


Figure 2. Surface morphologies of particles released in the drilling tests.

## Release scenarios in the sawing tests

### *Influence of types of nanofiller*

Compared to drilling, sawing resulted in clearly different particle concentrations, in different size ranges, for the various tested nanofiller composites, as shown in **Figure 3**. PU/CNT and the PU/SiO<sub>2</sub> produced equally high numbers of particles in the 0–300 nm size range (**Figure 3a**, left). PU/CB also generated higher particle numbers than the blank samples, but not as high as the other two composites. In comparison, in the 0.25–32 μm size range, the release level for the PU/CB sample was considerably higher than for the other three materials (**Figure 3a**, right). The PU/CNT registered minor increases over control materials, and the PU/SiO<sub>2</sub> samples remained nearly the same. The net particle number was roughly 1–2 orders of magnitude higher for the particles in the smaller size range than for those in the larger size range. The size distribution of

released particles in the 11–1083 nm size range is shown in **Figure 3b**. For all the sample types, a peak appeared in the 10–30 nm size range. A second mode size, around 100 nm, was recorded for the PU/CB and PU/CNT samples, but was not obvious for the PU and PU/SiO<sub>2</sub> samples. Close to the upper limit of the size spectrum (1 μm), particle numbers rose again. In general, the total particle concentrations measured using the SMPS were low (<200 #/cm<sup>3</sup>). The backgrounds were very clean and did not show signals in the SMPS scans.

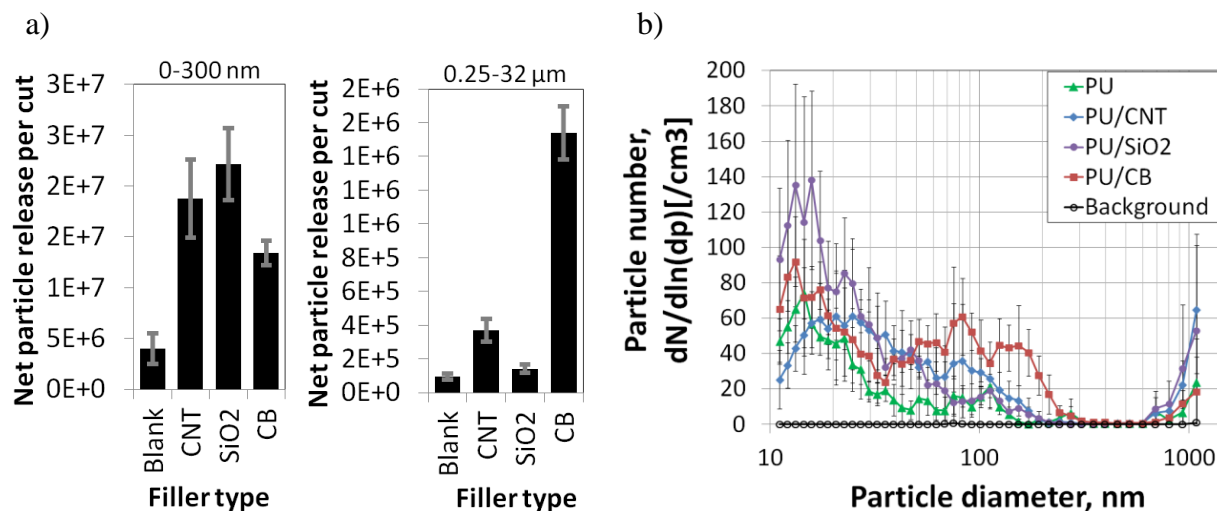


Figure 3. Influence of type of filler on particle release and size distribution: a) left, data from DISCmini (0–300 nm); right, data from the OPC (0.25–32 μm); b) data from the SMPS (10–1083 nm).

### Morphological analysis

The collected airborne samples were analyzed using TEM and SEM (**Figure 4** shows the example of SiO<sub>2</sub> containing composite). Large particles of a few microns in diameter (**Figure 4a,b,e**) and submicron particles (**Figure 4c**) were found. Small spherical particles around 100 nm or below were also present on the grid (**Figure 4a–d**: circled areas). A large particle likely to contain the structure of filler materials is shown in **Figure 4f**. After analyzing all TEM grid areas, only one particle that resembled a SiO<sub>2</sub> particle agglomerate was identified (**Figure 4g,h**). The diameter of one primary particle was measured using ImageJ software (v1.48S, National Institute of Health, USA) and the average value was 19.57 nm. This value corresponded to the manufacturer’s information on a primary particle size of 12–20 nm (batch No.AB111363, ABCR, Germany); this indicated that SiO<sub>2</sub> nanofiller particles were likely to have been released during

sawing. In the SEM characterizations, the particle morphologies were often seen as irregular, thick lumps, ranging from 1–10  $\mu\text{m}$ . The surfaces of PU/CB samples appeared to be different from those of other samples, showing scattered bright spots as was also observed for that material in the drilling tests (**Figure 4**). Individual nanofiller particles were not found in the SEM investigations. The particles collected seemed to be materials sawn from the polymer matrix, with a visible nanofiller texture on the surface of certain samples. An analysis of the chemical composition of the PU/SiO<sub>2</sub> sample surface (**Figure 4m**) identified nanofiller content. In addition, a large particle exhibiting a powdered surface and seeming to consist of smaller particles, also appeared on the filter (**Figure 4n**). Chemical analysis confirmed the presence of silicon in this particle.

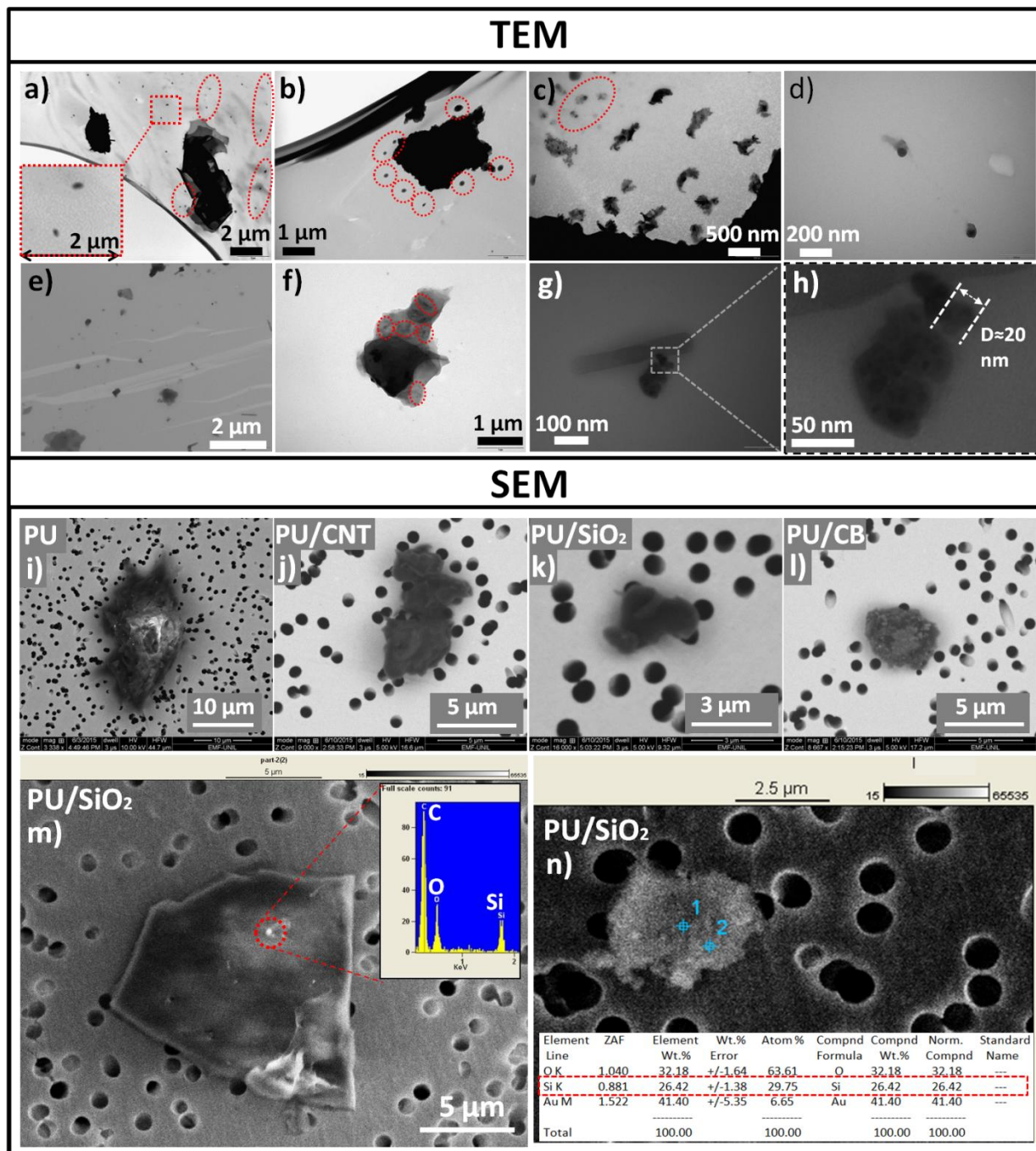


Figure 4. TEM and SEM observations of released particles from the sawing tests: a–d, PU; e–h, PU/SiO<sub>2</sub>.

Particle diameters in the order of 100 nm would be indicative of polymer fumes. This phenomenon is known from an aerosol monitoring study on injection molding sites, where polymer extrusion temperatures reach 200°C and above [158]. In our tests, each sawing session

typically lasted 5–7 min, which was much longer than the drilling process (~50 seconds). The blade may heat up due to the repeated sawing action, up to a point where the matrix starts to degrade and generate polymer fumes. To test this hypothesis, the blade's temperature was monitored during sawing (Figure S7). The thermocouple sensor was fixed to the blade using a metallic tape in order to detect temperature changes during sawing sessions. The temperature started to rise as soon as sawing began, and it rapidly (within approximately 1.5 min) reached a stable value of about 120°C. The test's nanocomposite samples were synthesized between 80°C and 100 °C, thus it is likely that matrix materials at the sawing line were degraded by the blade's heat and subsequently released polymer fume particles. This may also explain the particle diameters below 100 nm, as shown in the number size distribution from the SMPS (**Figure 3b**).

## DISCUSSION

### Effects of nanofillers

We observed that nanofiller particles and fibers were present on the surface of released matrix materials; this corresponds with earlier reports [49, 71, 159-162]. The protrusion of CNTs was attributed to their greater tensile strength; they were pulled out of the fracture interface as the matrix is ripped into particles [163]. However, Wohlleben et al. did not observe protruding CNTs from sanding fragments; they attributed this to the reflow behavior of the soft TPU matrix (600% elongation at break) around the filler particles during destruction [69]. In our tests, the stronger, partially cross-linked PU matrix was expected to limit flow processes, which explains why the nanofillers were exposed on the particle surfaces. The hollow structures shown on the surface of PU/SiO<sub>2</sub> (**Figure 2**) seemed to be cavities left behind by detached SiO<sub>2</sub> nanofillers. The cavity sizes (100–200 nm) corresponded roughly to the size of the agglomerates observed in the TEM characterization of the raw sample cross-sections (Figure S1). The white spots present on PU/CB (**Figure 2** and **Figure 4**) particle surfaces were likely to be individual or agglomerated filler particles, and this was also suggested by the higher electron density in comparison to the surrounding material.

The very low release level of filler particles in our tests may be due to the low nanofiller content in the composites tested (0.09% w/w). Greater releases of nanofiller particles have been reported for dental materials that had nanofiller contents of 12–84.5 wt% [164] and 73–84.5 wt% [165].

Free CNTs were observed when epoxy composites loaded with 4 wt% CNTs were sanded, but they were not when samples with lower loadings were sanded; this was attributed to incomplete dispersion [163]. The epoxy-alumina-CNT composites in the dry drilling tests contained 1.3%–2.2% of nanofillers, and airborne clusters of CNTs were released during the treatment [61]. The dispersion and agglomeration levels of the nanofiller particles in the matrix also influence the possibility that they will detach during mechanical processes. Poor distribution of fillers in composites, as well as their agglomeration, can act as failure points during the destruction process. Clearly different release scenarios were observed between samples with poor filler dispersion and those showing good distribution [154]; this led the authors to suggest that agglomerates of CNTs are more likely to be aerosolized and released than individual CNTs bound to the matrix.

The distinct release scenarios from the three types of nanocomposite may be attributable to nanofillers' properties. The interlocking and reinforcement effects of MWCNTs can reduce particle generation and increase particle size. The tensile modulus of the carbon nanotubes is much larger than that of a PU matrix. Their long, tube-like geometries may help connect different parts of the composite and prevent large-scale destruction. The same effect has been observed in the dry machining of nanocomposites: fewer airborne particles were generated from a CNT-alumina composite than from the base alumina composite alone [61, 73]. Furthermore, PU/CNT composites generated larger fragments than the control matrix [69]. A similar strengthening effect was also seen during drilling activities after nanoclay fillers were added to a PA6 matrix [155]. During the shredding of nanoclay-reinforced resin plaques, fewer nanoparticles were produced than with the standard plaques [166]. In these cases, the nanoclay fillers may act in the same way as CNTs do to reinforce the matrix materials, thus altering the release scenarios for such composites. The higher particle generation from drilling and sawing PU/CB composites may be caused by increased brittleness of the matrix. There is evidence of embrittlement when carbon black was added to polymer matrices [167-169]. This effect on particle release is similar to that caused by different types of matrix (e.g., harder vs. softer matrices), and this is discussed in the following sections. The identification of SiO<sub>2</sub> filler particles after the sawing tests may be in part due to their stronger agglomeration states.

Furthermore, the primary particles exhibited a sphere-like morphology. These characteristics increased the probability that the embedded particles would escape from the matrix.

### **Effects of process characteristics**

The treatment types (drilling and sawing) and test conditions (e.g., tool geometry and speed) also influenced the number and size of the particles released. Highly dynamic processes such as sanding, drilling, and grinding are more efficient at destroying solid materials than less dynamic processes including abrasion, sawing/scratching, and mechanical shock. Furthermore, processes treating larger surface areas on samples are likely to detach more materials from the matrix (e.g., sanding). Golanski et al. provided evidence that rotating steel brushes and graving tools were more efficient at removing CNTs from hard polymer coating surfaces than other abrasion processes [154]. Also, metallic rakes were effective at detaching nanoparticles from fabric nanomaterials by scratching. In our tests, sawing may be considered to be a mixed process of cutting and polishing, which favors the detachment of filler particles in a way resembling the above-mentioned processes. The greater numbers of particles released using faster rotation speeds and larger drill bits in our tests can be linked to the higher energy levels existing under those conditions. Similar results have been seen during solid core drilling of epoxy-based composites [61].

Treatments featuring a significant generation of heat may thermally decompose the polymer matrix and release nanoscale fume particles. This phenomenon is often observed in studies investigating high-temperature processes. Particle numbers decreased by 99.9% when a 190°C thermodenuder was used, which implies that the nanoscale particles released were likely to have been volatile, high-melting-point contents that evaporated due to the heat friction caused by grinding [159]. A visible smoke plume was generated during the dry drilling of epoxy composites [61]. Volatile organic compounds, peaking at 70 nm diameter, were released during the thermal cutting of PS and its derivatives [62]. SEM analysis revealed that most of the particles were spherical, and liquid particles were also present.

### **Matrix effects**

Studies investigating mechanical processes have commonly revealed irregular shapes and significant surface roughness on matrix particles [69, 70, 159, 164, 170]. This was attributed to

the ductile nature of polymers that stems from the viscoelastic nature of polymer materials and their special molecular arrangement [171]. The deformation occurring under external loads results in the molecular chains rearranging themselves into new positions and structures [172]. As a consequence, there is a tendency for surfaces to become rough, producing lumps, flakes, or layers of materials (**Figure 2** and **Figure 4**).

The nature of the composite matrix material seems to play an important role in the release process. In general, harder materials tend to be more brittle, which means they break more easily into small pieces under deformation. There is a propensity for crevices and cracks to form in brittle materials [173]. The cross-linked PU used in our test is relatively soft compared to the materials used in previously reported studies, such as epoxy [61, 153], PA [155], PVC [154], PS [62, 159], and inorganics including bricks [174] or cement paste [170]. The dry drilling of Al<sub>2</sub>O<sub>3</sub>-epoxy-CNT composites resulted in  $3.9 \times 10^6$  to  $1 \times 10^7$  #/cm<sup>3</sup> particle concentrations in the 5.6–560 nm range, using a similar set of drilling speeds (725–1355 rpm) and drill bit diameters (1/4" and 3/8", = 0.64 and 0.95 cm, respectively) to our study [61]. Thermal cutting of PS-based polymer foams led to particle release concentrations in the order of  $10^6$  #/cm<sup>3</sup> for submicron particles. In comparison, Wohlleben et al. recorded airborne particle numbers below 1000 #/cm<sup>3</sup> during abrasion tests on thermoplastic PU composites (TPU) [69]; this is close to the values seen in our tests. The majority of the particles released in these studies were found to be the matrix materials containing nanofillers. The relatively low particle number concentrations obtained in our experiments were in line with the suggestion made by Wohlleben et al. that matrix rigidity has a greater influence on the properties of the released aerosol than the nanofiller materials do. Softer matrices are less likely to release filler particles and tend to produce larger fragments; this was observed in several other studies [150, 152, 175].

## CONCLUSIONS AND OUTLOOK

In this study, we compared scenarios involving the release of nano-objects resulting from two distinct mechanical processes: drilling and sawing. Automatic, machine drilling released greater numbers of particles than manual sawing did. Different drilling parameters modified the intensity of particle release by up to several orders of magnitude. Different types of nanofiller did not substantially influence the results of the release scenarios. The only significant difference was

seen with the PU/CNT samples that produced larger aerosol particles due to the interlocking effect of the nanotubes. Free particles of the filler material were not observed. Instead, the filler particles were visible as protrusions on the surface of cut PU residues. In comparison, the sawing tests generated relatively low particle number concentrations. However, the process produced intense heat and, consequently, polymer fumes. Furthermore, the PU/CB samples produced higher particle number concentrations for micron-sized particles. Individual nanoparticle agglomerates were identified from the sawdust of PU/SiO<sub>2</sub> samples.

Although it was possible to detect free SiO<sub>2</sub>-filler particles from the sawing sessions, the majority of the released particles were matrix materials containing the nanofiller. It is conceivable that the amount of filler, as well as how well it is distributed within the matrix, plays an important role in determining the intensity of particle release during such machining. Future studies should further characterize the influences of these two variables. To extrapolate to risk assessment, the literature emerging on the hazards posed by the aerosols released during very similar drilling or sanding setups also indicates that fragments of polymer matrix with protrusions of engineered nanomaterials show no more toxicity than fragments of control polymer without nanofiller [69, 170, 176, 177].

The fact that polymer-fume condensates at the nanoscale were identified in our sawing experiments highlights the importance of investigating process-determined release. This is of direct relevance to risk because at elevated temperatures the products of the thermal decomposition of polymers can lead to medical symptoms such as the influenza-like illness known as “polymer fume fever” [178-180]. However, even below thermal release thresholds, energy-intensive processes such as drilling have a greater potential to release particles. The same principle applies to other process parameters in our drilling tests that are associated with higher energy inputs—faster speeds and larger tool geometry—resulting in higher shear rates. This is in agreement with previous findings [181]. The possibility that nanofiller particle release is process-dependent cannot be ruled out. Compared to the control samples, the PU/SiO<sub>2</sub> samples generated far more particle release in the sawing experiments than in the drilling ones. Therefore, processing conditions do indeed seem to be the most important factor in determining particle release; they should be considered in detail for the laboratory simulation of particle release

phenomena. The present study only tested one matrix material, but the literature indicates that the matrix properties themselves are very important determinants of release rates—rates that are merely modulated by the embedded nanomaterials. These differences are typically less than one order of magnitude and have been systematically explored in the present contribution, paving the way for a mechanistic understanding of particle release processes.

## **SUPPORTING INFORMATION**

More details on the characterization of raw materials, experimental setups, data analysis methods (determination of average peak concentrations), reproducibility analysis, and drilling and sawing temperature monitoring are available on the website (<http://pubs.acs.org>).

## **ACKNOWLEDGEMENT**

This research was funded by the European Research Council under the European Union's Seventh Framework Programme (FP/2007-2013) / ERC Grant Agreement n.263215. We thank Mr. Gregory Plateel and Dr. Nicolas Concha-Lozano for their excellent support in the laboratory and Mr. Antonio Mucciolo for his assistance in SEM/TEM characterizations at the University of Lausanne's Electron Microscopy Facility.

## **AUTHORS' CONTRIBUTIONS**

YD set up the experiments, collected and analyzed the data, and wrote the article. WW proposed the research idea, contributed to the development of the research design in the BASF laboratory, supervised activities there and the associated data analysis, and contributed to data interpretation and the writing of the manuscript. At the BASF laboratory, MB performed supplemental drilling experiments, and KV developed the automatic drilling setup. MR contributed to the development of the research design at the IST laboratory, supervised activities there and the associated data analysis, contributed to data interpretation, and supervised and contributed to the writing of the manuscript.

**\*Citations in this article are compiled in the complete reference list at the end of this report.**

## SUPPORTING INFORMATION

**Supporting information F-S1.** Visual appearance of the four sample types tested and transmission electron microscope (TEM) characterizations of the morphology and distribution of the filler particles. The added nanomaterials were well distributed in the PU matrix; only smaller agglomerates of a few hundred nanometers were visible in the TEM images.

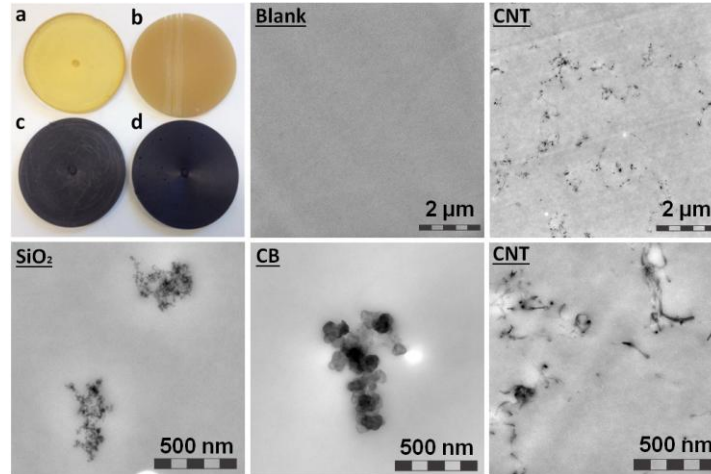


Figure S1. Photo of tested samples (a, PU; b, PU/SiO<sub>2</sub>; c, PU/CB; d, PU/MWCNT) and TEM images of a cross-section of the blank sample and the samples with the three filler types.

**Supporting information F-S2.** The drilling and sawing setups.

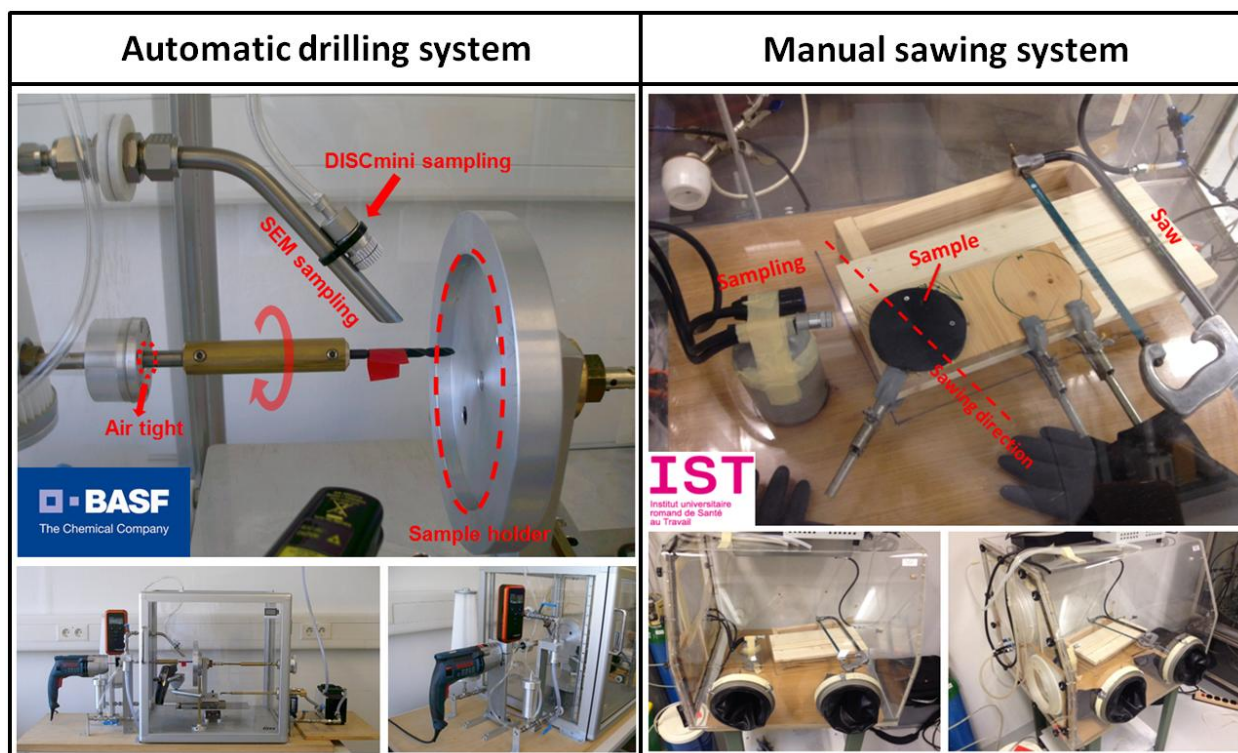


Figure S2. Photos of the two experimental systems used for testing. Left, automated drilling system at BASF; right, manual sawing system at IST.

**Supporting information F-S3.** Illustration of the method used to determine the average peak concentration for calculating net particle release from a single drilling test.

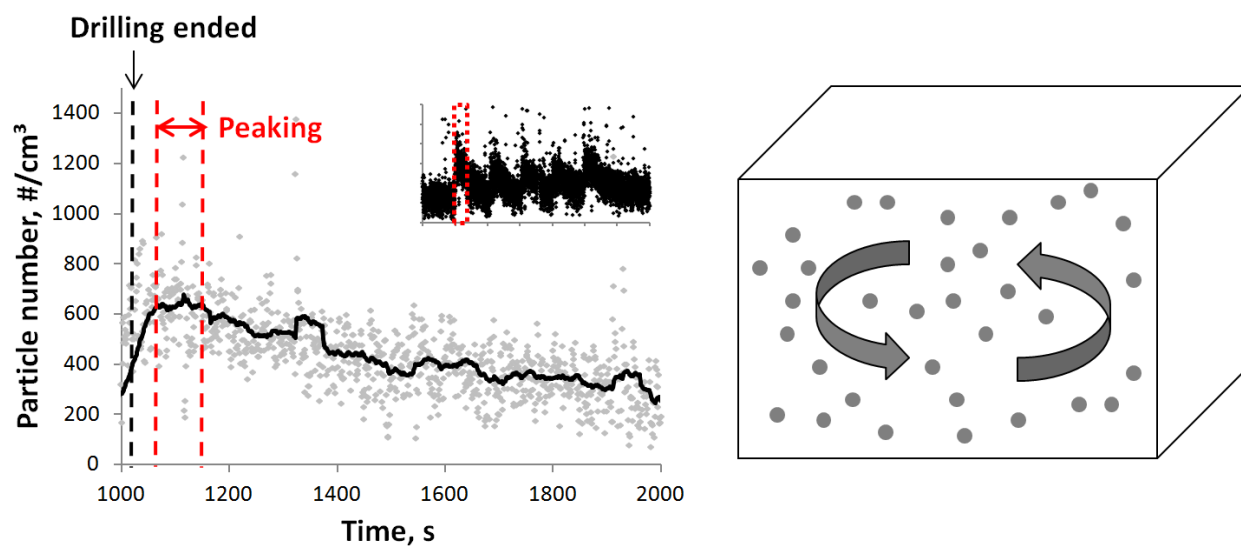


Figure S3. Left: peak period considered for determining average particle number concentration; the black line is the 50-second moving average. Right: the assumption of a well-mixed chamber was used for calculating total particle release throughout the drilling experiment.

**Supporting information F-S4.** Evolution of the particle number concentration and diameter during one complete drilling test (containing five drilling events). During the test, particle concentration started to rise as soon as drilling began. Figure S4 shows the pattern of particle number concentrations and the mean geometric diameters. The readings during the events varied considerably, with peaks reaching several thousand particles per  $\text{cm}^3$ . Maximum concentrations of the moving average reached 600–800  $\text{#/cm}^3$  shortly after drilling ended. The particle number concentration decreased gradually to the background level upon flushing. The evolution of the mean particle size is shown in Figure S4 (right). Before the first event, only few data points were available because particle size is not provided when the particle number concentration is near the device's lower detection limit (100  $\text{#/cm}^3$ ). In a pattern similar to the particle number concentration, particle size increased rapidly when drilling started and decreased when the chamber was flushed.

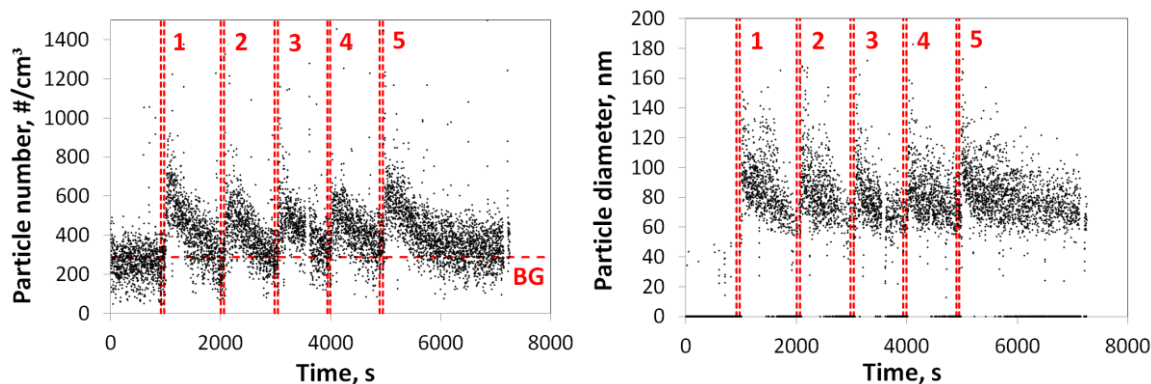


Figure S4. Peaks in particle number concentrations (left) and mean geometric diameter (right) in the 10–300 nm size range during one complete drilling test involving five drilling events, numbered 1–5 (data from DISCmini; material, PU/CNT;  $\Phi$ /drill, 4 mm; drill speed setting, S5). Red lines indicate start and stop times of the five drilling events (each of about 45 seconds).

**Supporting information T-S1.** Reproducibility of drilling test results. The particle number concentration and mean size obtained from replicate tests for the different materials were repeatable with standard deviations of <8% (number) and <15% (diameter), as shown in Table

S1. Background particle concentrations were usually around 200 #/cm<sup>3</sup>. The average particle number concentrations were 500–600 #/cm<sup>3</sup>. The results were significantly statistically different, both in number and size, for PU and PU/CNT. For the other two composite types, the release scenarios did not differ from that of the PU control sample.

Replicate Test	PU		PU/CNT		PU/SiO <sub>2</sub>		PU/CB	
	N, #/cm <sup>3</sup>	D, nm	N, #/cm <sup>3</sup>	D, nm	N, #/cm <sup>3</sup>	D, nm	N, #/cm <sup>3</sup>	D, nm
Background	262	-	288	-	186	-	141	-
Drill 1	743	63.7	626	101.5	649	85.3	581	59.7
Drill 2	648	54.1	540	97.7	732	65.6	610	53.1
Drill 3	651	51.1	577	89.7	651	60.9	573	53.8
Drill 4	640	71.0	501	94.7	656	60.8	558	55.1
Drill 5	695	52.0	585	100.5	-	-	693	58.8
Mean	675	58.4	566	96.8	680	68.1	603	56.1
S.D.	38.8	7.7	42.2	4.3	37.4	10.1	48.0	2.7
S.D., %	5.74%	13.27%	7.46%	4.42%	5.50%	14.78%	7.95%	4.78%

Table S1. Particle number concentration, N (#/cm<sup>3</sup>), and geometric mean diameter, D (nm), for replicate tests (Φ/drill, 4 mm; drill speed setting, S5). All measurements recorded with a DISCmini (size range 10–300 nm)

**Supporting information F-S5.** Evolution of particle number concentration during a complete sawing test (containing 4 sawing events). The OPC covers a broader size range (into microns), whereas the DISCmini only counts particles below 300 nm. The peak number concentrations were 4000–6000 #/cm<sup>3</sup>, measured using the OPC, corresponding to the sawing event numbers 1–4 (Figure S5, left). The peak heights decreased gradually as sawing proceeded. This could be due to the fact that the distance between the sawing location to the sampling ports became longer as the sample was cut from left to right (sampling tubes were on the left side of the sample). Immediately after each event, the particle concentration dropped as a filtered air flushed the

compartment. The two different slopes visible during this process are due to the different air flows introduced: the first, sampling air flow at 6 L/min and the second, stronger, flushing air flow at 50 L/min to rapidly clean out any remaining particles. Figure S5 (right) shows the repeated pattern of the particle number concentration, in the smaller size range, with regard to the start and end points of the sawing events (red dashed lines). The background particle concentration was normally below 10 #/cm<sup>3</sup>. Data points were much denser in the 100 #/cm<sup>3</sup> range as soon as sawing started, which indicated that the process was releasing small particles.

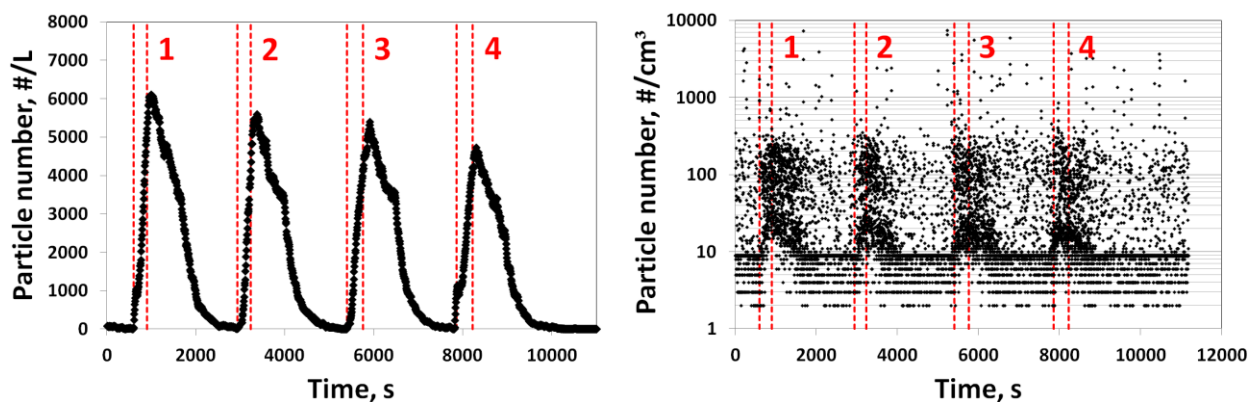


Figure S5. Evolution of particle number concentration while sawing the PU/CB nano-composite, measured using the OPC (left) and DISCmini (right).

**Supporting information T-S2.** Reproducibility of the sawing test results. The precise values of particle number concentrations measured by the two devices are summarized in Table S2. The standard deviation of the results was generally below 20% for the OPC data, whereas it was higher (almost up to 40% for the blank) for the DISCmini data. These large deviations may be caused by background particle levels very close to the total particle numbers (30–90 #/cm<sup>3</sup> compared to 53–167 #/cm<sup>3</sup>). Nevertheless, such variations were to be expected for a manual process and are generally considered acceptable.

	OPC (250 nm to 32 μm)				DISCmini (10–300 nm)			
	Blank	CNT	SiO <sub>2</sub>	CB	Blank	CNT	SiO <sub>2</sub>	CB
Background	1.2	1.4	20.6	20.0	39.7	36.0	89.2	30.1
Cut 1	405	1715	540	6045	75.9	101.7	151.5	87.3

Cut 2	285	1350	510	5600	70.4	99.2	155.2	76.1
Cut 3	410	1070	615	5310	40.5	86.3	207.0	73.6
Cut 4	260	1280	405	4735	27.5	85.6	154.6	71.6
Cut 5	320	1075	-	-	54.3	137.0	-	-
<b>Mean</b>	<b>336.0</b>	<b>1298.0</b>	<b>517.5</b>	<b>5422.5</b>	<b>53.7</b>	<b>102.0</b>	<b>167.0</b>	<b>77.1</b>
S.D.	68.7	236.1	87.0	549.0	20.2	20.9	26.6	7.0
S.D., %	20.4%	18.2%	16.8%	10.1%	37.6%	20.5%	16.0%	9.1%

Table S2. Summary of particle number concentration results for different samples during the sawing process. The difference in DISCmini mean particle concentrations for the four sample types was significant ( $p=0.000$ ); pairwise differences were significant for PU-PU/MWCNT ( $p=0.012$ ) and for PU-PU/SiO<sub>2</sub> ( $p=0.000$ ), but not for PU-PU/CB ( $p=0.626$ ).

**Supporting information F-S6.** Temperature evolution of drilling site during the experiment.

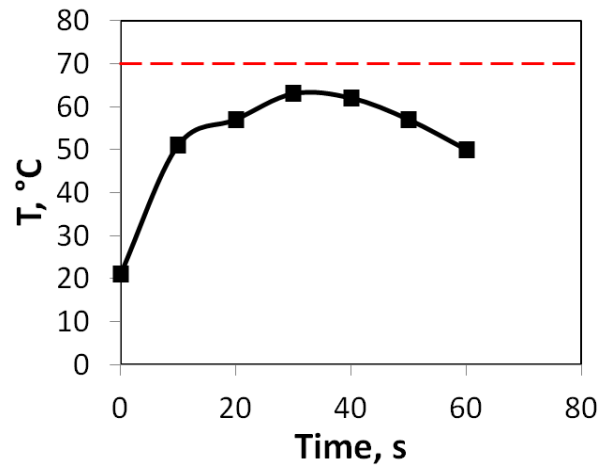


Figure S6. Evolution of local temperature against drilling time.

**Supporting information F-S7.** Temperature changes for the saw blade during the experiment.

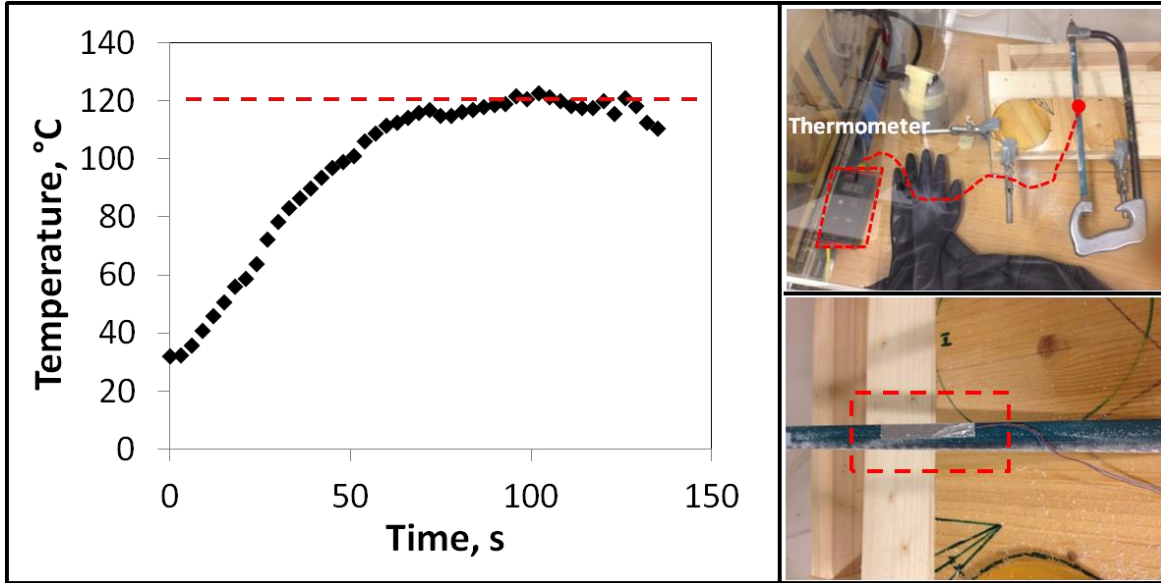


Figure S7. Evolution of blade temperature during sawing tests on PU samples.

## 8. ENMS RELEASES IN INDUSTRY AND RESEARCH ENVIRONMENTS

### Publication 5

Airborne Engineered Nanomaterials in the Workplace—a Review of Release and Worker Exposure during Nanomaterial Production and Handling Processes

Yaobo Ding<sup>1</sup>, Thomas A.J. Kuhlbusch<sup>2</sup>, Martie Van Tongeren<sup>3</sup>, Araceli Sánchez Jiménez<sup>3</sup>, Ilse Tuinman<sup>4</sup>, Rui Chen<sup>5</sup>, Iñigo Larraza Alvarez<sup>6</sup>, Urszula Mikolajczyk<sup>7</sup>, Carmen Nickel<sup>2</sup>, Jessica Meyer<sup>2</sup>, Heinz Kaminski<sup>2</sup>, Wendel Wohlleben<sup>8</sup>, Burkhard Stahlmecke<sup>2</sup>, Simon Clavaguera<sup>9</sup>, Michael Riediker<sup>1,10</sup>

<sup>1</sup> *Institute for Work and Health (IST), Universities of Lausanne and Geneva, Route de la Corniche 2, 1066, Epalinges, Switzerland*

<sup>2</sup> *Institute of Energy and Environmental Technology (IUTA), Air Quality & Sustainable Nanotechnology Unit, Bliersheimer Straße 58-60, 47229, Duisburg, Germany*

<sup>3</sup> *Centre for Human Exposure Science, Institute of Occupational Medicine (IOM), Research Avenue North, Edinburgh EH14 4AP, United Kingdom*

<sup>4</sup> *TNO, Lange Kleiweg 137, Rijswijk, The Netherlands*

<sup>5</sup> *CAS Key Lab for Biomedical Effects of Nanomaterials and Nanosafety, National Center for Nanoscience and Technology of China, Beijing 100190, P. R. China*

<sup>6</sup> *ACCIONA Infrastructure, Materials Area, Innovation Division, C/Valportillo II 8, 28108, Alcobendas, Spain*

<sup>7</sup> *Nofer Institute of Occupational Medicine, Lodz, Poland*

<sup>8</sup> *Dept. Material Physics, BASF SE, Advanced Materials Research, Ludwigshafen, Germany*

<sup>9</sup> *NanoSafety Platform, Commissariat à l'Énergie Atomique et aux Énergies Alternatives (CEA), Univ. Grenoble Alpes, Grenoble, 38054, France*

<sup>10</sup> *SAFENANO, IOM Singapore, 30 Raffles Place #17-00 Chevron House, Singapore, 048622, Singapore*

*Corresponding author: Michael Riediker; Tel. +41 21 314 74 53; Fax +41 21 314 74 30*

*E-mail address: Michael.Riediker@alumni.ethz.ch*

## **Abstract**

For exposure and risk assessment in occupational settings involving engineered nanomaterials (ENMs), it is important to understand the mechanisms affecting their release and how those mechanisms are influenced by factors such as the ENM itself, the matrix material's properties, and process characteristics. The release of ENMs from a source can result in workplace emissions and subsequent worker exposure. The latter is dependent on on-site conditions and control methods, such as room size and air flow as well as personal protective measures. This review summarizes studies providing information on ENM release in occupational settings, during different industrial activities and using various nanomaterials. It also assesses the contextual information that was collected — such as the amounts of materials handled, protective measures, and measurement strategies — in order to understand which release scenarios can result in exposure. Similar types of process activities exhibit similar release patterns in terms of particle concentrations and size distributions. High-energy processes such as synthesis, spraying, and machining are associated with the release of large numbers of predominantly small-sized particles. Low-energy processes, including laboratory handling, cleaning, and industrial bagging activities, usually resulted in slight or moderate releases of relatively large agglomerates. The present analysis suggests that process-based release potential can be ranked, thus helping to prioritize release assessments, which is useful for tiered exposure assessment approaches and for guiding the implementation of workplace safety strategies. The contextual information provided in the literature was often insufficient to directly link release to exposure. The studies that did allow an analysis of these links suggested that significant worker exposure might mainly occur when engineering safeguards and personal protection strategies were not carried out as recommended.

Keywords: nanoparticles, emission, grouping, occupational exposure, risk assessment

## **Introduction**

Engineered nanomaterials (ENMs) possess different physical and chemical properties than their bulk counterparts and, because of this, are used in manufacturing processes for a variety of applications [8]. However, during their production and use, ENMs may be released into the workplace, resulting in workers' exposure. Understanding release is important for accurately

describing the exposure scenarios that are helpful for risk assessment and management [182], which are required under regulatory schemes such as REACH in the EU [183].

Release can be referred to as the detachment of nanomaterials from a body of powder, a suspension, or a solid matrix [184]. This can be expressed as a rate describing the amount of material released per unit of time. In workplaces, the release of ENMs can occur throughout their entire lifecycle — manufacturing, use, and recycling. Release mechanisms depend on the physical state of the material (powder, suspension, or solid) and the amount of energy introduced by specific processes. For powders, environmental humidity and the moisture content of the raw powder have a significant influence on the release level, as suggested by dustiness studies [142]. Liquid suspensions containing ENMs can release nanoparticles from the solution's surface when external energies are applied, such as stirring [185], sonication [43, 185], centrifuging, [186] or spraying [185, 187]. The release rate from liquids depends on factors such as the ENM concentration and its solubility in the solution. Release from solid matrices is mainly caused by the mechanical treatment of nanocomposites, including drilling, sawing, and sanding [61, 72, 188]. Parameters such as the ENM's concentration and distribution within the composite matrix and the process conditions (e.g., treatment type, temperature, or relative humidity) play important roles in determining release levels.

To prevent or reduce ENM releases, it is important to understand the determinants of release related to nanomaterials, the matrix in which they are embedded (if at all), and the process and/or activity involved. Tsai *et al.* [42] reported that handling 100 g of nano-alumina powder resulted in a much higher released particle concentrations than handling 15 g. High-energy processes, such as pouring, generate more particles than less vigorous processes, such as transferring. Johnson *et al.* [43] found that the sonication of functionalized multi-walled carbon nanotubes (MWCNTs) in reconstituted water containing natural organic matter resulted in particle concentrations three times higher than sonicating raw MWCNTs in the same medium.

Material that was detached (i.e., released) from a powder body, a liquid, or a solid matrix can be emitted depending on the process specifications and on-site control measures in place. **Figure 1** depicts a typical occupational setting from which ENMs could be released, emitted, and transported, resulting in exposure to workers. If the release rate cannot be directly calculated from a predefined release mechanism, it may still be possible to estimate it from the information

on source concentrations, near-field volume flow rates, and the release start point and duration. Some of the released particles might be captured by engineering controls (e.g., ventilation or enclosure); the escaped portion, which subsequently disperses into working environments, is called emission. Transmission describes the process during which emitted aerosols are transported to the immediate receptors, which then results in exposure.

Amongst the metrics used to characterize the release of nanomaterials, particle number and mass concentration are the two most widely used parameters for airborne ENMs in occupational settings [124], possibly due to the availability of sampling equipment and mature sampling procedures. Such data allow the creation of rankings for the release potential of common industrial processes and the study of how release is influenced by factors such as the quantity of material needed, how it is treated, the energy levels associated, and variable human factors.

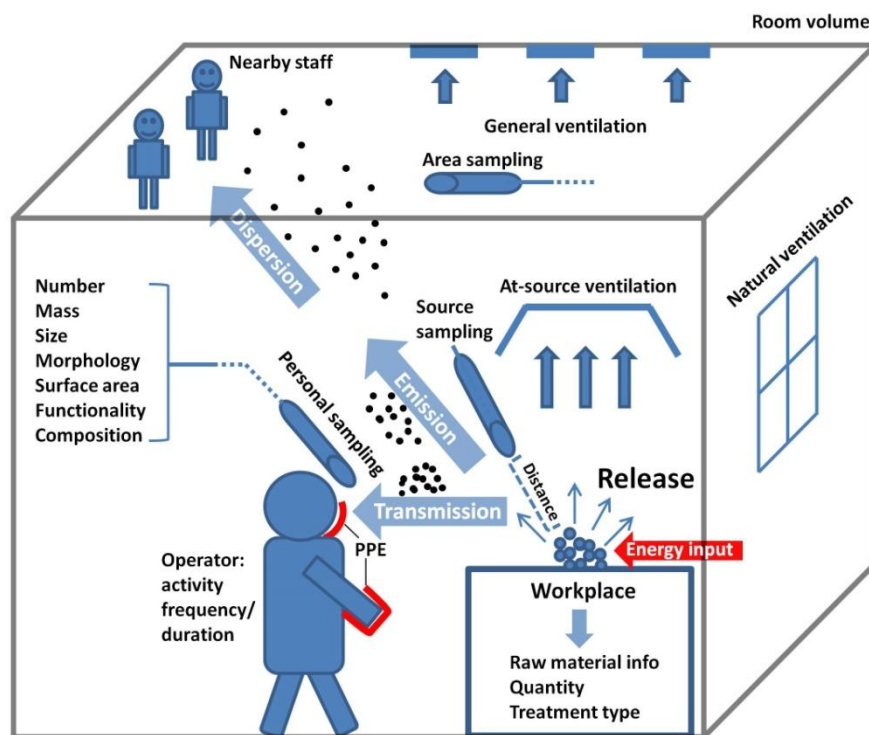


Figure 12. Diagram representing various elements and processes in an occupational exposure scenario

In addition to the characterization of the ENMs released, a comprehensive exposure assessment should also include the necessary contextual information. Clark *et al.* [182] pointed out that the

level of relevant detailed information in the existing literature on exposure is often insufficient for an in-depth understanding of the situation being studied. Parameters such as ventilation type, the personal protective equipment (PPE) used, sampling locations, frequency and duration of worker activity, and personal sampling data are not always fully described. This information is critical to transform upstream release data into downstream exposure estimates. Only sufficiently detailed meta-data will allow the development of exposure scenarios that are valid for risk assessment purposes and that can be used for establishing health and safety strategies.

This paper reviews the information on ENM release and exposure in the scientific literature and assesses how they inform us about the related human exposure in workplaces. The availability of the contextual information needed for exposure and risk assessment was assessed to identify potential gaps in data collection and reporting. The characteristics of released ENMs—including number concentration, mean size, and morphology—were compared for different processes involved in order to facilitate a general grouping and ranking of release potential. Measurement strategies, such as the equipment types and sampling locations used in field studies, were evaluated to give a better understanding of release and exposure data. Furthermore, production capacities and amounts handled were compared across different activities and materials in order to identify processes with a possibility of high occupational exposure. Finally, the types and efficiencies of engineering controls were summarized in order to describe the overall level of protection for workers in nanotechnology workplaces.

## **Method**

### **Literature collection strategies**

We conducted a systematic review of scientific publications describing real-world measurements of airborne ENM release and exposure in industry and research laboratories. The goal was to cover a wide range of relevant studies on this topic and describe the current information and knowledge about ENM release in workplaces.

The studies examined were collected from multiple literature sources. As a first step, 26 publications were identified in the NANEX database. The NANEX project's goal was to build a comprehensive library of occupational exposure scenarios for ENMs throughout their entire lifecycle [189]; it includes scientific literature and large surveys which generally contain

descriptions of the material, the processes and activities, release levels of airborne nanoparticles, and subsequent exposure estimates under specific environments. The literature covered scenarios related to the production of ENMs at a research-scale, as well as in industrial settings and downstream uses. The information available was a very good fit with the context of our review. Thus, the list of literature in the NANEX database was used to target relevant publications.

In a second step, we searched public online databases such as PUBMED and ScienceDirect. Keywords were chosen by analyzing the frequency with which they appeared in the titles of the selected NANEX publications. The most common words were *release*, *exposure*, *workplace(s)*, *airborne*, *nanoparticle(s)*, and *characterizations*. Combinations of these terms were then used in the searches. The names of specific materials were also used—such as *titanium dioxide (TiO<sub>2</sub>)*, *carbon nanotubes (CNTs)*, and *silver (Ag)*—to ensure the completeness of the search. Articles were screened and then retained if they fulfilled the following three conditions: 1) they at least partly addressed release associated with airborne ENMs; 2) their measurements were conducted in occupational settings (industrial or research facilities); 3) they comprised quantitative descriptions of ENM release scenarios, such as particle number or mass concentrations. All the collected articles were written in English..

Additional potentially relevant publications were identified using the *related citations* function, as suggested by the online databases when searching for specific items. This is usually a very efficient method for quickly identifying target articles.

### **Information processing**

An Excel spreadsheet was used to store the information extracted from the literature. The following key sub-categories were included: activity description, contextual information (e.g., engineering controls, PPEs, work duration and frequency, room dimensions), information on the bulk material, measurement strategy (e.g., equipment types, sampling distance to source, location), and airborne particle characterization (e.g., morphology, chemical composition, particle number and mass concentrations, diameter, surface area and functionality).

The present review specifically assessed the release characteristics of different industrial and laboratory processes. This involved evaluating the completeness of the information in activity descriptions, especially the process parameters that influence release scenarios. It also looked at

whether the information collected would allow a calculation of actual release rates, such as the sampling distance to source and ventilation rates. Finally, the review considered whether information on a material's properties and the quantities treated in a specific process were sufficiently detailed to inform us about the characteristics of released particles, including concentration and size distribution.

Attention was also given to the description of the general situation of worker exposure to ENMs in relation to release at nanotechnology workplaces. Exposure-related background information was essential for this purpose. We therefore identified the reported types and efficiencies of safety control measures used to limit ENM emission rates into the working environment, as well as any PPE that might influence a worker's level of exposure in the breathing zone. Additional data collected included production capacities and the amounts of raw materials handled, the frequency and duration of workers' activities, and ambient conditions such as relative humidity, the room volume, and any other information that might help to understand aerosol dispersion behaviors.

To ensure that the information extraction process was carried out in a systematic and repeatable manner, one person first coded all the information. Subsets of reference articles were then coded by several co-authors with the same coding rules. This control coding resulted in an almost perfect match.

## **Linking release to exposure: literature analysis**

### **Literature identified in the review**

The articles collected and reviewed are summarized in **Table S1** (Supplementary information, SI) by year, type (research or industry), material and activity. The years of publication range from 2004 to 2013. This represents the period when nanotechnologies were developing rapidly, and there was increased reporting on issues regarding exposure to ENMs. Most of the studies focused on exposure assessments reporting contaminant concentrations in workplace air. Thirty percent of publications investigated laboratory activities, 60% looked at industrial processes, and the remaining 10% investigated both. A large part of this literature focused on exposure to carbonaceous materials, followed by various metals and metal oxides. In some cases, the information provided failed to indicate the material type. Activity types included synthesis,

processing, handling, cleaning, machining, and others, during different phases of ENM lifecycles.

### Information availability

We first assessed which of the elements considered as important for linking release to exposure—when developing exposure scenarios—were available in the articles selected. **Figure 13** shows how available each of these elements of information was in the publications reviewed. It is divided into three sub-groups: contextual information, measurement strategy, and characterizations.

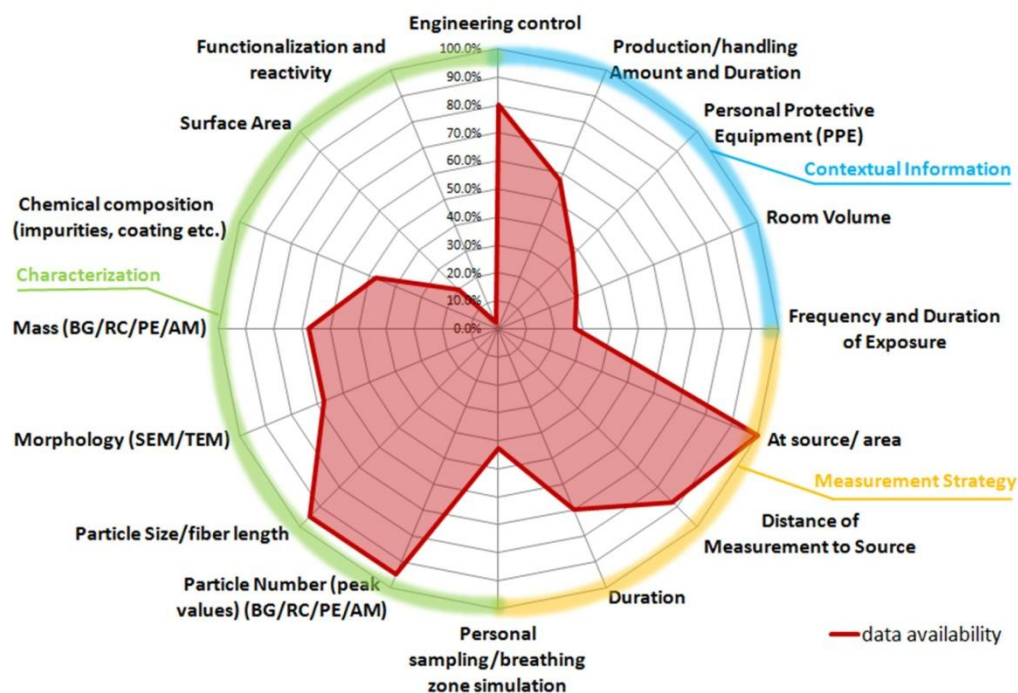


Figure 13. Summary of the percentage of articles providing essential elements of release- and exposure-relevant information

Types of engineering controls were frequently provided as contextual information. In contrast, only about half of the articles described the quantity of material being treated, and only about a third indicated the PPE used, the volume of the room involved, and the frequency and duration of the activity. As part of measurement strategies, at-source and area measurements were normally conducted for release and background characterizations. The sampling duration and distance to the source were usually given in the description of measurement methods. However, personal

breathing-zone data or simulations were only available in less than half of the publications. For particle characterizations, most studies provided number- and mass-based concentrations, size distributions, and a particle morphology analysis. The chemical compositions of airborne ENM samples were less frequently reported. Other physical and chemical properties—such as surface area, surface reactivity, and functionality—were less often or rarely characterized. Due to readily available equipment and mature, established procedures, the characterization of particle number and mass concentrations were relatively easy to carry out. For other metrics, such as surface area and coating type, collecting suitable data might have been difficult due to a lack of reliable equipment for on-line or off-line analysis of these properties.

### Activities and released materials

The industrial processes and laboratory activities identified were investigated for their potential to release airborne ENMs. They were grouped by the nature of the processes and activities and the types of particles identified in them. **Figure 14** (left) shows the percentage of publications for each category of activity. Collecting and sorting materials during production were the most commonly described activities. The most frequently assessed groups of processes are further described in **Table 1**. **Figure 14** (right) shows the fractions of release and exposure literature that contains each type of nanomaterial listed. In total, 43 materials were identified. CNTs were the most frequently investigated, followed by TiO<sub>2</sub>, Ag, iron oxides, carbon black, carbon fibers, aluminum oxide, silicon oxide, and fullerenes. A series of studies also described types of unexpectedly released particles, such as plastic materials generated from hot-sealing collection bags during packaging [38] and nanoscale particles emitted by forklifts in warehouses [185, 190-192].

Table 1. Types of activities most often described as causing airborne ENM release, together with typical examples

<b>Activity type</b>	<b>Examples from the literature review</b>
Collecting and sorting during	Collecting end-product materials from chemical synthesis [46]; batch collection by industrial cyclone [193]; emptying and tipping powder materials from bucket to bucket [40]; scooping spilt materials off a table [40]; opening a furnace and

ENM productions	transferring materials to vials [185]; manually loading and unloading trays [185]; dumping materials into a mixing tank [185]; detaching and removing CNTs from growth substrate using a razor blade [39].
Physical /chemical synthesis	Gas-phase production of metal-based nanoparticles [194]; flame spray pyrolysis technique (FSP) [195, 196]; induced coupled plasma with electric atomizer [197]; reaction collection [46]; electric arc reaction [198]; hot-wall reaction [38]; combustion reaction [75]; chemical vapor deposition [37, 39, 59, 199, 200].
Weighing /mixing	Handling nanopowders in an exhaust hood [196]; transferring from storage container to a balance [43]; weighing inside a fume hood [201]; mixing nanofibers with solvents [201].
Machining /abrasion	Wet-sawing nanocomposites [185]; cutting and winding coated substrate during electrospinning deposition onto a cellulose substrate [185]; band-sawing nanocomposites [73]; cutting composites using a water-cooled, dust-suppressed table saw [201]; chopping extrude composites [201]; fettling (removal of excess molding materials by sawing) [202].
Cleaning /maintenance	Cleaning a pyrolysis system [196]; cleaning an enclosure after laser ablation synthesis [40]; vacuum cleaning an enclosure in High-Pressure CO Conversion [40]; vacuum cleaning after creating and spray-drying slurries [185]; reactor cleanout [185]; cleaning/brushing down a plasma torch in a radio-frequency induction plasma reactor [185]; cleaning-up spilled materials from dumping operations [48]
Others	Spraying and filtration of CNT solutions [59]; spraying solution onto a bulk absorbent [185]; changing a spray dryer drum [185]; spraying a suspension [187]; flame-spraying for surface coating and modification [203]; sonicating materials with different surface coatings in a hood [185]; sonication in an unventilated enclosure [43]; pelletizing and bagging products in a warehouse [204].

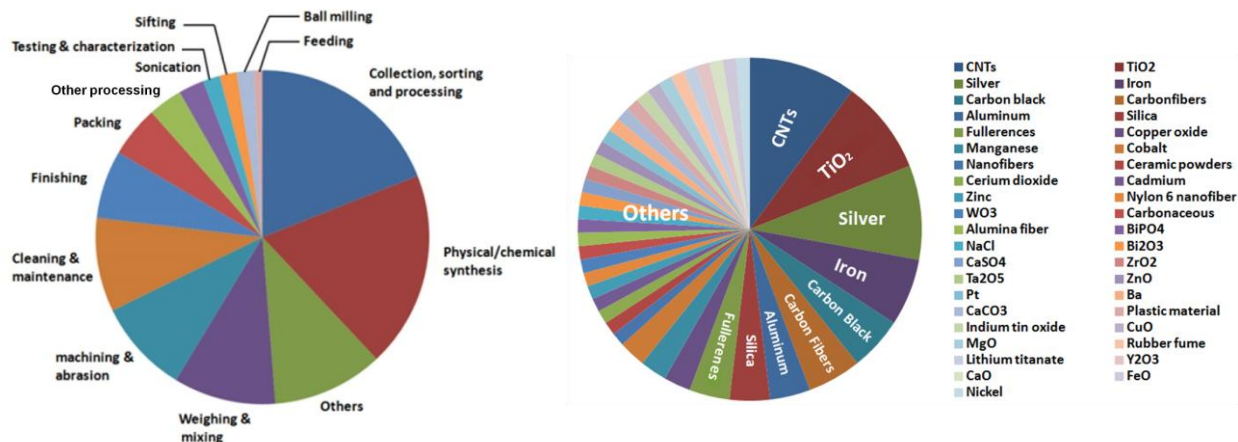


Figure 14. Proportions of activity types (left) and materials (right) identified from the literature review

### Release or near field/workplace area particle characteristics

When describing their release scenarios, most studies provided particle number and mass concentrations and at least some information about size distribution. Background measurements were frequently used as references. **Figure 14** (SI) provides an overview of metrics used for describing different activities and process types, as well as the measurement results for airborne particle concentrations and sizes. Number concentrations were mostly reported in the size range below 1  $\mu\text{m}$ , usually obtained by SMPS or FMPS, and often presented as continuous curves showing concentration evolution (changes) over time. Mass concentrations were reported in the fine ( $< 4 \mu\text{m}$  or  $< 2.5 \mu\text{m}$ , depending on the convention applied) or respirable particle ( $< 10 \mu\text{m}$ ) size ranges. For non-continuous actions, such as handling [59] and cleaning [40], peak ranges were frequently used to document the release. Mass concentrations were usually values averaged over certain periods of time. **Figure 4** ranks the near-source number concentrations by different production and handling activities. Correspondingly, particle size information, grouped by different processes, is shown in **Figure 5**.

Several studies investigated airborne ENM releases from laboratory sonication activities. The surface properties of sonicated materials seemed to strongly influence the release process. Sonication of raw MWCNTs in de-ionized water resulted in 2,200–2,800 particles/ $\text{cm}^3$  below 1  $\mu\text{m}$  in the air above the water bath, whereas the same procedure done with functionalized MWCNTs (hydroxyl group addition) resulted in only about one third of this value [185].

However, another study showed a higher release of functionalized CNTs ( $158 \text{ \#/cm}^3$ ) in water containing natural organic matter, than normal CNTs ( $56 \text{ \#/cm}^3$ ) in the same media [43]. Furthermore, sonicating carbon black led to five times more particles being released than sonicating fullerenes in de-ionized water. Lee *et al.* reported that fine particles between 120–300 nm were released (at 2–3 times the background level) during the ultrasonic dispersion of MWCNTs in a fume hood, which was differentiated from fugitive particles ( $< 100 \text{ nm}$ ) generated by other processes [59].

Cleaning was an activity often associated with the release of airborne particles in large sizes. Cleaning a pyrolysis system prior to operation resulted in a 10-fold increase in the airborne mass concentration, but no distinct change in particle numbers [196]. Vacuum cleaning following the chemical synthesis of single-walled carbon nanotubes (SWCNTs) led to the release of very large microsized agglomerates into the air [108]. In another case, where vacuum cleaners without HEPA filters were used to clean up after the creation of titanium slurries during spray drying, 10- to 50-fold increases in number concentrations were measured for particles in the 300–1000 nm range [185]. In a clean-out activity following the gas-phase condensation manufacture of silver nanoparticles, five times more particles were measured in the 500–1000 nm range [185]. Similarly, cleaning the filter chamber and cyclone of a radio-frequency induction plasma reactor for aluminum production was associated with  $15,580 \text{ p/cm}^3$  of air, with more

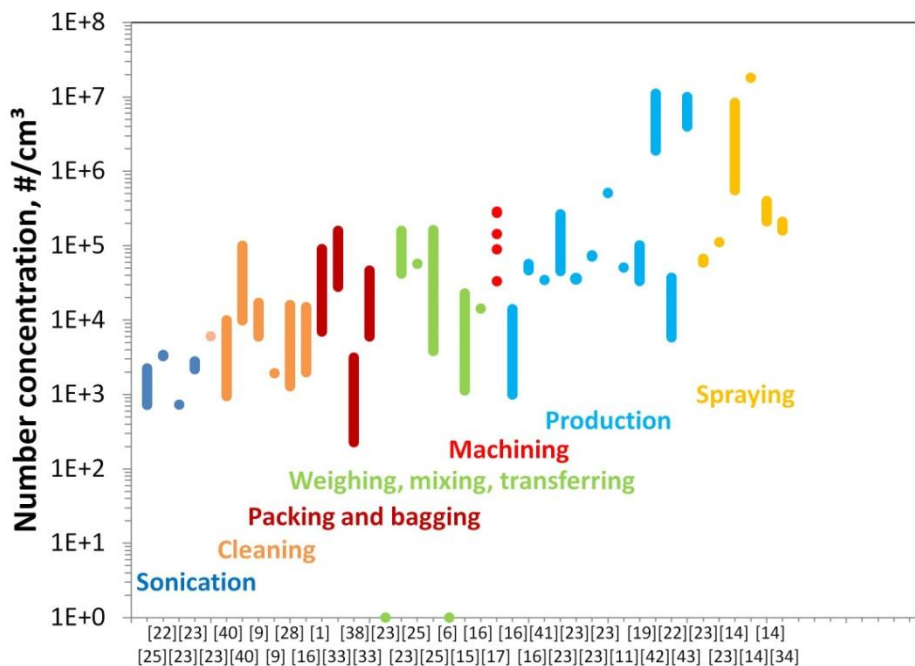


Figure 4. Near-source airborne ENM particle concentrations in workplaces, ranked by production and handling activities. Horizontal axis numbers refer to the reference list of articles in the supplementary information (SI).

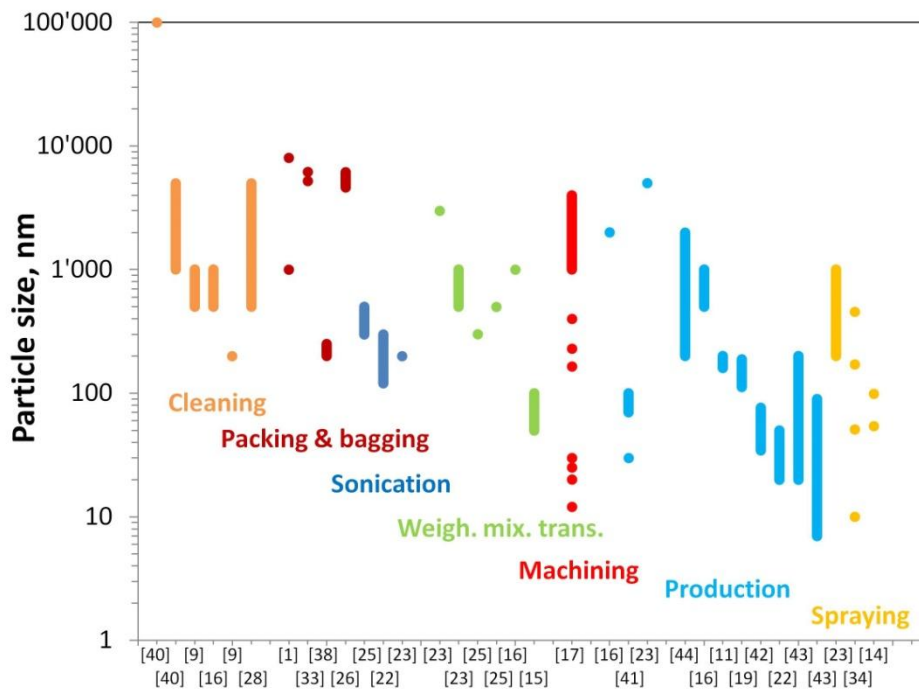


Figure 5. Diameter of airborne ENM particles released from production and handling activities (modal size or estimation from transmission electron microscopy analysis). Horizontal axis numbers refer to the reference list of articles in the supplementary information (SI).

than ten times more particles in the 300–1000 nm range [185]. Furthermore, sweeping up spilled materials from a dumping operation also slightly increased the mass concentration of respirable particles [205].

Industrial packaging and bagging activities often released large ENM particle agglomerates into the air. Kuhlbusch *et al.* reported a four- to eight-fold increase of PM10 mass concentrations, mostly for particles larger than 400 nm, during the bagging of carbon black [190]. In another study investigating the same material, the number concentration was elevated for particles > 100 nm [191]. During the removal of fullerenes from a storage tank, airborne particles larger than 1000 nm were identified [47]: the fullerenes existed mainly as aggregates and agglomerates in the air. TiO<sub>2</sub> aerosols were found to be released at diameters up to 6.0 μm during packing [192].

Bagging carbon nanofiber end-products released 230–3,130 carbon nanofiber p/cm<sup>3</sup> of air [205]. Area sampling resulted in a 0.5–1.1 mg/m<sup>3</sup> mass concentration, mainly made up of carbon nanofibers.

Weighing and mixing processes usually resulted in only minor or moderate increases in airborne ENM particle concentrations. No significant releases were recorded during the handling of synthetic ceramic nanopowders [196], transferring carbonaceous materials [43], or the laboratory handling of metal oxides [187]. During the weighing and transfer of different nanomaterials, release scenarios varied [43]. Handling raw MWCNTs and fullerenes generated much higher particle counts than the background, whereas treating functionalized MWCNTs and carbon black generated no significant release. In contrast, handling nanofibers generated particle concentrations up to 15,000 p/cm<sup>3</sup>, which was six to twenty times above the background level [196].

Physical and chemical synthesis were associated with potential releases of airborne ENM particles in smaller sizes. No significant release was observed in comparison to background levels during the experimental-scale production of nanofibers [196], pyrolysis production of TiO<sub>2</sub> [196], CVD growth of CNTs [39] and MWCNTs [199], and synthesis of Ag by mixing sodium citrate with silver nitrate [206]. In contrast, one study showed significant at-source releases from the CVD production of CNTs at sizes below 100 nm (probably carbonaceous by-products) and from 7–200 nm [207]; using higher injection temperatures released more particles of reduced diameters (from 20–200 to 7–90 nm). Synthesis of TiO<sub>2</sub> generated noticeable particle concentrations with a bimodal distribution (< 30 nm and 70–100 nm) [206], whereas induced-coupled-plasma production of Ag resulted in significant releases in the 20–30 nm range. Flame synthesis of metal oxides registered particle emissions in the 112–185 nm and 24–29 nm ranges, depending on the materials produced. Process parameters, such as filter-to-flame distance, precursor-to-oxygen ratio, and flame numbers appeared to influence the release scenarios [195]. For industrial processes, the reaction-collection of carbon black and the electric arc reaction of other carbonaceous materials mostly released particles in the 10–100 nm range [46, 198]. Gas-phase production of metal-based nanoparticles resulted in submicron particle releases at modes in the 160–200 nm range [194]. In vapor grown synthesis of carbon nanofibers, the nanofibers were found to be the dominant source of elementary carbon, but iron-rich soot-like particles at 20

nm were also identified [200]. Combustion reaction processes were shown to emit particles smaller than 300 nm [75]. In all these studies, the mass concentrations measured were often low, which indicates that mainly small particles were released.

Machining and abrasion of nanocomposites were often shown to release matrix materials with embedded ENM fillers. Furthermore, the release mechanisms varied by process type, parameters, and matrix as well as the filler materials. Wet-sawing of carbon nanofiber composites showed high particle release in terms of mass but not in numbers [185, 208]. A dry process was associated with a much lower particle emission than a wet process using the same materials [153]. In wet treatments, it is likely that the detected nanoscale particles were primarily water droplets. Comparing different materials, alumina fiber/CNT composites showed the least particle release, whereas alumina composites resulted in elevated particle generation. The thickness of the composite layer also affected particle release. No primary CNT structures or bundles were identified in the released particles.

Spraying process mostly led to high levels of airborne particles of very small sizes. In flame-spray processes used for coating and the surface modification of materials, the highest releases (160,000–210,000 p/cm<sup>3</sup>) were seen during the active phases of the process (flame on, precursor on) [203]. The particle size distribution showed multiple modes in the 10–454 nm range. Changing spray dryer drum also released high airborne concentrations of spray materials [185]. One extreme case reported concentrations up to 18,000,000 p/cm<sup>3</sup> at 54 nm in the personal breathing zone [187]. Spraying suspensions and pyro silanization registered high releases in the 55–99 nm range.

Other sources of nanosized particles were reported for all types of activities. Forklift trucks were a common source of ultrafine particles (< 100 nm) in activities such as warehouse bagging and packaging of carbonaceous materials [190, 191, 209] and TiO<sub>2</sub> pigment [192]. Vacuum cleaners were also found to release nanoscale particles [47], especially when no HEPA filter was installed [185]. Other combustion sources, such as butane gas heaters [190], gas-fired radiant heaters [205], and hot-sealing plastic bags [38], were also found to release very small particles. Additionally, a rotary-type oil vacuum pump was identified as a source of 300 nm particles [199].

The studies were able to distinguish these secondary releases of nanoscale particles by comparing the aerosol profiles (size and concentration) obtained with and without their potential sources. Although toxicological studies focus mostly on ENMs, it might be of equal importance to characterize the accidentally released nanoparticles in workplaces.

In most of the cases, released airborne ENMs were agglomerates or aggregates, often resulting in complex particle morphologies, such as loose, porous clusters of metal oxides particles [185], densely packed Ag particles [210], entangled CNFs [196, 208] and chain-like structures of CNTs [207]. Only one study reported individual Ag vapor condensate particles [211].

The results from ENM release scenarios seemed to be largely determined by process energy. High energy processes such as synthesis, spraying, and machining released large amounts of airborne ENM particles in the nanometer range. Low energy processes including laboratory handling, packing and bagging on production lines, and cleaning usually resulted in slight or moderate increases in ENM particle concentrations in the air. The particles released by these processes were often large agglomerates with sizes up to several micrometers. Furthermore, release mechanisms were found to be influenced by process parameters, material properties, and environmental conditions. These included, for example, material quantities, ambient humidity [42], and surface functionality [185] during material handling. Smaller quantities, hydrophilic surfaces, and higher humidity seemed to reduce particle concentrations. During sonication, the solubility of materials in the liquid media played an important role [43]. More soluble materials had lower chances of escaping from the solution and becoming airborne. During physical and chemical synthesis, reactor setup and process temperature both affected release levels [195]. Dynamic reaction processes and poor filtration resulted in higher ENM particle emissions. During the mechanical processing of nanocomposites, the filler type, its distribution in the matrix, and the treatment conditions (dry or wet) modified the release scenario [153, 185, 208]. Lower filler contents and humid atmospheres helped reduce particle emissions and personal exposure during processing.

### **Emission rate calculations**

Very few of the studies reviewed estimated ENM release rates for the processes that they investigated. Nevertheless, a few scenarios were identified where a rough estimation of release

rates might be possible because approximate room size and air exchange information had been provided together with the process characteristics and ENM particle concentrations over time. In one laboratory study in which only basic mechanical ventilation was used, the rate of room air change (or air changes per hour, ACH) and the room's dimensions were given [153]. In this case, the release rate can be estimated by integrating particle concentrations over time and the volume flow rate of the air in the room. The average particle concentration in the room can be calculated from source or area measurements, taking into account aerosol transport and diffusion mechanisms (e.g., near- and far-field models). In another study, investigating a laboratory synthesis process, the room's ACH was known, and the ENM emission rate was estimated from the average particle concentration using a one-box model assuming homogeneously mixed room air [36]. On the other hand, if natural ventilation is used [48, 192, 197], such as windows and doors, the room's ACH can be estimated from the ambient environmental conditions (e.g., wind speed, open surface area) assuming normal conditions as described in technical manuals, such as the EPA Exposure Factors Handbook (EPA 2011) or other literature [212, 213].

### **Measurement strategy**

The selected studies were also analyzed with regard to the types of measurement devices used, their detection limits, and the size range they could give information about for specific scenarios. Scanning mobility particle sizers (SMPS) were the most frequently used equipment for measuring particle numbers and size distributions below 1  $\mu\text{m}$ . A Nano-SMPS is sometimes used to obtain a greater size resolution below 100 nm [40]. Other frequently used devices were: the fast mobility particle sizer (FMPS), which was found to be particularly useful in environments with rapidly changing particle concentrations [73, 192]; optical devices such as the aerodynamic particle sizer (APS, size range up to 32  $\mu\text{m}$ ) were used for micro-sized particles [190, 196]; and filters were often used to collect airborne samples in order to assess mass concentrations gravimetrically [185, 199, 214]. A few studies also assessed the surface area of particles [38, 73, 209]. Morphological and elemental analyses were mostly done using electron microscopes [37, 185, 208, 215].

Sampling locations were assessed in order to understand whether source or near-field measurements had been carried out and whether personal breathing zone concentrations—which could provide information about particle transmission from sources to receptors—had been

measured. The review showed that source sampling had normally been conducted as close as possible to the potential emission points. For handling nanopowders under fume hoods, the distance was in the centimeter range [42, 187]. For flame and flame-spray production, the measurement position was in several tens of centimeters range or at the nearest opening [38, 198, 203, 216]. For large-scale manufacturing and processing activities, typical sampling locations were a few meters away from the suspected emission sources [47, 185, 191, 197, 199, 217]. Personal exposure characterization was usually conducted near workers [40, 196], sometimes even next to their noses [42], whereas others measured working positions near the assumed breathing zone of sitting or standing workers [36, 37, 194, 198, 204]. Filter samplers were mostly clipped to workers' collars, and personal nephelometers were attached to their belts [214]. Area sampling was used either as a background reference or to estimate the general exposure levels in working areas. Background reference levels were collected in production areas away from the immediate vicinity of the processes [37, 42, 43, 185, 198], or even outdoors [200]. In order to monitor air quality in normal working areas, near field (2.5 m) and far field (7.8 m) concentrations were measured [36]. Maintenance areas and conference rooms were sometimes monitored as well [200].

### **ENM production capacities and quantities handled**

The quantities of ENMs being handled varied from a few milligrams to many tons per year. **Table 2** gives an overview on the quantities involved in nanomaterial production and handling in research laboratories and in industry. The production of metals and metal oxides in research laboratories was mostly in the range of grams to kilograms. For carbonaceous materials (CNTs, carbon nanofibers, carbon nanopearls), production was often limited to just a few milligrams. In contrast, mass production by industrial manufacturers often ranged from kilograms per batch to tons per year. In research environments, the amounts of materials handled were also significantly lower than those in large-scale production facilities. The quantities treated were usually in the milligram range for activities such as weighing [185] and sonication [43]. For common materials, e.g., alumina powder, up to hundreds of grams could be handled for different purposes [42]. In industrial settings, normal handling activities such as end-product collection, packaging, and bagging of materials were in the same ranges as those seen for the manufacture of these nanomaterials. The largest quantities of novel nanomaterials were reported for titanium dioxide

powders, which were processed in kilograms per minutes [193] and bagged in 25–800 kg batches [192]. Traditional materials subject to huge demand, such as CaCO<sub>3</sub> and carbon black, could be handled in quantities as much as 60 tons per day [191].

Table 2. Information on ENM production capacities and amounts handled, from the literature

Production (laboratory)		Production (industry)		Handling (laboratory)— weighing/mixing/sonication		Handling (industry) —collecting, spraying, mixing, bagging	
Material	Quantity	Material	Quantity	Material	Quantity	Material	Quantity
TiO <sub>2</sub>	20 g/b [206]	Silicon	kg/d[38]	Alumina	15/100g[42]	TiO <sub>2</sub>	1 kg/min[193]
M. oxides	6 g/d[36]	TiO <sub>2</sub>	5–10 kg/b [185]	TiO <sub>2</sub> , CuO, Ag	mg/b[185]	TiO <sub>2</sub>	25 kg/800 kg bag[192]
Selenide	g/b[185]	Mn/Ag/Co/Fe	kg/b[216]	Full./MWCNT	4–200 mg[185]	CaCO <sub>3</sub>	22.5 ton/d[191]
Al	kg/b[185]	Catalysts	1 kg/d[216]	CNTs	4–200 mg[43]	Silica-iron	kg/b[185]
Ag	1–5 kg/d[197]	Metal oxides	1 kg/d[218]	CNMs	100 mg/L[43]	SiO <sub>2</sub>	40 kg/600 kg/b[191]
MWCNT	1–2 mg/b[185]	Ag	1200 kg/b[211]			Fullerene	40 ton/y[47]
CBF	500 mg/b[185]	CBF	10–20 kg/s[185]			CNF	7 kg/bag [48]
CBNPs*	200 mg/b. [185]	CNF	14.1 ton/y[200]			CB	60 ton/d[191]
		Silica aerogel	0.5 ton/y[59]				

\*CBF, carbon nanofiber; CBNPs; carbon nanopearls; Full.: fullerenes; CNMs, carbon based nanomaterials; b, batch; s, shift; d, day; m, month; y, year

## Ventilation and PPE

Engineering control systems and PPE play important roles in preventing or reducing personal exposure to hazardous substances in workplaces. The engineering controls described in the reviewed literature can be broadly grouped into four categories:

- a. Laboratory fume hoods
- b. Local exhaust ventilation (LEV) systems
- c. Process-specific enclosures
- d. General/centralized ventilation and natural ventilation

Typical PPE includes laboratory clothes, a full-body protection suit, glasses, gloves, and a mask.

Laboratory fume hoods were commonly used when handling small quantities of potentially hazardous materials for activities such as weighing, mixing, transferring [201], sonication [59], and creating solutions [185]. They were also used for experimental-scale physical [198] and chemical synthesis [36, 37, 42, 197]. The design and use of laboratory hoods has been greatly influenced their effectiveness at removing released particles: constant velocity hoods were found to work best during the pouring and transferring of nanopowders, followed by bypass (compensating) hoods, and then conventional hood [42].

LEV systems were often employed in industrial environments for controlling particle concentrations at their sources, such as furnaces [214], bagging machines, production lines [187], and during reactor cleanout processes [216]. The efficiency of LEV has been described. While cleaning up after a gas phase condensation of silver, particle release in the 500–1000 nm size range increased by five times. When a LEV system was used, the particle concentration fell to the background level [185]. During another cleaning process involving nanoscale metal catalytic materials, a properly maintained LEV system was shown to reduce particle mass concentration by 75% to 96% (mean: 88%), with a similar efficiency for number concentrations [216].

Enclosures of both small and large volumes were seen in fixed installations. These included a ventilated chamber for the electrospinning deposition of nanofibers [185], a positive-pressure glove box during the synthesis and manipulation of quantum dots [185], and a ventilated chamber for spraying a solution, followed by fiberization of absorbent material [185]. Distinct differences in particle concentrations were observed inside and outside such enclosures. One aerosol enclosure chamber significantly reduced particle concentrations during the collection of end products using an industrial cyclone [193]. Enclosing and ventilating the furnace during the production of multi-walled carbon nanotubes (MWCNTs) using chemical vapor deposition (CVD), minimized workers' exposure down to non-detectable levels [199]. In a spraying process, particle emission was shown to be much lower outside the spray enclosure than inside [185]. During flame spraying, average particle number and mass concentrations were 6–46 and 5 times lower, respectively, when a protective enclosure was installed [203]. Discussions on the efficiency of engineering controls can also be found in other studies [46, 75, 199, 206].

Centralized mechanical ventilation and natural ventilation have both been used in large-volume workplaces—such as warehouses and manufacturing areas—in order to help reduce particle concentrations. Rooftop exhaust fans were often seen above production lines [216] where large-scale processing activities such as drying [185], milling, spraying and blending [199], bagging, and packaging [38, 47] were taking place.

PPE was commonly used during material synthesis [216] and handling [59], cleaning, and the mechanical treatment of nanocomposites [185]. The equipment types included gloves, wrist-to-elbow cotton arm covers, full-body Tyvek suits, and full-face positive-pressure airline respirators [216], skin protection, half masks [59], shoe covers, and particulate respirators [185]. In a study of how well 3M FFP2/FFP3 and dräger 680 (FFP3) masks filtered 200 nm metal-based nanoparticles resulting from gas-phase production, they retained between 96.66% (FFP2) and 99.99% (dräger) of the number concentration of particles, respectively, under production conditions [194].

### **Limitations of the literature to date and suggestions for improvements**

This review found that ENM release characteristics could be grouped by activity type. Process characteristics, such as energy input and system parameters, influenced release levels. The information derived from this analysis provides a good qualitative understanding of the release mechanisms from different activities and processes. However, quantitative determinations of release and exposure remain difficult to achieve. This could be significantly improved by collecting and providing sufficient contextual information.

The literature reviewed in this study contained various types of ENMs in both industrial and laboratory settings. This enabled us to establish a preliminary ranking for nanoparticle release potentials, which could, for example, be used to define priorities for ENM release and occupational exposure assessments. It could also become a guide for the definition of precautionary measures. In our review, release levels and characteristics were comparable within the different types of defined groups of processes; they seemed to be linked to the energy levels associated. Understanding the relationships between specific process parameters and release levels—such as system setups, reaction temperatures, environmental humidity, and material properties—could help to prevent significant releases through safe-by-design approaches.

Morphological analyses showed that most of the ENM particles released were in an agglomerated state, which is important to bear in mind for an understanding of their potential impacts on human health. However, it is possible that these agglomerates are later broken up into smaller or primary nanoparticles. Studies have shown a possibility for the deagglomeration for nanoparticle agglomerates in the human respiratory system [63, 64], or when the particles are subject to external forces [65, 67, 101]. Therefore, in the future, information about the stability of nanoparticle agglomerates may be needed, together with the size information, when characterizing human exposure to ENMs and the risks associated.

Most of the studies assessed focused on the characterization of the released particles' properties close to their source. Only a few of them also provided relevant contextual information for estimating short-term and long-term personal exposure. Often, missing information included the properties and amounts of raw materials handled; this would provide information about the material's dustiness and the maximum possible release levels in subsequent exposure estimations. Furthermore, there was little information available that would allow estimations of exposure duration and frequency (e.g., hours/day, days/month, months/year)—data needed to estimate the total exposure dose and its effects of accumulating exposure over the long run. Unfortunately, information useful for an understanding of release was often missing, for example, information on the volume of the workplace, which provides the basis for simulating the potential distribution behavior of released aerosol particles. The same information would permit an estimation of exposure levels in general working areas, which are not often measured. Clark *et al.* [182] made a detailed discussion of the limitations of data reporting in exposure assessments and gave recommendations for future methodological improvements. We also recommend that release studies include the collection of exposure-relevant data so that they can have an even better impact and contribution to our understanding of exposure to airborne ENMs.

One significant limitation of the literature to date on airborne ENM release is that it has rarely provided either particle release rates or the contextual data that would allow an estimation of those rates. Most studies only provided near-source concentrations together with sampling distances. Few provided proxies for the near-field flow rate, such as the ventilation rates of local exhaust controls. Thus, the particle concentrations reported in this review are merely indicative of the release potential of the various processes analyzed: they cannot be interpreted

mechanistically as actual release levels. Use of a harmonized data collection strategy in future studies may facilitate the assessment of the real release rates of the processes concerned. There is also an opportunity to develop better data collection methods in measurement campaigns. For example, personal exposure levels (breathing zone) were rarely assessed, though this information would allow a validation of models that estimate workers' exposure doses from the source concentration and include physical and contextual parameters. Only a few studies have included data collection that has improved our understanding of particle transmission and dispersion in real world situations, although this would be useful for constructing particle distribution maps.

Another important limitation—one that is relevant to regulators and risk managers—is that the literature reviewed mainly covered the production and use phases of ENM lifecycles. There was very limited information available on the end-of-life treatment of ENMs at the time the literature was collected. However, these release and exposure scenarios are also important for making an overall risk assessment of ENMs. More recently published studies have started to address this data gap. For example, Massari *et al.* [219] looked at the behavior of TiO<sub>2</sub> nanoparticles during the incineration of solid paint waste. Reijnders [220] discussed safety issues during the recycling of materials containing persistent inorganic and carbon nanoparticles. Such information allows the current gaps in knowledge to be filled and will complete the data needed for doing risk assessments of ENMs throughout their lifecycles.

A preliminary ranking of the release potential for airborne ENMs could be used to develop a tiered approach to release assessment, resembling the concern-driven approaches used in exposure, hazard, and risk assessments [54]. The first step would be a qualitative assessment of the concern levels for specific processes from read-across, by assessing the possibilities for significant exposure and hazard. The second step could then be a quantitative evaluation (e.g., concentration, size, or chemical composition) of field measurements or laboratory simulations. The third step could be a systematic and comprehensive characterization of airborne ENM release scenarios from a process, using different conditions and parameters. This approach would allow the identification of the most critical or at-risk occupational activities in a cost-effective manner.

## **Acknowledgement**

The research leading to these results has received funding from the European Research Council under the European Union's Seventh Framework Programme (FP/2007-2013) / ERC Grant Agreement n.263215.

**\*Citations in this article are compiled in the complete reference list at the end of this report.**

## Supplementary Information (SI)

Table S3. Types of facilities, particle types and processes described in the review of literature from 2004 to 20

Year	Facility	ENMs	Activity type
2004 [40, 217]	R/I [40]; I [217]	SWCNT [40]; CB [217]	Cleaning/handling [40]; Processing [217]
2006 [46, 221, 222]	I [46, 221, 222]	CB [46]; Unknown [221, 222]	Synthesis/handling [46]; Other [221, 222]
2007[201]	R [201]	CNF [201]	Machining/handling[201]
2008[39, 47, 194, 198, 199, 216]	I [47, 194, 198, 216]; R[[39, 199]	CNT [39]; MWCNT [199] ; Carbonaceous [198]; Fullerenes [47]; Metal-based [194, 216]	Synthesis [194, 198]; Synthesis/handling [39, 199]; Cleaning [216]; Cleaning/handling [47]
2009[36, 37, 42, 73, 187, 196, 202, 215, 223]	R [36, 37, 42, 73, 187, 196]; I [202, 215, 223]	S/M-WCNT [37]; TiO <sub>2</sub> , NF [196]; Ag [215]; Alumina, CNT [73]; Alumina, Ag [42]; ITO, ZnO [187]; Lithium titanate [223]; Metal oxides [36]; Unknown [202]	Synthesis [36, 37, 223] Synthesis/handling/cleaning [196]; Handling [42, 187, 215]; Processing [202]; Machining [73]
2010[43, 48, 59, 185, 192, 204, 214, 218]	R [43]; I [48, 192, 204, 214, 218]; R/I[59, 185]	MWCNT, metals [59]; Fullerenes, CNT, CB [43, 204]; CNF [48]; TiO <sub>2</sub> [192]; TiO <sub>2</sub> , Ag [185, 214]; Metal oxides [218]	Synthesis/handling [59]; Handling [43, 192]; Cleaning [218]; Cleaning/handling [48]; Processing [204, 214]; Machining/cleaning [185]
2011[75, 191, 197, 200]	I [75, 191, 200]; R/I [197]	CNF [200]; TiO <sub>2</sub> , Ag [197]; SiO <sub>2</sub> , CB, CaCO <sub>3</sub> [191]; Metal oxides [75]	Synthesis [200]; Synthesis/handling [75, 197]; Handling [191]
2012[38, 193, 203]	I [38, 193, 203]	TiO <sub>2</sub> [193]; Silicon [38]; CeO <sub>2</sub> [203]	Handling [193]; Processing [203]; Processing/synthesis [38];
2013[224]	I [224]	Rubber fumes [224]	Other [224]

R, research laboratory(ies); I, industrial setting(s)

CNF, carbon nanofiber; NF, nanofiber; CB, carbon black; Ful., fullerenes; SWCNT, single-walled carbon nanotubes; MWCNT, multi-walled carbon nanotubes. Synthesis includes physical or chemical synthesis; handling includes transferring, weighing, mixing, collecting, sorting, and sonication; processing includes feeding, finishing, drying, spraying, filtering, packing, and bagging.

Act.	Ref.	Materials	BG, #/cm <sup>3</sup>	Number concentration, #/cm <sup>3</sup>	BG, mg/m <sup>3</sup>	Mass concentration, mg/m <sup>3</sup>	Mean size	Morphology
Weighing, mixing, transferring	[185]	Composite materials	700–19,500	4,000	0.015–0.019	0.064–0.221	0.5 x 3 µm	Aggl.
	[185]	MWCNT	14,700	57,000–157,800	N/A	N/A	0.5–1 µm	Aggl.
	[201]	CNF	N/A	N/A	N/A	Surface deposition: 0.39-17.5 ug/cm <sup>2</sup>	N/A	N/A
	[43]	C <sub>60</sub> fullerenes	14,922	72,085	N/A	N/A	~ 300 nm	Aggl.
	[43]	MWCNT	14,922	18,782–177,155	N/A	N/A	~ 500 nm	Aggl.
	[201]	CNF	10,000–20,000	10,000–20,000	0.015-0.019	0.03-0.055 (AM), 0.064-0.221	N/A	Aggl.
	[42]	Alumina, Ag	BG subtracted	1,575–13,260 (PBZ); 1,131–22,932	N/A	N/A	50–100 nm, 200 nm aggl.	Aggl.
[196]	Nanofibers	700	15,000 (peaks), 6 to 20 time increase	N/A	N/A	10 x 1000 nm	Aggl.	
Sonification	[43]	MWCNT, CB	724–1,250	1,450–3,500	N/A	N/A	300–500 nm	Aggl.
	[59]	MWCNT	2,000–3,000	5,276–6,399	N/A	0.0078–0.1609 (P, AM)	120–300 nm	N/A
	[185]	C60, MWCNT	N/A	730, 2200–2800	N/A	N/A	~ 200 nm	Aggl.
Packing and bagging	[217]	CB	1,000–10,000	8,000–100,000	0.01–0.045 (PM10)	0.027–0.34 (PM10)	1 µm, 8 µm, < 100 nm (forklifts)	Aggl.
	[191]	Nano-CB	22,000	50,000–180,000	0.169±0.116	0.159±0.052	6.1 um	Aggl.
	[205]	CNF, other particles	< 0.5e+5	(0.8–1.15)e+6 (total), 230–3130 (CNFs)	< 0.1	0.5–1.1	15–25 nm (radiant gas heater), 200–250 nm	N/A
	[191]	CaCO <sub>3</sub>	4,000	10,000–50,000	0.169±0.116	0.154±0.074	50–250 nm (forklifts), 5.2 µm	Aggl.
	[192]	TiO <sub>2</sub>	N/A	N/A	N/A	0.08–0.8 (AM)	30–60 nm (forklifts), 5.52–7.25 µm	N/A
Spraying	[185]	Silica-iron	13,300–20,300	79,700	< 0.0003	45.7 (Fe)	200–1000 nm	Slight aggl.
	[185]	TiO <sub>2</sub>	33,500	144,800	N/A	N/A	N/A	N/A
	[187]	ITO, ZnO	13,020	566,857–8,351,915 (PBZ 18,000,000)	N/A	N/A	54/99 nm	N/A
	[187]	ITO, ZnO	13,020	225,000–413,000	N/A	1.37–2.63	Large agglomeration	Aggl.
	[203]	CeO <sub>2</sub>	N/A	160,000–210,000; 4,600–9,200(AM)	N/A	0.32(0.125-63)	<10/51/171/454 nm	N/A
Other processes	[187]	ITO, ZnO	13,020	638,000 (AM)	N/A	1.37–2.63 (PBZ), 0.07 (AM)	55 nm	N/A
	[211]	Ag	5,000–50,000	>1,000,000	N/A	0.013–0.094	10–100 nm	Single
	[193]	TiO <sub>2</sub>	N/A	22,055–25,771 (no enclosure) / 7,500–10,000 (enclosure)	N/A	N/A	124.2 nm, 524.4 nm	Aggl.
	[185]	TiO <sub>2</sub>	13,000	177,600	N/A	N/A	N/A	N/A
	[191]	Fumed silica	3,700	10,000–19,000	0.169±0.116	1.963±1.051	4.6 µm	Aggl.
	[199]	CNT	N/A	172.9–193.6	N/A	0.21–0.43	2–3 µm	Sing.& Aggl.

Note: size range for number concentration < 1 µm; mass concentrations are measured for a wider size range, into microns; mean particle size was taken from the mode sizes in number size distributions or estimated from TEM/SEM images. BG, background; Aggl., agglomerate.								
Act.	Ref.	Materials	BG, #/cm <sup>3</sup>	Number concentration, #/cm <sup>3</sup>	BG, mg/m <sup>3</sup>	Mass concentration, mg/m <sup>3</sup>	Mean size	Morphology
Cleaning	[185]	Silver	N/A	6100	< 0.001	1.7–6.7	N/A	Aggl.
	[108]	SWCNT	< 50	1,000–10,000/10,000–100,000	N/A	< 0.05	1–5, 100 µm	Aggl.
	[216]	Ag,Mn,Co	12,146	18,196–29,063 (no LEV), 10,556–14,071 (LEV)	Not detected	0.71–6.7 (no LEV), 0.041–1.7 (LEV)	200 nm, 500–1000 nm	Aggl.
	[218]	Ag,Cu,Ni,Fe,Mn	N/A	1,300–16,000 (BG subtracted)	N/A	0.016–1.467 (PBZ), 0.17–0.754	0.5–5 µm	Aggl.
	[196]	TiO <sub>2</sub>	7,000–20,000	22,000	0.1–0.2	1.7	0.5–1 µm	Aggl.
Production	[196]	TiO <sub>2</sub>	7,000–20,000	21,000	0.1–0.2	0.4	0.5–1 µm	Aggl.
	[196]	Specific ENMs	5,500–15,000	62,000 (477,000)	N/A	N/A	2 µm	Aggl.
	[206]	TiO <sub>2</sub>	11,418	45,889	N/A	0.33–4.99	< 30nm, 70–100 nm	Aggl.
	[185]	Carbon nanofiber	13,600	59,000–279,700	0.012–0.015	0.031–1.839	0.1 x 5 µm	Slight aggl.
	[185]	MWCNT	6,600	42,400	N/A	N/A	N/A	N/A
	[185]	Metals/metal oxides	12,000–14,000	85,900	N/A	N/A	N/A	N/A
	[185]	Al	37,700	548,500	< 0.0004	0.246	N/A	N/A
	[194]	Metals	8,512	59,100 (136,000)	0.052	0.188 (1.34, AM)	160–200 nm	N/A
	[36]	Metals/metal oxides	2,109	Peaks: 35,494–102,708	0.009	0.463	112–188 nm	N/A
	[210]	Ag	(4.63–7.9)e+6	(6.54–18.92)e+6	N/A	N/A	34.6–76.4 nm	Aggl.
	[59]	CNT/catalyst	N/A	5,840–37,350 (75,000)	N/A	0.0813 (AM), 0.1063 (PBZ)	20–50 nm	Aggl.
	[207]	CNT	< 2,000	< 2,000(PBZ), (4–10)e+6	N/A	N/A	7–90 nm, 20–200 nm	Aggl.
	[200]	CNF	N/A	N/A	0.00187	0.0034–0.032 (AM), 0.045–0.08 (PE)	0.2–5 µm	Slight aggl.
[225]	Lithium titanium	15,000	20,000–30,000 (AM)	< limit of detection	0.026–0.118 (~39% lithium titanium, AM)	> 200 nm, a few micrometers	Aggl.	
Machining	[73]	Carbon fiber	4,820	94,000	N/A	N/A	165 nm	N/A
	[73]	CNT/ carbon fiber	4,820	153,000 (PBZ), 294,000	N/A	N/A	12 nm, 20 nm,230 nm, 1 µm	Aggl.
	[73]	Carbon fiber	4,820	319,000 (PBZ), 283,000	N/A	N/A	12 nm, 20 nm, 230 nm	Aggl.
	[73]	MWCNT, Al <sub>2</sub> O <sub>3</sub> fiber	4,820	28,000 (PBZ), 38,000	N/A	N/A	12 nm, 25 nm,1–4 µm	Aggl.
	[73]	Alumina fibers	4,820	88,000 (PBZ), 148,000	N/A	N/A	12 nm, 30 nm, 1–2 µm	Aggl.
	[20 41]	Carbon nanofiber	10,000–20,000	10,000–20,000	0.015–0.019	1.094	400 nm	Aggl.

Table S2. Release characterizations grouped into different activity type.

## 9. SUMMARY OF RESULTS

The established aerosolization system was able to generate aerosols with stable particle number and size distribution over a sufficiently long period of time needed for sampling purposes. The resulting number concentration ranges were comparable to the existing aerosolization and dustiness testing methods, when compared for the same materials and suggested the same order of dustiness. The shear forces induced by pressure drop over a critical orifice decreased mean particle size for nearly all tested nanopowder aerosols, except for the one with the lowest mean diameter under the reference condition (i.e. without using the orifice). The particle size distribution spectrums were shifted to smaller size ranges when the aerosols were treated with pressure drops. The results were highly reproducible. The applied shear force conditions significantly increased the particle generation from several folds up to 2-3 orders of magnitude. The number fraction of particles below 100 nm were enhanced, and that of large particles (>350 nm) reduced. The morphological analysis confirmed the reduction of mean size by higher pressure drops. Most particles were still in agglomeration states after passing through the orifice. The results varied for different types of tested materials with distinct surface properties, primary particle sizes and shapes. Agglomerates with hollow structures consisting of non-spherical primary particles (e.g., needle-like) registered the most significant size reductions and number increases by pressure drop. Moreover, aerosols with the largest mean size seen under the reference condition were affected by applied shear forces.

The comparison of different aerosolization systems for the same materials showed that properties of generated nanopowder aerosols varied depending on specific testing methods. The particle mode diameters obtained with the four test setups ranged from 0.1  $\mu\text{m}$  to above 1  $\mu\text{m}$ , and the number concentrations spanned in the range of  $10^3 - 10^6 \text{ \#/cm}^3$ . The systems were robust in producing repeatable results. The aerosolization energies from these systems could be roughly ranked by the velocity of the air flow interacting with the powder particles flow (thus degree of aerodynamic drag by the air to the particles), and this seemed to be related to the resultant aerosol profiles. A comparison of the van der Waals interaction between primary two particles with the drag force ranges in the experiments showed the possibility of deagglomeration under energy input levels of the used setups. The continuous drop method, which featured the lowest energy input only from the drag of surrounding air during the free fall of powder particles,

resulted in the largest mode size of aerosols. In comparison, the air jet method using high speed flows to active a powder seemed to efficiently break particle agglomerates down to nanoscale. The two tested materials with distinct surface hydrophilicity produced aerosols in different number concentrations and size distributions. The testing methods also played a role in this process. The hydrophobic aerosols (NM103) had similar mode sizes in the four systems, whereas the sizes of their hydrophilic counterparts (NM104) differed much more. Comparing the two materials using the same aerosolization method, NM103 had a smaller mode diameter but a higher particle concentration than NM104. However, it was the contrary for particle number when using the air jet system.

Introduction of varied relative humidity in testing the mechanical stability of airborne nanoparticle agglomerates resulted in altered effects of the pressure drop in critical orifices. Shear forces under 50-150 kPa pressure drops were found to effectively decrease mean particle size of aerosols created from hydrophilic and hydrophobic nanopowders. Accordingly, particle number concentration increased under these conditions. However, increasing relative humidity of the system environment reduced these effects of pressure drop. For example, 50 kPa condition had already a significant influence on total particle number of the aerosols under dry condition. When humidity increased, 100 kPa pressure drop was required to have predominant effects. Humid atmosphere itself was shown to increase particle diameter and reduce total number when pressure drop was not applied. It had more significant influences for the number of small particles than for that of large particles. The hydrophilic aerosols were more sensitive to humidity changes regardless of the testing methods, but the responses of the hydrophobic particles differed depending on test systems.

The nanoparticle releases from mechanical treatments of nanomaterial composites was found to be varied by process type and parameters as well as nanofiller type. Overall, the drilling tests released higher numbers of particles than the sawing tests did. In the drilling experiments, faster speeds and larger bit size released greater numbers of particles. Samples reinforced by carbon nanotubes released less particles but in larger diameters, compared to the blank samples. All other composite types did not show a different release level. In the sawing experiments, the added nanofillers modified the release scenarios. PU/CB samples released greater numbers of micro-sized particles compared to the blank samples. All nanofiller reinforced samples generated

higher levels of nanoscale particles. Morphological analysis showed that in both processes the majority of particles released were matrix materials with nanofillers embedded or protruded from the surface. Only one individual nanoparticle agglomerate was identified from sawing PU/SiO<sub>2</sub> samples. Moreover, nano-sized polymer fumes were released in the sawing tests.

The review of airborne ENMs releases from industrial as well as research environments suggests that properties of released aerosols and resultant exposure can be linked to the process and activity type and associated energy level. The same types of activities exhibited similar release scenarios. High energy processes, such as mechanical machining, synthesis and spraying normally resulted in great generations of small particles. In comparison, low energy processes, including manual cleaning, common laboratory handling practices (e.g., mixing, pouring, transferring) and industrial bagging and packing are often associated with minor or moderate releases. Various engineering controls methods (e.g., ventilation, masks) were developed and used to protect worker exposures at nanotechnology workplaces. Although the quality of these protective equipments are often satisfactory, it nevertheless requires correct operating procedures when using them in order to maximize their performances. The assessment of exposure relevant data in the literature suggests that there is still a need to better report this information together with the release data. Currently the contextual information necessary for assessing human risks in occupational exposure studies are not always available.

## **10. DISCUSSION AND CONCLUSIONS**

Understanding properties of nanomaterial aerosols released from workplace environments is very important for assessing their exposure risks to humans. In this work, we combined the review of real-life release and exposure scenarios with laboratory release simulations, aiming at achieving a mechanistic understanding on nanomaterial release processes and linking it to real-world situations. The relationship between process energies and released aerosol properties were identified both from reviewing the real life exposure scenarios as well as from laboratory experiments on powder aerosolization and deagglomeration and nanocomposite treatments. The observations from our literature review as well as from the simulation work were consistent in that a higher energy input level, whether obtained from a different process or by varying its parameters, is likely to generate a greater release of airborne particles in smaller size ranges. The different aerosol profiles created using distinct aerosolization methods in the comparison study

indicates that the energy of workplace activities that resemble these laboratory processes (common powder handlings) may determine the properties of nanopowder aerosols when they are released. After being aerosolized, the airborne particles might experience further deagglomeration by external energies applied, as seen in our simulation study using critical orifices. In addition to the energy range, the level of deagglomeration may be also dependent of the aerosol profiles themselves, seen that larger particles seemed to deagglomerate more easily [65]. This was evidenced in comparing two of our deagglomeration systems (the funnel and the stirrer). The changes of aerosol properties started at low shear force levels and the effects decreased gradually at high forces, which indicates that not only high-energy but also low-energy activities (may be the case for majority of the industrial ENMs handlings) have the potential to trigger deagglomeration. Nanoparticles released from treating solid materials may also depend on process energies, as observed in our study investigating nanocomposites based a common polymer matrix (PU) and nanofiller types.

Although the airborne particle stability and their deagglomeration potentials were studied in a broad energy range, it is still difficult to compare these release scenarios with those from specific processes in real life. This is mainly due to the lack of a realistic method in estimating the exact energy level of an occupational activity. There are studies that investigated the effects of impact velocities to powder particle dispersion in drop tests [226]. However, few studies looked at aerodynamic shears as a form of energy from workplace processes that are responsible for potential changes in aerosol properties. In fact, this type of interaction exist in various processes, such as falling, transferring and pouring of powder materials, and turbulence in ambient air caused by human or process factors. After generalizing the way of estimating aerosolization energies in the different setups used, we propose to use the relative velocity between powder particles and aerosolization flow as a potential parameter for assessing energy levels in relevant industrial processes. It is relatively easy to be quantified both in real life situations and in laboratory simulation studies. It links experimental results to real situations and make them better indicative for release and exposure assessments.

The developed fluidized-bed aerosolization system using laboratory funnels was proven to be a robust aerosol generation method, allowing good control of particle number concentration and size distribution. Controlling these factors is not only important for correct characterization of nanopowder aerosol properties using slow systems such as the SMPS, but could be also useful

for other applications where well-controlled aerosol generation are needed, such as in nanotoxicological studies. The comparison of its particle concentration ranges with existing dustiness data for similar materials indicates that the system may also serve as a dustiness testing platform only consuming very small quantities of raw powder (down to 200 mg/test), supplementing the standard rotating drum as well as the continuous drop methods which use relatively larger amount of materials. We propose to use our system for routine testing of nanomaterial deagglomeration potentials. A ranking on this aerosol property would benefit occupational exposure and risk assessments in providing more accurate predictions on aerosol size changes during their emission, transmission or immission processes.

The relative humidity, as one of the most common environmental variables in worker exposure scenarios, can be controlled to reduce release of potentially hazardous nanoparticles. Our study results can be explained by capillary force from water condensation on particle surface and inside their capillaries, which seem to be sufficiently strong to counter the dispersion energy range incurred in the experiments. The implication for real-life situations, therefore, is that increasing moisture content in workplace air will stabilize the size of airborne particles, it may even enhance their agglomeration, and thus may be an effective mean to contribute to the control of workers' exposure levels. This might be especially useful for nano-sized particles which are of great concern in exposure and risk assessments. Water spraying is a common way in reducing airborne particle concentrations [227]. A water-spraying system was used to suppress fugitive dust and linear dependence of the dust level to relative humidity was observed [228].

The difference in aerosol properties obtained from the two types of powders seen under dry conditions indicates that the hydrophilic particles may have already absorbed certain level of moisture content during storage. This might influence their responses to small humidity gradient created in the experiments. Pre-treatments such as thermal drying can be used to eliminate moisture content absorbed in raw powder, and this might further enhance the particles' sensitivity to humidity variations.

The influences of nanofiller and process types as well as matrix materials on nanocomposite releases in mechanical processing were also observed in other studies investigating drilling [61, 70], sawing [72], sanding [51, 188], and abrasion [154, 229]. Process conditions seemed to be the most influential factor for determining release. For example, higher-energy treatment seemed

to facilitate airborne particle generation. Thus they should be carefully controlled in laboratory simulations on release mechanism. The effects of nanofillers on composite release may be also process-dependent. The fact that majority of the released particles were mixes of matrix and nanofiller materials in micro-size range might raise the concern of their toxicological effects to humans. However, current literature indicates that polymer matrix fragments with protrusions of ENMs do not exhibit higher toxicity compared to pure polymer particles [69, 170, 176]. Nevertheless, we also observed nanoscale polymer fume particles produced by process heat, and they may pose unexpected health problems such as the so called “polymer fume fever” [178].

The information derived from the review on industrial ENMs release can be possibly used to rank the release potentials of different workplace activities. The resulted ranking helps determine priorities of specific industrial processes for exposure and risk assessments. This is especially useful in a tiered assessment strategy which aims at defining the concern level of potential relevant processes in its first step. Furthermore, the results can inform policy makers and safety officers on activities associated with potentially high level of ENMs exposure, and thus guide efforts towards risk prevention in these activities.

The lack of exposure relevant data in ENMs release studies calls for the need for better data reporting practice, as suggested by Clark et al. [182]. This information allows for predicting human exposure levels associated with specific processes, as well as uses in future meta-analysis. The contextual information can be also used to estimate release rate, facilitating a mechanistic understanding on ENMs releases.

Several aspects of this work can be further improved in the future:

1. Due to the fact that capillary force level from water condensation in airborne particles is influenced by primary particle diameter, surface chemistry, roughness and shape, future studies can use different particle profiles to analyze their responses to environmental humidity changes. The R.H. level can be further increased up to 90%, to reveal particle behaviors under such extreme conditions.
2. In investigation of nanocomposite release scenarios, only one matrix material was tested. However, current literature suggests that polymer matrix is also a very important determinant in nanocomposite release level. Systematic comparison of different matrix materials in their effects on release mechanisms can be further studies in the future.

3. The end-of-life treatments of ENMs and ENMs-enabled products becomes a more and more important material life cycle stage for human exposure assessment. These processes may feature different conditions from production and use phases of ENMs, such as high temperature in incineration and various destruction methods in mechanical disintegration. Researchers have started to realize the needs in investigating these activities, and studies have been conducted to reveal relevant release mechanisms [219, 230, 231].

## References

1. Koole, R., E. Groeneveld, D. Vanmaekelbergh, A. Meijerink, and C. de Mello Donegá, *Size Effects on Semiconductor Nanoparticles*, in *Nanoparticles*, C. de Mello Donegá, Editor. 2014, Springer Berlin Heidelberg. p. 13-51.
2. Meyers, M.A., A. Mishra, and D.J. Benson, *Mechanical properties of nanocrystalline materials*. Progress in Materials Science, 2006. **51**(4): p. 427-556.
3. Spitalsky, Z., D. Tasis, K. Papagelis, and C. Galiotis, *Carbon nanotube–polymer composites: Chemistry, processing, mechanical and electrical properties*. Progress in Polymer Science, 2010. **35**(3): p. 357-401.
4. Yurkov, G.Y., A.S. Fionov, Y.A. Koksharov, V.V. Koleso, and S.P. Gubin, *Electrical and magnetic properties of nanomaterials containing iron or cobalt nanoparticles*. Inorganic Materials, 2007. **43**(8): p. 834-844.
5. Xiong, Y., J. Hu, Z. Shen, V. Pouchly, and K. Maca, *Preparation of Transparent Nanoceramics by Suppressing Pore Coalescence*. Journal of the American Ceramic Society, 2011. **94**(12): p. 4269-4273.
6. Chaturvedi, S., P.N. Dave, and N.K. Shah, *Applications of nano-catalyst in new era*. Journal of Saudi Chemical Society, 2012. **16**(3): p. 307-325.
7. Schmid, K. and M. Riediker, *Use of nanoparticles in Swiss Industry: a targeted survey*. Environ Sci Technol, 2008. **42**(7): p. 2253-60.
8. Schmid, K., B. Danuser, and M. Riediker, *Nanoparticle usage and protection measures in the manufacturing industry--a representative survey*. J Occup Environ Hyg, 2010. **7**(4): p. 224-32.
9. Lewicka, Z.A., W.W. Yu, B.L. Oliva, E.Q. Contreras, and V.L. Colvin, *Photochemical behavior of nanoscale TiO<sub>2</sub> and ZnO sunscreen ingredients*. Journal of Photochemistry and Photobiology A: Chemistry, 2013. **263**: p. 24-33.
10. Yang, L., S. Zhou, and L. Wu, *Preparation of waterborne self-cleaning nanocomposite coatings based on TiO<sub>2</sub>/PMMA latex*. Progress in Organic Coatings, 2015. **85**: p. 208-215.
11. Abreu, A.S., M. Oliveira, A. de Sá, R.M. Rodrigues, M.A. Cerqueira, A.A. Vicente, and A.V. Machado, *Antimicrobial nanostructured starch based films for packaging*. Carbohydrate Polymers, 2015. **129**: p. 127-134.
12. Ki, H., J. Kim, S. Kwon, and S. Jeong, *A study on multifunctional wool textiles treated with nano-sized silver*. Journal of Materials Science, 2007. **42**(19): p. 8020-8024.
13. !!! INVALID CITATION !!! (Castranova, 2011 #577; Hsiao, 2011 #98; Lewinski, 2008 #681).
14. Brown, D., M. Wilson, W. MacNee, V. Stone, and K. Donaldson, *Size-dependent proinflammatory effects of ultrafine polystyrene particles: a role for surface area and oxidative stress in the enhanced activity of ultrafines*. Toxicol Appl Pharmacol, 2001. **175**: p. 191 - 199.

15. Chuang, H.-C., L.-C. Chen, Y.-C. Lei, K.-Y. Wu, P.-H. Feng, and T.-J. Cheng, *Surface area as a dose metric for carbon black nanoparticles: A study of oxidative stress, DNA single-strand breakage and inflammation in rats*. Atmospheric Environment, 2015. **106**(0): p. 329-334.
16. Cho, W.S., R. Duffin, F. Thielbeer, M. Bradley, I.L. Megson, W. Macnee, C.A. Poland, C.L. Tran, and K. Donaldson, *Zeta potential and solubility to toxic ions as mechanisms of lung inflammation caused by metal/metal oxide nanoparticles*. Toxicol Sci, 2012. **126**(2): p. 469-77.
17. Geiser, M. and W. Kreyling, *Deposition and biokinetics of inhaled nanoparticles*. Particle and Fibre Toxicology, 2010. **7**(1): p. 2.
18. Muller, J., F. Huaux, N. Moreau, P. Misson, J.-F. Heilier, M. Delos, M. Arras, A. Fonseca, J. Nagy, and D. Lison, *Respiratory toxicity of multi-wall carbon nanotubes*. Toxicol Appl Pharmacol, 2005. **207**: p. 221 - 231.
19. Schaeublin, N.M., L.K. Braydich-Stolle, A.M. Schrand, J.M. Miller, J. Hutchison, J.J. Schlager, and S.M. Hussain, *Surface charge of gold nanoparticles mediates mechanism of toxicity*. Nanoscale, 2011. **3**(2): p. 410-20.
20. Di Bona, K.R., Y. Xu, P.A. Ramirez, J. DeLaine, C. Parker, Y. Bao, and J.F. Rasco, *Surface charge and dosage dependent potential developmental toxicity and biodistribution of iron oxide nanoparticles in pregnant CD-1 mice*. Reproductive Toxicology, 2014. **50**: p. 36-42.
21. Fröhlich, E., *The role of surface charge in cellular uptake and cytotoxicity of medical nanoparticles*. International Journal of Nanomedicine, 2012. **7**: p. 5577-5591.
22. Andreati, T., C.P. Kiill, A.L.R.d. Souza, J.F. Fangueiro, L. Fernandes, S. Doktorovová, D.L. Santos, M.L. Garcia, M.P.D. Gremião, E.B. Souto, and A.M. Silva, *Surface engineering of silica nanoparticles for oral insulin delivery: Characterization and cell toxicity studies*. Colloids and Surfaces B: Biointerfaces, 2014. **123**: p. 916-923.
23. Bermudez, E., J.B. Mangum, B.A. Wong, B. Asgharian, P.M. Hext, D.B. Warheit, and J.I. Everitt, *Pulmonary responses of mice, rats, and hamsters to subchronic inhalation of ultrafine titanium dioxide particles*. Toxicol Sci, 2004. **77**(2): p. 347-57.
24. Oberdörster, G., J. Ferin, and B.E. Lehnert, *Correlation between particle size, in vivo particle persistence, and lung injury*. Environmental Health Perspectives, 1994. **102**(Suppl 5): p. 173-179.
25. Oberdorster, G., E. Oberdorster, and J. Oberdorster, *Nanotoxicology: an emerging discipline evolving from studies of ultrafine particles*. Environ Health Perspect, 2005. **113**(7): p. 823-39.
26. Rothen-Rutishauser, B., C. Muhlfeld, F. Blank, C. Musso, and P. Gehr, *Translocation of particles and inflammatory responses after exposure to fine particles and nanoparticles in an epithelial airway model*. Particle and Fibre Toxicology, 2007. **4**(1): p. 9.
27. Manke, A., L. Wang, and Y. Rojanasakul, *Mechanisms of Nanoparticle-Induced Oxidative Stress and Toxicity*. Biomed Res Int, 2013. **2013**: p. 942916.
28. Li, N., T. Xia, and A.E. Nel, *The role of oxidative stress in ambient particulate matter-induced lung diseases and its implications in the toxicity of engineered nanoparticles*. Free Radical Biology and Medicine, 2008. **44**(9): p. 1689-1699.
29. Zhu, M.-T., B. Wang, Y. Wang, L. Yuan, H.-J. Wang, M. Wang, H. Ouyang, Z.-F. Chai, W.-Y. Feng, and Y.-L. Zhao, *Endothelial dysfunction and inflammation induced by iron oxide nanoparticle exposure: Risk factors for early atherosclerosis*. Toxicology Letters, 2011. **203**(2): p. 162-171.
30. Chen, J., M. Tan, A. Nemmar, W. Song, M. Dong, G. Zhang, and Y. Li, *Quantification of extrapulmonary translocation of intratracheal-instilled particles in vivo in rats: Effect of lipopolysaccharide*. Toxicology, 2006. **222**: p. 195 - 201.
31. Kreyling, W., W. Moller, M. Semmler-Behnke, and G. Oberdorster, *Particle dosimetry: deposition and clearance from the respiratory tract and translocation towards extra-pulmonary sites*. Particle Toxicology, 2007: p. 47 - 74.

32. Kreyling, W., M. Semmler-Behnke, J. Seitz, W. Scymczak, A. Wenk, P. Mayer, S. Takenaka, and G. Oberdorster, *Size and material dependency of translocation of inhaled iridium or carbon nanoparticles from the lungs of rats to blood*. *Inhal Toxicol*, 2009. **21**(S1): p. 55 - 60.
33. Moller, W., W. Kreyling, O. Schmid, M. Semmler-Behnke, and H. Schulz, *Deposition, Retention and Clearance, and Translocation of Inhaled Fine and Nano-Particles in the Respiratory Tract (Chapter 5)*. *Particle-Lung Interactions*, 2009: p. 79 - 107.
34. Oberdoerster, G., Z. Sharp, V. Atudorei, A. Elder, R. Gelein, W. Kreyling, and C. Cox, *Translocation of inhaled ultrafine particles to the brain*. *Inhal Toxicol*, 2004. **16**: p. 437 - 445.
35. Petitot, F., P. Lestaevel, E. Tourlonias, C. Mazzucco, S. Jacquinet, B. Dhieux, O. Delissen, B.B. Tournier, F. Gensdarmes, P. Beaunier, and I. Dublineau, *Inhalation of uranium nanoparticles: Respiratory tract deposition and translocation to secondary target organs in rats*. *Toxicology Letters*, 2013. **217**(3): p. 217-225.
36. Demou, E., W.J. Stark, and S. Hellweg, *Particle Emission and Exposure during Nanoparticle Synthesis in Research Laboratories*. *Annals of Occupational Hygiene*, 2009. **53**(8): p. 829-838.
37. Tsai, S.J., M. Hofmann, M. Hallock, E. Ada, J. Kong, and M. Ellenbecker, *Characterization and Evaluation of Nanoparticle Release during the Synthesis of Single-Walled and Multiwalled Carbon Nanotubes by Chemical Vapor Deposition*. *Environmental Science & Technology*, 2009. **43**(15): p. 6017-6023.
38. Wang, J., C. Asbach, H. Fissan, T. Hulser, H. Kaminski, T.A.J. Kuhlbusch, and D.Y.H. Pui, *Emission measurement and safety assessment for the production process of silicon nanoparticles in a pilot-scale facility*. *Journal of Nanoparticle Research*, 2012. **14**(4).
39. Bello, D., A.J. Hart, K. Ahn, M. Hallock, N. Yamamoto, E.J. Garcia, M.J. Ellenbecker, and B.L. Wardle, *Particle exposure levels during CVD growth and subsequent handling of vertically-aligned carbon nanotube films*. *Carbon*, 2008. **46**(6): p. 974-977.
40. Maynard, A.D., P.A. Baron, M. Foley, A.A. Shvedova, E.R. Kisin, and V. Castranova, *Exposure to carbon nanotube material: Aerosol release during the handling of unrefined single-walled carbon nanotube material*. *Journal of Toxicology and Environmental Health-Part A*, 2004. **67**(1): p. 87-107.
41. Methner, M., C. Beaucham, C. Crawford, L. Hodson, and C. Geraci, *Field Application of the Nanoparticle Emission Assessment Technique (NEAT): Task-Based Air Monitoring During the Processing of Engineered Nanomaterials (ENM) at Four Facilities*. *J Occup Environ Hyg*, 2012. **9**(9): p. 543-555.
42. Tsai, S.J., E. Ada, J.A. Isaacs, and M.J. Ellenbecker, *Airborne nanoparticle exposures associated with the manual handling of nanoalumina and nanosilver in fume hoods*. *Journal of Nanoparticle Research*, 2009. **11**(1): p. 147-161.
43. Johnson, D.R., M.M. Methner, A.J. Kennedy, and J.A. Steevens, *Potential for Occupational Exposure to Engineered Carbon-Based Nanomaterials in Environmental Laboratory Studies*. *Environmental Health Perspectives*, 2010. **118**(1): p. 49-54.
44. Ji, J.H., D. Woo, S.B. Lee, T. Kim, D. Kim, J.H. Kim, and G.N. Bae, *Detection and characterization of nanomaterials released in low concentrations during multi-walled carbon nanotube spraying process in a cleanroom*. *Inhal Toxicol*, 2013. **25**(14): p. 759-65.
45. Rowley, J. and D. Crump, *Measurements of the dispersal of aerosol sprays in a room and comparison to a simple decay model*. *J Environ Monit*, 2005. **7**(10): p. 960-3.
46. Kuhlbusch, T.A. and H. Fissan, *Particle characteristics in the reactor and pelletizing areas of carbon black production*. *J Occup Environ Hyg*, 2006. **3**(10): p. 558-67.
47. Fujitani, Y., T. Kobayashi, K. Arashidani, N. Kunugita, and K. Suemura, *Measurement of the physical properties of aerosols in a fullerene factory for inhalation exposure assessment*. *J Occup Environ Hyg*, 2008. **5**(6): p. 380-389.

48. Evans, D.E., B.K. Ku, M.E. Birch, and K.H. Dunn, *Aerosol Monitoring during Carbon Nanofiber Production: Mobile Direct-Reading Sampling*. *Annals of Occupational Hygiene*, 2010. **54**(5): p. 514-531.
49. A. Hellmann, K.S., S. Ripperger, M. Berges, *Release of ultrafine dusts during the machining of nanocomposites*. *Gefahrstoffe – Reinhalt. Luft*, 2012. **72**(11/12): p. 473-476.
50. Busquets-Fité, M., E. Fernandez, G. Janer, G. Vilar, S. Vázquez-Campos, R. Zanasca, C. Citterio, L. Mercante, and V. Puentes, *Exploring release and recovery of nanomaterials from commercial polymeric nanocomposites*. *Journal of Physics: Conference Series*, 2013. **429**(1): p. 012048.
51. Göhler, D., A. Nogowski, P. Fiala, and M. Stintz, *Nanoparticle release from nanocomposites due to mechanical treatment at two stages of the life-cycle*. *Journal of Physics: Conference Series*, 2013. **429**(1): p. 012045.
52. EU, *Amending Regulation (EU) No 1169/2011 of the European Parliament and of the Council on the provision of food information to consumers as regards the definition of 'engineered nanomaterials'*. *Official Journal of the European Union*, 2013. **No 1363/2013**.
53. NRC, *Science and Decisions: Advancing Risk Assessment*. 2009.
54. Oomen, A.G., P.M. Bos, T.F. Fernandes, K. Hund-Rinke, D. Boraschi, H.J. Byrne, K. Aschberger, S. Gottardo, F. von der Kammer, D. Kuhnelt, D. Hristozov, A. Marcomini, L. Migliore, J. Scott-Fordsmand, P. Wick, and R. Landsiedel, *Concern-driven integrated approaches to nanomaterial testing and assessment--report of the NanoSafety Cluster Working Group 10*. *Nanotoxicology*, 2014. **8**(3): p. 334-48.
55. Hamaker, H.C., *The London—van der Waals attraction between spherical particles*. *Physica*, 1937. **4**(10): p. 1058-1072.
56. Schneider, T. and K.A. Jensen, *Relevance of aerosol dynamics and dustiness for personal exposure to manufactured nanoparticles*. *Journal of Nanoparticle Research*, 2009. **11**(7): p. 1637-1650.
57. Rabinovich, Y.I., J.J. Adler, M.S. Esayanur, A. Ata, R.K. Singh, and B.M. Moudgil, *Capillary forces between surfaces with nanoscale roughness*. *Advances in Colloid and Interface Science*, 2002. **96**(1–3): p. 213-230.
58. Hinds, W., *Aerosol technology - properties, behaviour, and measurement of airborne particles*. 2nd edition ed. 1982, New York: John Wiley & Sons.
59. Lee, J.H., S.B. Lee, G.N. Bae, K.S. Jeon, J.U. Yoon, J.H. Ji, J.H. Sung, B.G. Lee, J.H. Lee, J.S. Yang, H.Y. Kim, C.S. Kang, and I.J. Yu, *Exposure assessment of carbon nanotube manufacturing workplaces*. *Inhal Toxicol*, 2010. **22**(5): p. 369-381.
60. Hagendorfer, H., C. Lorenz, R. Kaegi, B. Sinnet, R. Gehrig, N. Goetz, M. Scheringer, C. Ludwig, and A. Ulrich, *Size-fractionated characterization and quantification of nanoparticle release rates from a consumer spray product containing engineered nanoparticles*. *J Nanopart Res*, 2010. **12**(7): p. 2481 - 2494.
61. Bello, D., B. Wardle, J. Zhang, N. Yamamoto, C. Santeufemio, M. Hallock, and M. Virji, *Characterization of exposures to nanoscale particles and fibers during solid core drilling of hybrid CNT advanced composites*. *Int J Occup Environ Health*, 2010. **16**: p. 434 - 450.
62. Zhang, H., Y.-Y. Kuo, A.C. Gerecke, and J. Wang, *Co-Release of Hexabromocyclododecane (HBCD) and Nano- and Microparticles from Thermal Cutting of Polystyrene Foams*. *Environmental Science & Technology*, 2012. **46**(20): p. 10990-10996.
63. Li, W.-I., M. Perzl, J. Heyder, R. Langer, J.D. Brain, K.H. Englmeier, R.W. Niven, and D.A. Edwards, *Aerodynamics and aerosol particle deaggregation phenomena in model oral-pharyngeal cavities*. *Journal of Aerosol Science*, 1996. **27**(8): p. 1269-1286.
64. Li, W.-I. and D.A. Edwards, *Aerosol particle transport and deaggregation phenomena in the mouth and throat*. *Advanced Drug Delivery Reviews*, 1997. **26**(1): p. 41-49.

65. Ding, Y. and M. Riediker, *A system to assess the stability of airborne nanoparticle agglomerates under aerodynamic shear*. Journal of Aerosol Science, 2015. **88**(0): p. 98-108.
66. Fonda, M., M. Petach, C.F. Rogers, J. Huntington, D. Stratton, K. Nishioka, and M. Tipo, *Resuspension of Particles by Aerodynamic Deagglomeration*. Aerosol Science and Technology, 1999. **30**(6): p. 509-529.
67. Stahlmecke, B., S. Wagener, C. Asbach, H. Kaminski, H. Fissan, and T. Kuhlbusch, *Investigation of airborne nanopowder agglomerate stability in an orifice under various differential pressure conditions*. J Nanopart Res, 2009. **11**(7): p. 1625 - 1635.
68. Schneider, T. and K. Jensen, *Combined Single-Drop and Rotating Drum Dustiness Test of Fine to Nanosize Powders Using a Small Drum*. Ann Occup Hyg, 2008. **52**(1): p. 23 - 34.
69. Wohlleben, W., M.W. Meier, S. Vogel, R. Landsiedel, G. Cox, S. Hirth, and Z. Tomovic, *Elastic CNT-polyurethane nanocomposite: synthesis, performance and assessment of fragments released during use*. Nanoscale, 2013. **5**(1): p. 369-380.
70. Sachse, S., F. Silva, A. Irfan, H. Zhu, K. Pielichowski, A. Leszczynska, M. Blazquez, O. Kazmina, O. Kuzmenko, and J. Njuguna, *Physical characteristics of nanoparticles emitted during drilling of silica based polyamide 6 nanocomposites*. IOP Conference Series: Materials Science and Engineering, 2012. **40**(1): p. 012012.
71. Schlagenhaut, L., B.T.T. Chu, J. Buha, F. Nüesch, and J. Wang, *Release of Carbon Nanotubes from an Epoxy-Based Nanocomposite during an Abrasion Process*. Environmental Science & Technology, 2012. **46**(13): p. 7366-7372.
72. Gomez, V., M. Levin, A.T. Saber, S. Irusta, M. Dal Maso, R. Hanoi, J. Santamaria, K.A. Jensen, H. Wallin, and I.K. Koponen, *Comparison of dust release from epoxy and paint nanocomposites and conventional products during sanding and sawing*. Ann Occup Hyg, 2014. **58**(8): p. 983-94.
73. Bello, D., B.L. Wardle, N. Yamamoto, R.G. deVilloria, E.J. Garcia, A.J. Hart, K. Ahn, M.J. Ellenbecker, and M. Hallock, *Exposure to nanoscale particles and fibers during machining of hybrid advanced composites containing carbon nanotubes*. Journal of Nanoparticle Research, 2009. **11**(1): p. 231-249.
74. Methner, M., C. Crawford, and C. Geraci, *Evaluation of the Potential Airborne Release of Carbon Nanofibers During the Preparation, Grinding, and Cutting of Epoxy-Based Nanocomposite Material*. J Occup Environ Hyg, 2012. **9**(5): p. 308-318.
75. Curwin, B. and S. Bertke, *Exposure Characterization of Metal Oxide Nanoparticles in the Workplace*. J Occup Environ Hyg, 2011. **8**(10): p. 580-587.
76. Koivisto, A.J., J. Lyyranen, A. Auvinen, E. Vanhala, K. Hameri, T. Tuomi, and J. Jokiniemi, *Industrial worker exposure to airborne particles during the packing of pigment and nanoscale titanium dioxide*. Inhal Toxicol, 2012. **24**(12): p. 839-849.
77. Bourdon, J.A., A. Williams, B. Kuo, I. Moffat, P.A. White, S. Halappanavar, U. Vogel, H. Wallin, and C.L. Yauk, *Gene expression profiling to identify potentially relevant disease outcomes and support human health risk assessment for carbon black nanoparticle exposure*. Toxicology, 2013. **303**(0): p. 83-93.
78. Paur, H.-R., F.R. Cassee, J. Teeguarden, H. Fissan, S. Diabate, M. Aufderheide, W.G. Kreyling, O. Hänninen, G. Kasper, M. Riediker, B. Rothen-Rutishauser, and O. Schmid, *In-vitro cell exposure studies for the assessment of nanoparticle toxicity in the lung—A dialog between aerosol science and biology*. Journal of Aerosol Science, 2011. **42**(10): p. 668-692.
79. Zhang, Z. and C. Kleinstreuer, *Computational analysis of airflow and nanoparticle deposition in a combined nasal–oral–tracheobronchial airway model*. Journal of Aerosol Science, 2011. **42**(3): p. 174-194.

80. Rissler, J., E. Swietlicki, A. Bengtsson, C. Boman, J. Pagels, T. Sandström, A. Blomberg, and J. Löndahl, *Experimental determination of deposition of diesel exhaust particles in the human respiratory tract*. Journal of Aerosol Science, 2012. **48**(0): p. 18-33.
81. Noël, A., K. Maghni, Y. Cloutier, C. Dion, K.J. Wilkinson, S. Hallé, R. Tardif, and G. Truchon, *Effects of inhaled nano-TiO<sub>2</sub> aerosols showing two distinct agglomeration states on rat lungs*. Toxicology Letters, 2012. **214**(2): p. 109-119.
82. Gomez, V., S. Irusta, F. Balas, N. Navascues, and J. Santamaria, *Unintended emission of nanoparticle aerosols during common laboratory handling operations*. Journal of Hazardous Materials, 2014. **279**(0): p. 75-84.
83. Islam, N. and M.J. Cleary, *Developing an efficient and reliable dry powder inhaler for pulmonary drug delivery – A review for multidisciplinary researchers*. Medical Engineering & Physics, 2012. **34**(4): p. 409-427.
84. Yang, M.Y., J.G.Y. Chan, and H.-K. Chan, *Pulmonary drug delivery by powder aerosols*. Journal of Controlled Release, 2014. **193**(0): p. 228-240.
85. Froeschke, S., S. Kohler, A.P. Weber, and G. Kasper, *Impact fragmentation of nanoparticle agglomerates*. Journal of Aerosol Science, 2003. **34**(3): p. 275-287.
86. Stahlmecke, B., S. Wagener, C. Asbach, H. Kaminski, H. Fissan, and T.A.J. Kuhlbusch, *Investigation of airborne nanopowder agglomerate stability in an orifice under various differential pressure conditions*. Vol. 11. 2009: J Nanopart Res.
87. Blum, J. and J. Blum, *Dust Agglomeration*. European Astronomical Society Publications Series, 2009. **35**: p. 195-217.
88. Bach, S. and E. Schmidt, *Determining the Dustiness of Powders—A Comparison of three Measuring Devices*. Annals of Occupational Hygiene, 2008. **52**(8): p. 717-725.
89. Breum, N.O., *The rotating drum dustiness tester: Variability in dustiness in relation to sample mass, testing time, and surface adhesion*. Annals of Occupational Hygiene, 1999. **43**(8): p. 557-566.
90. Morgeneyer, M., O. Le Bihan, A. Ustache, and O. Aguerre-Chariol, *Experimental study of the aerosolization of fine alumina particles from bulk by a vortex shaker*. Powder Technology, 2013. **246**(0): p. 583-589.
91. Saleh, K., M.-T. Moufarej Abou Jaoude, M. Morgeneyer, E. Lefrancois, O. Le Bihan, and J. Bouillard, *Dust generation from powders: A characterization test based on stirred fluidization*. Powder Technology, 2014. **255**(0): p. 141-148.
92. CEN, *FprEN 15051 Workplace exposure: measurement of the dustiness of bulk materials; Part 1: Requirements and choice of test methods; Part 2: Rotating drum method; Part 3: Continuous drop method*. Brussels, Belgium: European Committee for Standardization. 2013.
93. Evans, D.E., L.A. Turkevich, C.T. Roettgers, G.J. Deye, and P.A. Baron, *Dustiness of Fine and Nanoscale Powders*. Annals of Occupational Hygiene, 2013. **57**(2): p. 261-277.
94. O'Shaughnessy, P.T., M. Kang, and D. Ellickson, *A Novel Device for Measuring Respirable Dustiness Using Low-Mass Powder Samples*. Journal of Occupational and Environmental Hygiene, 2011. **9**(3): p. 129-139.
95. Ahmed Mahmoud, E., T. Nakazato, S. Nakajima, N. Nakagawa, and K. Kato, *Separation rate of fine powders from a circulating powder-particle fluidized bed (CPPFB)*. Powder Technology, 2004. **146**(1–2): p. 46-55.
96. Ammar, Y., A. Dehbi, and M. Reeks, *Break-Up of Aerosol Agglomerates in Highly Turbulent Gas Flow*. Flow, Turbulence and Combustion, 2012. **89**(3): p. 465-489.
97. Kulkarni, P., P.A. Baron, and K. Willeke, *Aerosol Measurement - Principles, Techniques, and Applications*. 2011, Hoboken, New Jersey: John Wiley & Sons, Inc.,.

98. Tsai, C., C. Wu, M. Leu, S. Chen, C. Huang, P. Tsai, and F. Ko, *Dustiness test of nanopowders using a standard rotating drum with a modified sampling train*. J Nanopart Res, 2009. **11**(1): p. 121 - 131.
99. Dahmann, D. and C. Monz, *Determination of dustiness of nanostructured materials*. Gefahrstoffe - Reinhaltung der Luft, 2011. **71**(11/12): p. 481 - 487.
100. Isamu Ogura, H.S.a.M.G., *Dustiness testing of engineered nanomaterials*. Journal of Physics: Conference Series, 2009. **170**: p. 012003.
101. Sosnowski, T.R., K. Giżyńska, and Ł. Żywczyk, *Fluidization and break-up of powder particle aggregates during constant and pulsating flow in converging nozzles*. Colloids and Surfaces A: Physicochemical and Engineering Aspects, 2014. **441**(0): p. 905-911.
102. Chen, S.-C., C.-J. Tsai, C.-H. Wu, D.Y.H. Pui, A.A. Onischuk, and V.V. Karasev, *Particle loss in a critical orifice*. Journal of Aerosol Science, 2007. **38**(9): p. 935-949.
103. Schaefer, K. and A. Miszczyk, *Improvement of electrochemical action of zinc-rich paints by addition of nanoparticulate zinc*. Corrosion Science, 2013. **66**(0): p. 380-391.
104. Svintsitskiy, D.A., A.P. Chupakhin, E.M. Slavinskaya, O.A. Stonkus, A.I. Stadnichenko, S.V. Koscheev, and A.I. Boronin, *Study of cupric oxide nanopowders as efficient catalysts for low-temperature CO oxidation*. Journal of Molecular Catalysis A: Chemical, 2013. **368-369**(0): p. 95-106.
105. Gavrilă-Florescu, L., I. Sandu, A. Stan, E. Dutu, and I. Voicu, *Laser synthesized nanopowders for polymer-based composites*. Applied Surface Science, 2012. **258**(23): p. 9260-9262.
106. Zalite, I., N. Zilinska, and G. Kladler, *SiAlON ceramics from nanopowders*. Journal of the European Ceramic Society, 2008. **28**(5): p. 901-905.
107. Bansal, N.P., J.C. Goldsby, R.B. Rogers, M.A. Susner, and M.D. Sumption, *Chemical synthesis of superconducting MgB<sub>2</sub> nanopowder*. Journal of Alloys and Compounds, 2015. **622**(0): p. 986-988.
108. Maynard, A., P. Baron, M. Foley, A. Shvedova, E. Kisin, and V. Castranova, *Exposure to carbon nanotube material: Aerosol release during the handling of unrefined single walled carbon nanotube material*. J Toxic And Environ Health, 2004. **67**: p. 87 - 107.
109. Verlag, B., *European Norm 15051, Workplace exposure—measurement of the dustiness of bulk materials*. 2014.
110. M.A.E. Plinke, D.L., M.G. Boundy, F. Löffler, *Dust generation from handling powders in industry*. American Industrial Hygiene Association Journal, 1995. **56**(3): p. 251-257.
111. Cotogno Giulio, C.G., Gilliland Douglas, Jensen Keld Astrup et al., *Titanium Dioxide, NM-100, NM-101, NM-102, NM-103, NM-104, NM-105: Characterisation and Physico-Chemical Properties*. 2014.
112. Shi, H., R. Magaye, V. Castranova, and J. Zhao, *Titanium dioxide nanoparticles: a review of current toxicological data*. Part Fibre Toxicol, 2013. **10**: p. 15.
113. Turki, D. and N. Fatah, *Behavior and fluidization of the cohesive powders: agglomerates sizes approach* Brazilian Journal of Chemical Engineering, 2008. **Vol. 25** (No. 04): p. pp. 697 - 711.
114. Cheng, W., P.F. Dunn, and R.M. Brach, *Surface roughness effects on microparticle adhesion*. The Journal of Adhesion, 2002. **78**(11): p. 929-965.
115. Batsanov, S.S., *Van der Waals Radii of Elements*. Inorganic Materials, 2001. **37**(9): p. 871-885.
116. Bergström, L., *Hamaker constants of inorganic materials*. Advances in Colloid and Interface Science, 1997. **70**(0): p. 125-169.
117. Nishiyama, T., T. Inamuro, and S. Yasuda, *Numerical simulation of the dispersion of aggregated Brownian particles under shear flows*. Computers & Fluids, 2013. **86**(0): p. 395-404.
118. van Ommen, J.R., J. Valverde, and R. Pfeffer, *Fluidization of nanopowders: a review*. Journal of Nanoparticle Research, 2012. **14**(3): p. 1-29.

119. Zhu, C., Q. Yu, R.N. Dave, and R. Pfeffer, *Gas fluidization characteristics of nanoparticle agglomerates*. *AIChE Journal*, 2005. **51**(2): p. 426-439.
120. J. Ruud van Ommen, D.M.K., Alan Weimer, Robert Pfeer, Berend van Wachem. *Experiments and modelling of micro-jet assisted fluidization of nanoparticles*. in *The 13th International Conference on Fluidization - New Paradigm in Fluidization Engineering*. 2010. ECI Digital Archives.
121. Andrès, C., P. Réginault, M.H. Rochat, B. Chaillot, and Y. Pourcelot, *Particle-size distribution of a powder: Comparison of three analytical techniques*. *International Journal of Pharmaceutics*, 1996. **144**(2): p. 141-146.
122. *A guidebook to particle size analysis*. 2014, HORIBA Instruments, INC.
123. Israelachvili, J.N., *Chapter 13 - Van der Waals Forces between Particles and Surfaces*, in *Intermolecular and Surface Forces (Third Edition)*, J.N. Israelachvili, Editor. 2011, Academic Press: San Diego. p. 253-289.
124. Brouwer, D., *Exposure to manufactured nanoparticles in different workplaces*. *Toxicology*, 2010. **269**(2–3): p. 120-127.
125. Kuhlbusch, T., C. Asbach, H. Fissan, D. Gohler, and M. Stintz, *Nanoparticle exposure at nanotechnology workplaces: A review*. *Particle and Fibre Toxicology*, 2011. **8**(1): p. 22.
126. Fukui, H., M. Horie, S. Endoh, H. Kato, K. Fujita, K. Nishio, L.K. Komaba, J. Maru, A. Miyauhi, A. Nakamura, S. Kinugasa, Y. Yoshida, Y. Hagihara, and H. Iwahashi, *Association of zinc ion release and oxidative stress induced by intratracheal instillation of ZnO nanoparticles to rat lung*. *Chemico-Biological Interactions*, 2012. **198**(1–3): p. 29-37.
127. Sandra V. Pirela, I.R.M., Xiaoyan Lu, Vincent Castranova, Treye Thomas, Yong Qian, Dhimiter Bello, Lester Kobzik, Igor Koturbash, Philip Demokritou, *Effects of Laser Printer–Emitted Engineered Nanoparticles on Cytotoxicity, Chemokine Expression, Reactive Oxygen Species, DNA Methylation, and DNA Damage: A Comprehensive in Vitro Analysis in Human Small Airway Epithelial Cells, Macrophages, and Lymphoblasts*. *Environ Health Perspect*, 2015.
128. Castranova, V., *Overview of current toxicological knowledge of engineered nanoparticles*. *J Occup Environ Med*, 2011. **53**(6 Suppl): p. S14-7.
129. Xiong, S., Y. Tang, H.S. Ng, X. Zhao, Z. Jiang, Z. Chen, K.W. Ng, and S.C.J. Loo, *Specific surface area of titanium dioxide (TiO<sub>2</sub>) particles influences cyto- and photo-toxicity*. *Toxicology*, 2013. **304**(0): p. 132-140.
130. Calvert, G., M. Ghadiri, and R. Tweedie, *Aerodynamic dispersion of cohesive powders: A review of understanding and technology*. *Advanced Powder Technology*, 2009. **20**(1): p. 4-16.
131. Kousaka, Y., K. Okuyama, A. Shimizu, and T. Yoshida, *DISPERSION MECHANISM OF AGGREGATE PARTICLES IN AIR*. *Journal of Chemical Engineering of Japan*, 1979. **12**(2): p. 152-159.
132. Henry, F., J. Bouillard, P. Marchal, A. Vignes, O. Dufaud, and L. Perrin, *Exploring a new method to study the agglomeration of powders: Application to nanopowders*. *Powder Technology*, 2013. **250**(0): p. 13-20.
133. Parveen, F., F. Berruti, C. Briens, and J. McMillan, *Effect of fluidized bed particle properties and agglomerate shape on the stability of agglomerates in a fluidized bed*. *Powder Technology*, 2013. **237**(0): p. 46-52.
134. Ihalainen, M., T. Lind, T. Torvela, K.E.J. Lehtinen, and J. Jokiniemi, *A Method to Study Agglomerate Breakup and Bounce During Impaction*. *Aerosol Science and Technology*, 2012. **46**(9): p. 990-1001.
135. Ihalainen, M., T. Lind, A. Arffman, T. Torvela, and J. Jokiniemi, *Break-Up and Bounce of TiO<sub>2</sub> Agglomerates by Impaction*. *Aerosol Science and Technology*, 2013. **48**(1): p. 31-41.
136. Butt, H.-J. and M. Kappl, *Normal capillary forces*. *Advances in Colloid and Interface Science*, 2009. **146**(1–2): p. 48-60.

137. Price, R., P.M. Young, S. Edge, and J.N. Staniforth, *The influence of relative humidity on particulate interactions in carrier-based dry powder inhaler formulations*. International Journal of Pharmaceutics, 2002. **246**(1–2): p. 47-59.
138. Zhu, K., R.B.H. Tan, W. Kiong Ng, S. Shen, Q. Zhou, and P.W.S. Heng, *Analysis of the influence of relative humidity on the moisture sorption of particles and the aerosolization process in a dry powder inhaler*. Journal of Aerosol Science, 2008. **39**(6): p. 510-524.
139. Bérard, V., E. Lesniewska, C. Andrès, D. Pertuy, C. Laroche, and Y. Pourcelot, *Dry powder inhaler: influence of humidity on topology and adhesion studied by AFM*. International Journal of Pharmaceutics, 2002. **232**(1–2): p. 213-224.
140. Pakarinen, O.H., A.S. Foster, M. Paajanen, T. Kalinainen, J. Katainen, I. Makkonen, J. Lahtinen, and R.M. Nieminen, *Towards an accurate description of the capillary force in nanoparticle-surface interactions*. Modelling and Simulation in Materials Science and Engineering, 2005. **13**(7): p. 1175.
141. Ding, Y., B. Stahlmecke, A.S. Jiménez, I.L. Tuinman, H. Kaminski, T.A.J. Kuhlbusch, M. van Tongeren, and M. Riediker, *Dustiness and Deagglomeration Testing: Interlaboratory Comparison of Systems for Nanoparticle Powders*. Aerosol Science and Technology, 2015. **49**(12): p. 1222-1231.
142. Levin, M., E. Rojas, E. Vanhala, M. Vippola, B. Liguori, K. Kling, I. Koponen, K. Møhlhave, T. Tuomi, D. Gregurec, S. Moya, and K. Jensen, *Influence of relative humidity and physical load during storage on dustiness of inorganic nanomaterials: implications for testing and risk assessment*. Journal of Nanoparticle Research, 2015. **17**(8): p. 1-13.
143. Harrison, A.J., D.S. Corti, and S.P. Beaudoin, *Capillary Forces in Nanoparticle Adhesion: A Review of AFM Methods*. Particulate Science and Technology, 2015: p. 1-13.
144. Jog, J.P., *Crystallisation in polymer nanocomposites*. Materials Science and Technology, 2006. **22**(7): p. 797-806.
145. Hanemann, T. and D.V. Szabó, *Polymer-Nanoparticle Composites: From Synthesis to Modern Applications*. Materials, 2010. **3**(6): p. 3468.
146. Szeluga, U., B. Kumanek, and B. Trzebicka, *Synergy in hybrid polymer/nanocarbon composites. A review*. Composites Part A: Applied Science and Manufacturing, 2015. **73**(0): p. 204-231.
147. Poland, C.A., R. Duffin, I. Kinloch, A. Maynard, W.A.H. Wallace, A. Seaton, V. Stone, S. Brown, W. MacNee, and K. Donaldson, *Carbon nanotubes introduced into the abdominal cavity of mice show asbestos-like pathogenicity in a pilot study*. Nat Nano, 2008. **3**(7): p. 423-428.
148. Lin, W., Y.-w. Huang, X.-D. Zhou, and Y. Ma, *In vitro toxicity of silica nanoparticles in human lung cancer cells*. Toxicology and Applied Pharmacology, 2006. **217**(3): p. 252-259.
149. Hunt, G., I. Lynch, F. Cassee, R. Handy, T. Fernandes, M. Berges, T. Kuhlbusch, M. Dusinska, and M. Riediker, *Towards a Consensus View on Understanding Nanomaterials Hazards and Managing Exposure: Knowledge Gaps and Recommendations*. Materials, 2013. **6**(3): p. 1090.
150. Harper, S., W. Wohlleben, M. Doa, B. Nowack, S. Clancy, R. Canady, and A. Maynard, *Measuring Nanomaterial Release from Carbon Nanotube Composites: Review of the State of the Science*. Journal of Physics: Conference Series, 2015. **617**(1): p. 012026.
151. Kingston, C., R. Zepp, A. Andrady, D. Boverhof, R. Fehir, D. Hawkins, J. Roberts, P. Sayre, B. Shelton, Y. Sultan, V. Vejins, and W. Wohlleben, *Release characteristics of selected carbon nanotube polymer composites*. Carbon, 2014. **68**(0): p. 33-57.
152. Schlagenhauf, L., F. Nüesch, and J. Wang, *Release of Carbon Nanotubes from Polymer Nanocomposites*. Fibers, 2014. **2**(2): p. 108.
153. Bello, D., B. Wardle, N. Yamamoto, R. Guzman deVilloria, E. Garcia, A. Hart, K. Ahn, M. Ellenbecker, and M. Hallock, *Exposure to nanoscale particles and fibers during machining of*

- hybrid advanced composites containing carbon nanotubes*. Journal of Nanoparticle Research, 2009. **11**(1): p. 231-249.
154. Golanski, L., A. Guiot, M. Pras, M. Malarde, and F. Tardif, *Release-ability of nano fillers from different nanomaterials (toward the acceptability of nanoprodukt)*. Journal of Nanoparticle Research, 2012. **14**(7): p. 1-9.
  155. Sachse, S., F. Silva, H. Zhu, A. Irfan, A. Leszczy, K. Pielichowski, V. Ermini, M. Blazquez, O. Kuzmenko, and J. Njuguna, *The effect of nanoclay on dust generation during drilling of PA6 nanocomposites*. J. Nanomaterials, 2012. **2012**: p. 26-26.
  156. Canady, R., T. Kuhlbusch, M. Renker, E. Lee, and L. Tsytsikova, *NanoRelease Consumer Products Phase 2.5 Report 2013*.
  157. Nanocyl[2009], *Responsible care and nanomaterials case study Nanocyl. Presentation at European Responsible Care Conference*. Prague. Brussels, Belgium: The European Chemical Industry Council (CEFIC).
  158. Tsai, S., A. Ashter, E. Ada, J. Mead, C. Barry, and M. Ellenbecker, *Control of Airborne Nanoparticles Release During Compounding of Polymer Nanocomposites*. Nano, 2008. **3**(4): p. 301 - 309.
  159. Ogura, I., M. Kotake, M. Shigeta, M. Uejima, K. Saito, N. Hashimoto, and A. Kishimoto, *Potential release of carbon nanotubes from their composites during grinding*. Journal of Physics: Conference Series, 2013. **429**(1): p. 012049.
  160. Cena, L.G. and T.M. Peters, *Characterization and Control of Airborne Particles Emitted During Production of Epoxy/Carbon Nanotube Nanocomposites*. J Occup Environ Hyg, 2011. **8**(2): p. 86-92.
  161. Fleury, D., J.A.S. Bomfim, A. Vignes, C. Girard, S. Metz, F. Muñoz, B. R'Mili, A. Ustache, A. Guiot, and J.X. Bouillard, *Identification of the main exposure scenarios in the production of CNT-polymer nanocomposites by melt-moulding process*. Journal of Cleaner Production, 2013. **53**(0): p. 22-36.
  162. Devaprakasam, D., P.V. Hatton, G. Möbus, and B.J. Inkson, *Effect of microstructure of nano- and micro-particle filled polymer composites on their tribo-mechanical performance*. Journal of Physics: Conference Series, 2008. **126**(1): p. 012057.
  163. Huang, G., J. Park, L. Cena, B. Shelton, and T. Peters, *Evaluation of airborne particle emissions from commercial products containing carbon nanotubes*. Journal of Nanoparticle Research, 2012. **14**(11): p. 1-13.
  164. Van Landuyt, K.L., K. Yoshihara, B. Geebelen, M. Peumans, L. Godderis, P. Hoet, and B. Van Meerbeek, *Should we be concerned about composite (nano-)dust?* Dental Materials, 2012. **28**(11): p. 1162-1170.
  165. Van Landuyt, K.L., B. Hellack, B. Van Meerbeek, M. Peumans, P. Hoet, M. Wiemann, T.A.J. Kuhlbusch, and C. Asbach, *Nanoparticle release from dental composites*. Acta Biomaterialia, 2014. **10**(1): p. 365-374.
  166. Raynor, P.C., J.I. Cebula, J.S. Spangenberg, B.A. Olson, J.M. Dasch, and J.B. D'Arcy, *Assessing Potential Nanoparticle Release During Nanocomposite Shredding Using Direct-Reading Instruments*. Journal of Occupational and Environmental Hygiene, 2011. **9**(1): p. 1-13.
  167. Rudolph D, D. and P. Kalidas R, *Carbon Black Embrittlement of ABS*, in *Toughness and Brittleness of Plastics*. 1976, AMERICAN CHEMICAL SOCIETY. p. 256-262.
  168. R. Satheesh Raja, K.M., V. Manikandan *Effect of Carbon Black and Fly Ash Fillers on Tensile Properties of Composites* Key Engineering Materials. **471-472**: p. 26-30
  169. Kaynak, A., A. Polat, and U. Yilmazer, *Some microwave and mechanical properties of carbon fiber-polypropylene and carbon black-polypropylene composites*. Materials Research Bulletin, 1996. **31**(10): p. 1195-1206.

170. Wohlleben, W., S. Brill, M. Meier, M. Mertler, G. Cox, S. Hirth, B. von Vacano, V. Strauss, S. Treumann, K. Wiench, L. Ma-Hock, and R. Landsiedel, *On the Lifecycle of nanocomposites: Comparing Released Fragments and their In-Vivo Hazards from Three Release Mechanisms and Four Nanocomposites*. Small, 2011.
171. Van Krevelen, D.W. and K. Te Nijenhuis, *Chapter 13 - Mechanical Properties of Solid Polymers*, in *Properties of Polymers (Fourth Edition)*, D.W.V.K. by and K.T. Nijenhuis, Editors. 2009, Elsevier: Amsterdam. p. 383-503.
172. Jansen, J.A., *Understanding the consequence of ductile-to-brittle transitions in a plastic materials failure*. ANTEC 2008: p. 742.
173. Berry, J.P., *The morphology of polymer fracture surfaces*. Journal of Polymer Science Part C: Polymer Symposia, 1963. **3**(1): p. 91-101.
174. Shandilya, N., O. Le Bihan, and M. Morgenev, *Effect of the Normal Load on the Release of Aerosol Wear Particles During Abrasion*. Tribology Letters, 2014. **55**(2): p. 227-234.
175. Gohler, D., M. Stintz, M. Vorbau, and L. Hillemann, *Characterization of nanoparticle release from surface coatings by the simulation of a sanding process*. Ann Occup Hyg, 2010. **54**(6): p. 615 - 624.
176. Saber, A.T., I.K. Koponen, K.A. Jensen, N.R. Jacobsen, L. Mikkelsen, P. Moller, S. Loft, U. Vogel, and H. Wallin, *Inflammatory and genotoxic effects of sanding dust generated from nanoparticle-containing paints and lacquers*. Nanotoxicology, 2012. **6**(7): p. 776-88.
177. Saber, A.T., N.R. Jacobsen, A. Mortensen, J. Szarek, P. Jackson, A.M. Madsen, K.A. Jensen, I.K. Koponen, G. Brunborg, K.B. Gutzkow, U. Vogel, and H. Wallin, *Nanotitanium dioxide toxicity in mouse lung is reduced in sanding dust from paint*. Part Fibre Toxicol, 2012. **9**: p. 4.
178. Patel, M.M., M.A. Miller, and S. Chomchai, *Polymer fume fever after use of a household product*. The American Journal of Emergency Medicine, 2006. **24**(7): p. 880-881.
179. Testud, F., S. Sabouraud, and F. Lecoq-Jammes, *Fièvre des polymères après fartage intensif de snowboards en milieu confiné : 3 observations*. Archives des Maladies Professionnelles et de l'Environnement, 2010. **71**(6): p. 925-930.
180. Townsend, P.W., G.G. Vernice, and R.L. Williams, *'Polymer fume fever' without polymer*. Journal of Fluorine Chemistry, 1989. **42**(3): p. 441-443.
181. Le Bihan, O., Shandilya, N., Gheerardyn, L., Guillon, O., Dore, E. and Morgenev, M., *Investigation of the Release of Particles from a Nanocoated Product*. Advances in Nanoparticles, 2013(2): p. 39-44.
182. Clark, K., M. van Tongeren, F. Christensen, D. Brouwer, B. Nowack, F. Gottschalk, C. Micheletti, K. Schmid, R. Gerritsen, R. Aitken, C. Vaquero, V. Gkanis, C. Housiadas, J. de Ipiña, and M. Riediker, *Limitations and information needs for engineered nanomaterial-specific exposure estimation and scenarios: recommendations for improved reporting practices*. Journal of Nanoparticle Research, 2012. **14**(9): p. 1-14.
183. *Regulation (EC) No 1907/2006 of the European Parliament and of the Council*. Official Journal of the European Union, 18 December 2006.
184. *Scientific report: Workplace exposure to nanoparticles*. European Agency for Safety and Health at Work (EU-OSHA).
185. Methner, M., L. Hodson, A. Dames, and C. Geraci, *Nanoparticle Emission Assessment Technique (NEAT) for the Identification and Measurement of Potential Inhalation Exposure to Engineered Nanomaterials-Part B: Results from 12 Field Studies*. J Occup Environ Hyg, 2010. **7**(3): p. 163-176.
186. Imhof, C., K. Clark, T. Meyer, K. Schmid, and M. Riediker, *Research and development-where people are exposed to nanomaterials*. J Occup Health, 2015. **57**(2): p. 179-88.
187. Möhlmann, C., J. Welter, M. Klenke, and J. Sander, *Workplace exposure at nanomaterial production processes*. Journal of Physics: Conference Series, 2009. **170**(1): p. 012004.

188. Koponen, I., K. Jensen, and T. Schneider, *Comparison of dust released from sanding conventional and nanoparticle-doped wall and wood coatings*. J Expo Sci Env Epid, 2010: p. 1 - 10.
189. report, N.F., *Development of Exposure Scenarios for Manufactured Nanomaterials*. 2010.
190. Kuhlbusch, T., S. Neumann, and H. Fissan, *Number size distribution, mass concentration and particle composition of PM1, PM2.5, PM10 in bag filling areas of carbon black production*. J Occup and Environ Hyg, 2004. **1**: p. 660 - 671.
191. Tsai, C.J., C.Y. Huang, S.C. Chen, C.E. Ho, C.H. Huang, C.W. Chen, C.P. Chang, S.J. Tsai, and M.J. Ellenbecker, *Exposure assessment of nano-sized and respirable particles at different workplaces*. Journal of Nanoparticle Research, 2011. **13**(9): p. 4161-4172.
192. Huang, C.H., C.Y. Tai, C.Y. Huang, C.J. Tsai, C.W. Chen, C.P. Chang, and T.S. Shih, *Measurements of respirable dust and nanoparticle concentrations in a titanium dioxide pigment production factory*. Journal of Environmental Science and Health Part a-Toxic/Hazardous Substances & Environmental Engineering, 2010. **45**(10): p. 1227-1233.
193. Yang, Y., P. Mao, Z.P. Wang, and J.H. Zhang, *Distribution of Nanoparticle Number Concentrations at a Nano-TiO<sub>2</sub> Plant*. Aerosol and Air Quality Research, 2012. **12**(5): p. 934-940.
194. Demou, E., P. Peter, and S. Hellweg, *Exposure to Manufactured Nanostructured Particles in an Industrial Pilot Plant*. Annals of Occupational Hygiene, 2008. **52**(8): p. 695-706.
195. Demou, E., W. Stark, and S. Hellweg, *Particle emission and exposure during nanoparticle synthesis in research laboratories*. Ann Occup Hyg, 2009. **53**: p. 829 - 838.
196. Plitzko, S., *Workplace exposure to engineered nanoparticles*. Inhal Toxicol, 2009. **21 Suppl 1**: p. 25-9.
197. Lee, J.H., M. Kwon, J.H. Ji, C.S. Kang, K.H. Ahn, J.H. Han, and I.J. Yu, *Exposure assessment of workplaces manufacturing nanosized TiO<sub>2</sub> and silver*. Inhal Toxicol, 2011. **23**(4): p. 226-36.
198. Yeganeh, B., C.M. Kull, M.S. Hull, and L.C. Marr, *Characterization of Airborne Particles During Production of Carbonaceous Nanomaterials*. Environmental Science & Technology, 2008. **42**(12): p. 4600-4606.
199. Han, J.H., E.J. Lee, J.H. Lee, K.P. So, Y.H. Lee, G.N. Bae, S.B. Lee, J.H. Ji, M.H. Cho, and I.J. Yu, *Monitoring multiwalled carbon nanotube exposure in carbon nanotube research facility*. Inhal Toxicol, 2008. **20**(8): p. 741-749.
200. Birch, M.E., B.K. Ku, D.E. Evans, and T.A. Ruda-Eberenz, *Exposure and Emissions Monitoring during Carbon Nanofiber Production-Part I: Elemental Carbon and Iron-Soot Aerosols*. Annals of Occupational Hygiene, 2011. **55**(9): p. 1016-1036.
201. Methner, M.M., M.E. Birch, D.E. Evans, B.-K. Ku, K. Crouch, and M.D. Hoover, *Identification and characterization of potential sources of worker exposure to carbon nanofibers during polymer composite laboratory operations*. J Occup Environ Hyg, 2007. **4**(12): p. D125-30.
202. Elihn, K. and P. Berg, *Ultrafine Particle Characteristics in Seven Industrial Plants*. Annals of Occupational Hygiene, 2009. **53**(5): p. 475-484.
203. Leppanen, M., J. Lyyranen, M. Jarvela, A. Auvinen, J. Jokiniemi, J. Pimenoff, and T. Tuomi, *Exposure to CeO<sub>2</sub> nanoparticles during flame spray process*. Nanotoxicology, 2012. **6**(6): p. 643-651.
204. Wang, Y.F., P.J. Tsai, C.W. Chen, D.R. Chen, and D.J. Hsu, *Using a Modified Electrical Aerosol Detector To Predict Nanoparticle Exposures to Different Regions of the Respiratory Tract for Workers in a Carbon Black Manufacturing Industry*. Environmental Science & Technology, 2010. **44**(17): p. 6767-6774.
205. Evans, D., B. Ku, M. Birch, and K. Dunn, *Aerosol monitoring during carbon nanofiber production: Mobile direct-reading sampling*. Ann Occup Hyg, 2010. **54**(5): p. 514 - 531.
206. Lee, J., M. Kwon, J. Ji, C. Kang, K. Ahn, J. Han, and I. Yu, *Exposure assessment of workplaces manufacturing nanosized TiO<sub>2</sub> and silver*. Inhal Toxicol, 2011. **23**(4): p. 226 - 236.

207. Tsai, S., M. Hofmann, M. Hallco, E. Ada, J. Kong, and M. Ellenbecker, *Characterization and evaluation of nanoparticle release during the synthesis of single-walled and multiwalled carbon nanotubes by chemical vapor deposition*. *Env Sci Technol*, 2009. **43**: p. 6017 - 6023.
208. Mazzuckelli, L., M. Methner, M. Birch, D. Evans, B. Ku, K. Crouch, and M. Hoover, *Identification and characterization of potential sources of worker exposure to carbon nanofibres during polymer composite laboratory operations*. *J Occup and Environ Hyg*, 2007. **4**: p. D125 - D130.
209. Wang, Y., P. Tsai, C. Chen, D. Chen, and D. Hsu, *Using a modified electrical aerosol detector to predict nanoparticle exposure to different regions of the respiratory tract for workers in Carbon Black manufacturing industry*. *Environ Sci Technol*, 2010. **44**: p. 6767 - 6774.
210. Park, J., B. Kwak, E. Bae, J. Lee, Y. Kim, K. Choi, and J. Yi, *Characterization of exposure to silver nanoparticles in a manufacturing facility*. *J Nanopart Res*, 2009. **11**: p. 1705 - 1712.
211. Miller, A., P.L. Drake, P. Hintz, and M. Habjan, *Characterizing Exposures to Airborne Metals and Nanoparticle Emissions in a Refinery*. *Annals of Occupational Hygiene*, 2010. **54**(5): p. 504-513.
212. Hang, J., Z. Luo, M. Sandberg, and J. Gong, *Natural ventilation assessment in typical open and semi-open urban environments under various wind directions*. *Building and Environment*, 2013. **70**(0): p. 318-333.
213. You, Y., C. Niu, J. Zhou, Y. Liu, Z. Bai, J. Zhang, F. He, and N. Zhang, *Measurement of air exchange rates in different indoor environments using continuous CO2 sensors*. *Journal of Environmental Sciences*, 2012. **24**(4): p. 657-664.
214. Miller, A., P.L. Drake, P. Hintz, and M. Habjan, *Characterizing exposures to airborne metals and nanoparticle emissions in a refinery*. *Ann Occup Hyg*, 2010. **54**(5): p. 504-13.
215. Park, J., B.K. Kwak, E. Bae, J. Lee, Y. Kim, K. Choi, and J. Yi, *Characterization of exposure to silver nanoparticles in a manufacturing facility*. *Journal of Nanoparticle Research*, 2009. **11**(7): p. 1705-1712.
216. Methner, M.M., *Engineering case reports. Effectiveness of local exhaust ventilation (LEV) in controlling engineered nanomaterial emissions during reactor cleanout operations*. *J Occup Environ Hyg*, 2008. **5**(6): p. D63-9.
217. Kuhlbusch, T.A.J., S. Neumann, and H. Fissan, *Number size distribution, mass concentration, and particle composition of PM1, PM2.5, and PM10 in bag filling areas of carbon black production*. *J Occup Environ Hyg*, 2004. **1**(10): p. 660-671.
218. Methner, M.M., *Effectiveness of a Custom-fitted Flange and Local Exhaust Ventilation (LEV) System in Controlling the Release of Nanoscale Metal Oxide Particulates During Reactor Cleanout Operations*. *International Journal of Occupational and Environmental Health*, 2010. **16**(4): p. 475-487.
219. Massari, A., M. Beggio, S. Hreglich, R. Marin, and S. Zuin, *Behavior of TiO2 nanoparticles during incineration of solid paint waste: A lab-scale test*. *Waste Management*, 2014. **34**(10): p. 1897-1907.
220. Reijnders, L., *11 - Safe recycling of materials containing persistent inorganic and carbon nanoparticles*, in *Health and Environmental Safety of Nanomaterials*, J. Njuguna, K. Pielichowski, and H. Zhu, Editors. 2014, Woodhead Publishing. p. 222-250.
221. Peters, T.M., W.A. Heitbrink, D.E. Evans, T.J. Slavin, and A.D. Maynard, *The mapping of fine and ultrafine particle concentrations in an engine machining and assembly facility*. *Annals of Occupational Hygiene*, 2006. **50**(3): p. 249-257.
222. Thomassen, Y., W. Koch, W. Dunkhorst, D.G. Ellingsen, N.P. Skaugset, L. Jordbekken, P.A. Drablos, and S. Weinbruch, *Ultrafine particles at workplaces of a primary aluminium smelter*. *Journal of Environmental Monitoring*, 2006. **8**(1): p. 127-133.

223. Peters, T.M., S. Elzey, R. Johnson, H. Park, V.H. Grassian, T. Maher, and P. O'Shaughnessy, *Airborne Monitoring to Distinguish Engineered Nanomaterials from Incidental Particles for Environmental Health and Safety*. J Occup Environ Hyg, 2009. **6**(2): p. 73-81.
224. Kim, B., J.S. Lee, B.S. Choi, S.Y. Park, J.H. Yoon, and H. Kim, *Ultrafine Particle Characteristics in a Rubber Manufacturing Factory*. Annals of Occupational Hygiene, 2013. **57**(6): p. 728-739.
225. Peters, T., S. Elzey, R. Johnson, H. Park, V. Grassian, T. Maher, and P. O'Shaughnessy, *Airborne Monitoring to Distinguish engineered Nanomaterials from Incidental particles for environmental health and safety*. J Occup and Environ Hyg, 2009. **6**: p. 73 - 81.
226. Zafar, U., C. Hare, A. Hassanpour, and M. Ghadiri, *Drop test: A new method to measure the particle adhesion force*. Powder Technology, 2014. **264**: p. 236-241.
227. Faschingleitner, J. and W. Höflinger, *Evaluation of primary and secondary fugitive dust suppression methods using enclosed water spraying systems at bulk solids handling*. Advanced Powder Technology, 2011. **22**(2): p. 236-244.
228. Grundnig, P.W., W. Höflinger, G. Mauschwitz, Z. Liu, G. Zhang, and Z. Wang, *Influence of air humidity on the suppression of fugitive dust by using a water-spraying system*. China Particuology, 2006. **4**(5): p. 229-233.
229. Vorbau, M., L. Hillemann, and M. Stintz, *Method for the characterization of the abrasion induced nanoparticles release into air from surface coatings*. J Aerosol Sci, 2009. **40**(3): p. 209 - 217.
230. Buonanno, G., L. Stabile, P. Avino, and E. Belluso, *Chemical, dimensional and morphological ultrafine particle characterization from a waste-to-energy plant*. Waste Manag, 2011. **31**(11): p. 2253-62.
231. Sotiriou, G.A., D. Singh, F. Zhang, W. Wohlleben, M.-C.G. Chalbot, I.G. Kavouras, and P. Demokritou, *An integrated methodology for the assessment of environmental health implications during thermal decomposition of nano-enabled products*. Environmental Science: Nano, 2015. **2**(3): p. 262-272.

# LIST OF PUBLICATIONS

## *Journal articles*

(2015 Swiss Aerosol Award publication) **A system to assess the stability of airborne nanoparticle agglomerates under aerodynamic shear.**

Yaobo Ding & Michael Riediker. *Journal of Aerosol Science* (2015), 88(0), 98-108.

(DOI: <http://dx.doi.org/10.1016/j.jaerosci.2015.06.001>)

**Dustiness and deagglomeration testing - interlaboratory comparison of systems for nanoparticle powders.**

Yaobo Ding, Burkhard Stahlmecke, Araceli Sánchez Jiménez, Ilse L. Tuinman, Heinz Kaminski, Thomas A.J. Kuhlbusch, Martie van Tongeren, Michael Riediker. *Aerosol Science and Technology* (2015), 49:12, 1222-1231. (DOI: [10.1080/02786826.2015.1114999](https://doi.org/10.1080/02786826.2015.1114999))

**Influence of molecular architecture on the isothermal time-dependent response of amorphous shape memory polyurethanes.**

Charly Azra, Yaobo Ding, Christopher J.G. Plummer Jan-Anders, E. Månson. *European Polymer Journal* (2012) 49(1) pp. 184-193. (DOI: <http://dx.doi.org/10.1016/j.eurpolymj.2012.10.012>)

Expected publications :

**Linking release of engineered nanomaterials at workplaces to human exposure: a review.**

Yaobo Ding & Michael Riediker. (submitted NOV 2015)

**Nano-object release during machining of polymer-based nanocomposites depends on process factors and the type of nanofiller ?**

Yaobo Ding, Wendel Wohlleben, Mael Boland, Klaus Vilsmeier, Michael Riediker. (*in revision*)

**Deagglomeration potentials of airborne nanoparticle agglomerates under different humidity conditions – an interlaboratory comparison.**

Yaobo Ding, Burkhard Stahlmecke, Heinz Kaminski, Yunhong Jiang, Thomas A.J. Kuhlbusch, Michael Riediker.  
(*in revision*)

## *Scientific reports*

**Likelihood of airborne nanomaterials to deagglomerate under various conditions** (*submitted May 2015*)

Ding, Y., Stahlmecke, B., Sanchez, A., Tuinman, I., Kaminski, H., Brouwer, D., Kuhlbusch, T.A.J., Van Tongeren, M., Riediker. *Publication of European Union (public report)*.  
EU FP7 MARINA (MANaging Risk of NANomaterials) project, <http://www.marina-fp7.eu/>

**Release of engineered nanomaterials (ENMs) along their life cycles in small and large industries.** (submitted May 2015)

Ding, Y., Sanchez, A., Kuhlbusch, T.A.J., Van Tongeren, Stahlmecke, B., Tuinman, I., Brouwer, D., M., Riediker. *Publication of European Union (public report).*

EU FP7 MARINA (MANaging Risk of NANomaterials) project, <http://www.marina-fp7.eu/>

### **Book chapters**

**“The flows of engineered nanomaterials from production, use and disposal to the environment”**, Volume: indoor and Outdoor Nanoparticles - determinants of Release and Exposure Scenarios.

Bernd Nowack, Nikolaus Bornhöft, Yaobo Ding, Michael Riediker, Araceli Sánchez Jiménez, Tian yin Sun, Martie van Tongeren, Wendel Wohlleben.

*The Handbook of Environmental Chemistry*: pp 1-23. Springer International Publishing Switzerland, 2016. ISBN 978-3-319-23919-4.

*Contributions from Yaobo Ding: a section on estimation of environmental release of engineered airborne nanomaterials from nanotechnology workplaces was written. In addition, Yaobo Ding commented on other parts of the chapter and participated in discussions.*

### **Conferences**

**Investigating airborne stability of nanomaterials - aerosol generations and characterizations.**

Yaobo Ding, Michael Riediker. Oral presentation at the 10th International Scientific Conference of the International Hygiene Association, IOHA 2015, At London, Volume: *Annals of Occupational Hygiene (2015) 59 (suppl 1): 9.*

[DOI: 10.1093/annhyg/mev035](https://doi.org/10.1093/annhyg/mev035)

**Nano-objects release during drilling and sawing of nanofiller composites.**

Yaobo Ding, Michael Riediker. Oral presentation at the 10th International Scientific Conference of the International Hygiene Association, IOHA 2015, At London, Volume: *Annals of Occupational Hygiene (2015) 59 (suppl 1): 9.*

[DOI: 10.1093/annhyg/mev035](https://doi.org/10.1093/annhyg/mev035)

**Investigating the stability of airborne nanoparticles – a system to study de-agglomeration processes under different conditions.**

Yaobo Ding. Oral presentation at the Swiss Aerosol Group (SAG) annual meeting, 10th November 2014, Bern, Switzerland

**Investigating the stability of airborne nanoparticles – developing an effective system to trigger de-agglomeration under different conditions.**

Yaobo Ding, Oral presentation at *the Nanosafety Forum for Young Scientists* hosted by the EU NanoSafety Cluster, 8-9<sup>th</sup> October 2014, Sicily, Italy.

**Developing an integrated tool to investigate the likelihood of nanomaterial agglomerates to break apart into smaller or primary particles.**

Yaobo Ding, Michael Riediker, Poster presentation at *the 2014 International Aerosol Conference*, August 28 – September 2, 2014, BEXCO, Busan, Korea.

**Investigation of the likelihood of nanomaterial agglomerates to break apart into smaller agglomerates or primary particles – developing an integrated tool to identify nanomaterial release into the environment.**

Yaobo Ding, Michael Riediker, Oral presentation at *the Aerosol Technology Conference AT2014*, 16-18 June 2014, Karlsruhe, Germany. Abstract No.T230A12.

**A novel system to test the stability of airborne nanoparticles agglomerates.**

Ding Yaobo, Riediker Michael, *NanoTox 2014*, Poster presentation at *the 7th International Nanotoxicology Congress*, April 23-26, Antalya, Turkey. P. 231, 2014.

**Development of an system to test the stability of airborne nanoparticle agglomerates.**

Yaobo Ding, Oral presentation at *the 6th International Symposium on Nanotechnology, Occupational and Environmental Health (NanOEH)*, October 28-31, 2013, Nagoya, Japan.

**Development of an effective system to test the de-agglomeration process of airborne nanoparticles.**

Yaobo Ding, Michael Riediker, Poster presentation at *the 2<sup>nd</sup> Quality-Nano integrating conference “Quality in nanosafety assessment – driving best practice and innovation”*, 27<sup>th</sup> February – 1<sup>st</sup> March 2013, Prague, Czech Republic.

## GRANTS

Participation in the International Aerosol Conference (IAC 2014), August 28 – September 2, 2014, Busan, Korea, funded by Fondation pour l'Université de Lausanne, Lausanne, Switzerland.

Quality-Nano Transnational Access (TA) to the microscopy facilities at University of Leeds (U.K.), 6-10 January 2014, funded by QualityNano Research Infrastructure, Dublin, Ireland.

QualityNano is a Research Infrastructure for nanosafety assessment. It harnesses resources from across Europe and develop efficient, transparent and effective processes. The Transnational Access (TA) component for QualityNano is dedicated to providing users from the European nanosafety community access to nanomaterials processing, characterisation and exposure assessment facilities (TAFs).

## Acknowledgement

The thesis is a concentrate of the hard work over three and half years on laboratory experiments and theoretical studies. I would never achieve it without many of those who helped me along the journey.

Firstly, I would like to express my sincere gratitude to my thesis advisor Dr. Michael Riediker for the excellent supervision of my study and research activities, for his great motivation, patience and insights in the field, which is invaluable for a young researcher in his early years of professional career. His continuous guidance throughout the entire period of my project and manuscript writing ensured the timely progress of my study.

Besides my supervisor, I would like to thank the rest of my thesis committee: Prof. Gerhard Kasper, Dr. Keld Jensen, and Dr. Olivier Le Bihan, not only for their constant encouragement and insightful comments on my research, but also for the in-depth questions which incited me to perfect my research in various aspects.

My sincere thanks also goes to Dr. Guillaume Suarez, Dr. Jean-Jacques Sauvain, Gregory Plateel, Dr. Nicolas Concha-Lozano, Ferdinand Storti, Simon Deslarzes and Nicole Charrière for their very kind laboratory supports along the development of the experimental system, as well as the guidance on the work safety. Without their precious assistances my laboratory experiments would not proceed smoothly as planned.

I thank my fellow Ph.D. students Dr. Reto Meier (former), Dr. Jiayuan Zhao (former), Halshka Graczyk and the previous group member Dr. Nastassja Lewinski for their stimulating discussions on research topics, and also for the great time we spent together during various group activities.

I also appreciate the assistance of Antonio Mucciolo from the Electron Microscopy Facility of University of Lausanne, in TEM characterizations of my nanoparticle samples. In addition, I am grateful for the financial support of Fondation pour l'Université de Lausanne for my participation in the International Aerosol Conference (IAC 2014) in Busan, Korea.

I would like to express my genuine thank to the financial support of the QualityNano Research Infrastructure through the Transnational Access (TA) program, for using the research facility in a collaborating institute. The assistance of Dr. Yunhong Jiang in University of Leeds on the microscopic analysis of my samples is greatly appreciated.

I'd like also to thank the colleagues from partner institutes on the experiments, Dr. Burkhard Stahlmecke, Dr. Thomas A.J. Kuhlbusch, Dr. Araceli Sánchez Jiménez, Dr. Martie van Tongeren, Dr. Ilse L. Tuinman, and Dr. Derk Brouwer, for their valuable comments on my research as well as on drafting the manuscripts.

Last but not the least, my family members have been great supporters over the years with all their hearts to my studies: my dear wife, my cute little boy, and my family in China.



Yaobo Ding  
dyb450303@gmail.com

# CV

## EDUCATIONS

- PhD candidate, Engineered nanomaterial aerosols and occupational health** 2012 – 2015  
Institute for Work and Health, University of Lausanne, Lausanne, Switzerland
- MSc., Materials Science (Transformation of materials and production processes)** 2009 – 2011  
GPA 5.1/6.0, École Polytechnique Fédérale de Lausanne (EPFL), Switzerland
- BSc., Materials Science and Engineering** 2004 – 2008  
GPA 82/100, China University of Geosciences, Beijing. P.R.China

## PROFESSIONAL EXPERIENCES

- PhD candidate** Supervisor: Dr. Michael Riediker 2012-  
  - *Development of an aerosolization system for dry nanomaterial powders in producing controlled concentration and size distribution*
  - *Application of aerodynamic shear to nanoparticle agglomerates in airborne state using critical orifices to study the deagglomeration potentials of nanomaterials*
  - *Investigation of humidity influence on stability of agglomerates*
  - *Study release of nano-objects from mechanical treatments of nano-composites (sawing and drilling)*
  - *Systematic review on release of engineered nanomaterials at nanotechnology workplaces*
- Master Thesis** Laboratory of Polymer and Composite Technology, EPFL 2011  
**Design of novel shape memory polyurethanes (SMPUs) for microfluidic applications**  
Supervisor: Dr. Christopher Plummer  
  - *Investigation of influence of polydispersity, cross-linking density and chain extender on glass transition behaviour of SMPUs, modelling of stress relaxation process;*
  - *Synthesis/moulding setups design, network structure synthesis, inject moulding, curing;*
  - *Tests of thermal (DSC) and mechanical (DMA/shape memory test) properties.*
- R&D Internship** (4 months) Sika Technology AG, Zürich, Switzerland 2010 – 2011  
**Investigation of influence of blowing agent concentration and nucleation agents on the cell structure and expansion behavior of LDPE foams** Supervisor: Dr. Jügen Finter  
  - *Chemical Blowing Agent (CBA) and inorganic/organic nucleation agents were employed to investigate their influences in both free and constrained foaming process;*

- *Melt mixing at different temperatures and released-times (twin screw extruder/two-roll mill), determination of decomposition rate of CBA, foam density, cell size/density, ratio of open to closed cells and thermal/mechanical properties of foam products.*

**Master Research Project** (1 semester) Powder Technology Laboratory, EPFL **2009 – 2010**

Synthesis and characterization of transparent polycrystalline  $\alpha$ -alumina *Supervisor: Dr. Paul Bowen*

- *Seed production, thermal treatments (thermo-gravimetry, particle size distribution);*
- *Spark Plasma Sintering (SPS), microstructure analysis (SEM), atomistic modeling of dopants effect on interface structures (Metropolis Monte Carlo method).*

**Master Research Project** (1 semester) Ceramic Laboratory, EPFL **2009**

**Investigation of effect of substrate roughness on c-oriented AlN thin film** *Supervisor: Prof. Paul Muralt*

- *Investigation of influence of surface morphology of silicon substrate on internal stress of thin film;*
- *Thin film fabrication (Pulsed-dc magnetron sputtering), microstructure and surface morphology characterizations by X-ray diffraction (XRD) and Atomic Force Microscopy (AFM).*

**Bachelor Thesis** Laboratory of New Materials, Chinese Academy of Sciences, Beijing **2008**

**Preparation and characterization of PP/carbon nanotube composites** *Supervisor: Prof. Zhang Yihe*

- *Investigation of influence of multi-wall carbon nano-tubes concentrations (0.5-5%) on the fracture morphology, thermal and mechanical properties of polypropylene/CNTs composites.*
- *Melt-Blending (two-roll mill/internal mixer), injection moulding, thermogravimetry (TG), Infrared Spectroscopy (IR), DSC, XRD, SEM, notched impact strength, tensile and bending strength.*

## EXTRA-CURRICULAR ACTIVITIES

**“Swissinfo-Huawei” Basketball Tournament** Gymnasium Leonhard, Basel **05.2011**

- *Team player of Lasanne Chinese Students Association and had won the 3<sup>rd</sup> place in the championship*

**Student guest at 100-year anniversary of Sika group** Sika Schweiz AG Automotive **05.2010**

- *Learning of polymer composite technologies for automotive industry; visits to car manufacturers (Volkswagen, Renault); Practice in multilayer-foaming prototype process; social activities*

## HONORS AND AWARDS

Swiss Aerosol Award 2015 (*prize sponsored by the Swiss Lung Foundation for the best scientific publication in aerosol research written from within Switzerland, CHF 10,000*) 11.2015

Student funding for participation in scientific conference (University of Lausanne)	08.2014
Quality-Nano Transnational Access Grant (European Union-funded)	01.2014
EPFL Student Research Assistant Scholarship (2-year)	12.2008 – 09.2010
China University of Geosciences Academic Performance Scholarship	2005/2008
China University of Geosciences Excellent Youth League Member	2006/2007
Excellent Award in Beijing Universities Calligraphy Competition	09.2006
Excellent Leader of Student Community Association	12.2005

## **MEMBERSHIPS**

German Association for Aerosol Research (GAef), Student member

## **LANGUAGES**

- English (TOEFL, professional uses)
- French (CEFR – B1, independent user)
- Chinese (Native)

## **INTERESTS**

- Basketball, swimming and Chinese calligraphy



